5-2023

Determination of Effective Index of Refraction of Structured Materials (Photonic Crystals)

Md Arafat Hossain
The University of Texas Rio Grande Valley

DETERMINATION OF EFFECTIVE INDEX OF REFRACTION OF STRUCTURED MATERIALS (PHOTONIC CRYSTALS)

A Thesis

by

MD ARAFAT HOSSAIN

Submitted in Partial Fulfillment of the

Requirements for the Degree of

MASTER OF SCIENCE

Major Subject: Physics

The University of Texas Rio Grande Valley

May 2023

DETERMINATION OF EFFECTIVE INDEX OF REFRACTION OF STRUCTURED MATERIALS (PHOTONIC CRYSTALS)

A Thesis
by
MD ARAFAT HOSSAIN

COMMITTEE MEMBERS

Dr. Malik Rakhmanov
Chair of Committee

Dr. Nicholas Dimakis
Committee Member

Dr. Soma Mukherjee
Committee Member

Dr. Ahmed Touhami
Committee Member

May 2023

ABSTRACT

Hossain, Md Arafat, Determination of effective index of refraction of structured materials (photonic crystals). Master of Science (MS), May, 2023, 89 pp., 7 tables, 45 figures, references, 35 titles.

Photonic crystals have been widely studied by researchers due to their ability to control light propagation in all spatial directions. For example, 2D photonic crystals can be made of dielectric rods arranged in a square lattice. When light propagates through 2D photonic crystals, it experiences multiple scatterings by the crystal centers. The superposition of all scattered waves forms the transmitted field largely dependent upon the effective index of refraction of the structured material. We propose a method to determine the effective index of refraction through such materials with the Finite-Difference Time-Domain (FDTD) model. We set up the interface of two media, such as air and photonic crystal, modeled the refraction of the EM waves at the interface, collected the data from FDTD and analyzed the data in MATLAB using FFT2. The proposed method promises to be a simple tool for determining the effective index of refraction of structured materials.

DEDICATION

Dedicated to my Grandfather, Kazi Shaokat Ali, who always encouraged me to study hard and inspired me to dream big.

ACKNOWLEDGMENTS

I am grateful to my advisor Dr. Malik Rakhmanov for his invaluable guidance throughout my research work. Without his support, it would not be possible to finish this research work. Also, I would like to thank Dr. Nicholas Dimakis, Dr. Soma Mukherjee, and Dr. Ahmed Touhami for their support. I would like to thank Synopsis Optical Solutions Group for providing the simulation packages to finish this research.

TABLE OF CONTENTS

Page

LIST OF TABLES

Page

LIST OF FIGURES

Page

CHAPTER I

INTRODUCTION

Photonic crystals are made of periodic dielectric structures and have attracted enormous research interest nowadays. The propagation of light in photonic crystals has been studied for a long time [1, 2]. The photonic crystals inhibit light propagation over a specific band of frequencies while allowing others to propagate. This behavior gives rise to the concept of photonic band gap, which is analogous to the electronic band gap in semiconducting materials [3, 4, 5]. The propagation of EM waves in photonic crystals and photonic band gap have been studied extensively by several groups [6, 7, 8]. Their studies show that the periodic dielectric structures have photonic band gap.

Recently photonic crystals have garnered outstanding research interest due to their unique properties. The band gap of photonic crystals prohibits light propagation at certain frequencies. Therefore, light propagation can be controlled in certain ways, which is not possible in conventional materials. The photonic crystals have advantages over semiconductor materials due to low-loss, high speed, and wide-bandwidth properties [9]. All these properties have importance in telecommunications and optoelectronic devices. A few examples of devices based on photonic crystals are optical filter [10], wavelength division multiplexer (WDM) [11], optical sensor [12], and logic gates [13, 14].

The 2D photonic crystals, the counterpart of 3D, have also garnered research interest over the few years [15, 16]. The 2D photonic crystals come in various lattices such as square [15], triangular [17], and hexagonal [18]. This work focuses on 2D structured photonic crystals due to computational limitations. We studied 2D photonic crystals of square lattice considering transverse electric (TE) and transverse magnetic (TM) polarization.

The propagation of light in photonic crystals shows interesting phenomena. The light in the photonic crystals scattered strongly due to the high refractive index contrast. The scattered waves make constructive or destructive interference in the structure depending upon the wavelength of the incident light. The index of refraction of the constituent elements is different from the index of refraction of the structured photonic crystals. The propagation of light in strongly modulated 2D photonic crystals behaves as a material having a refractive index called effective refractive index. The photonic band gap of the photonic crystals can control the effective refractive index. The effective index in 2D photonic crystals has been studied by many theoretical [19, 20, 21] and experimental groups [22, 23]. It is possible to find positive and negative or zero refraction in the same structure depending upon their band structure and direction of propagation of the incident light in the photonic crystals [24].

The outline of this Thesis is as follows: Chapter II discusses Maxwell's equations and the propagation of EM waves in the homogeneous medium for TE and TM polarization. Chapter III discusses the periodic dielectric structures using Bravais lattice, reciprocal lattice, and Brillouin zone. This chapter also discusses the governing equation of photonic crystals, including numerical examples. Chapter IV introduces the Finite-Difference Time-Domain method (FDTD) based on Maxwell's equations and Yee's grid [25]. The discussion of a perfectly matched layer (PML) for absorbing outgoing waves is also included in this chapter. Chapter IV describes the method for determining the refractive index using Fast-Fourier Transformation. This chapter includes the numerical calculation of the refractive index using FFT2 tool. Chapter V discusses the effective index of refraction in 2D photonic crystals using the FDTD method. The relation between effective index and polarization is also discussed in this chapter. Chapter VI summarizes the results of this work, and the findings of this work are also discussed here.

CHAPTER II

EM WAVES IN HOMOGENEOUS MEDIA

2.1 Maxwell's Equations

Maxwell's equations are based on experimental fact and named after their discoverers, such as Faraday's law, Gauss' law, Ampere's law, and magnetic monopole. The physical quantities associated with Maxwell's laws are electric field **E**, electric displacement field **D**, magnetic field **H**, electric current density **J**, and charge density ρ. In linear and homogeneous media, Maxwell's equation in integral and differential form can be written as

Gauss' law: The differential form of Gauss' law is equivalent to the statement of Coulomb's law.

$$\oint_S \mathbf{D} \cdot d\mathbf{s} = \int_V \rho dv. \tag{2.1}$$

The differential form can be written as

$$\nabla \cdot \mathbf{D} = \rho. \tag{2.2}$$

It connects the electric charge density ρ for moving and stationary charges to the electric field **E**. Here V is the volume enclosed by the surface S.

Faraday's law: it is time-varying magnetic flux produces electromotive force.

$$\oint_C \mathbf{E} \cdot d\mathbf{I} = -\int_S \frac{\partial \mathbf{B}}{\partial t} \cdot d\mathbf{s}. \tag{2.3}$$

The differential form of Faraday's law is

$$\nabla \times \mathbf{E} = -\frac{\partial \mathbf{B}}{\partial t}. \tag{2.4}$$

where S is an arbitrary two-dimensional surface in three-dimensional space and C is its boundary.
Ampere's law: It is the line integral of the magnetic field **H** around any closed loops is equal to the total current density **J** enclosed by that loop.

$$\oint_C \mathbf{H} \cdot d\mathbf{I} = \int_S \mathbf{J} \cdot d\mathbf{s} + \int_S \frac{\partial \mathbf{D}}{\partial t} \cdot d\mathbf{s}. \tag{2.5}$$

The differential form of Ampere's law is

$$\nabla \times \mathbf{H} = \mathbf{J} + \frac{\partial \mathbf{D}}{\partial t}. \tag{2.6}$$

where S is a surface with boundary C. The first term in the right side of Eq.2.5 is the conduction current density and second term is the displacement current density.
Maxwell's fourth equation-this equation states that there are no magnetic monopoles. Sometimes, it is called Gauss' law for magnetism.

$$\oint_S \mathbf{B} \cdot d\mathbf{s} = 0. \tag{2.7}$$

The differential form of fourth equation is

$$\nabla \cdot \mathbf{B} = 0. \tag{2.8}$$

Where S is a surface with boundary C.

2.2 Boundary Conditions

In linear, isotropic, and homogeneous media the relation between fields are

$$\mathbf{D} = \varepsilon_r \varepsilon_0 \mathbf{E}, \qquad \mathbf{B} = \mu_r \mu_0 \mathbf{H}; \tag{2.9}$$

where ε_0 and μ_0 are the permittivity and permeability of the free space, and ε_r and μ_r are the relative permittivity and permeability of the materials, respectively. The speed of light $c = 299792548 m/s$, the value of μ_0 is $4\pi \times 10^{-7} H/m$. The permittivity of free space, $\varepsilon_0 = \frac{1}{c^2 \mu_0}$ and the value of ε_0 is

$8.854 \times 1^{-12} F/m$.

First Boundary Condition: The normal component of electric displacement field **D** is discontinuous across the boundary.

The boundary conditions for the normal components of **E** and **D** can be found by applying Gauss' law, Eq.2.1, to the loop *abcd*. At the limit, $\Delta h \to 0$, normal component of **D** yields

$$\mathbf{D}_1 \cdot \mathbf{n}_1 \Delta s + \mathbf{D}_2 \cdot \mathbf{n}_2 \Delta s = \rho_s \Delta s, \tag{2.10}$$

where $\mathbf{n}_1$ and $\mathbf{n}_2$ are unit normal vector to the top and bottom surfaces of the cylinder in Fig.2.1. But $\mathbf{n}_2 = -\mathbf{n}_1$, and Eq.2.10 yields

$$\mathbf{n}_2 \cdot (\mathbf{D}_1 - \mathbf{D}_2) = \rho_s, \tag{2.11}$$

where $\mathbf{D}_1$ and $\mathbf{D}_2$ are the normal component of displacement fields of D_{1n} and D_{2n}, respectively, and ρ_s is the surface charge density of the cylinder. So, Eq.2.11 can be written as

$$D_{1n} - D_{2n} = \rho_s. \tag{2.12}$$

The normal component of electric displacement field **D** is discontinuous across the boundary between two media. This is the second boundary condition for Maxwell's equation. Similarly for normal component of electric field, **E**, by applying Eq.2.9 to Eq.2.12 yields

$$\varepsilon_1 E_{1n} - \varepsilon_2 E_{2n} = \rho_s. \tag{2.13}$$

Second Boundary Condition: Tangential component of the electric field **E**. Let us consider a boundary between two media having permittivities ε_1, ε_2, and permeabilities μ_1, μ_2, respectively, as shown in Fig.2.1 By applying Faraday's law, Eq.2.3, to the loop *abcd* in Fig.2.1 we get

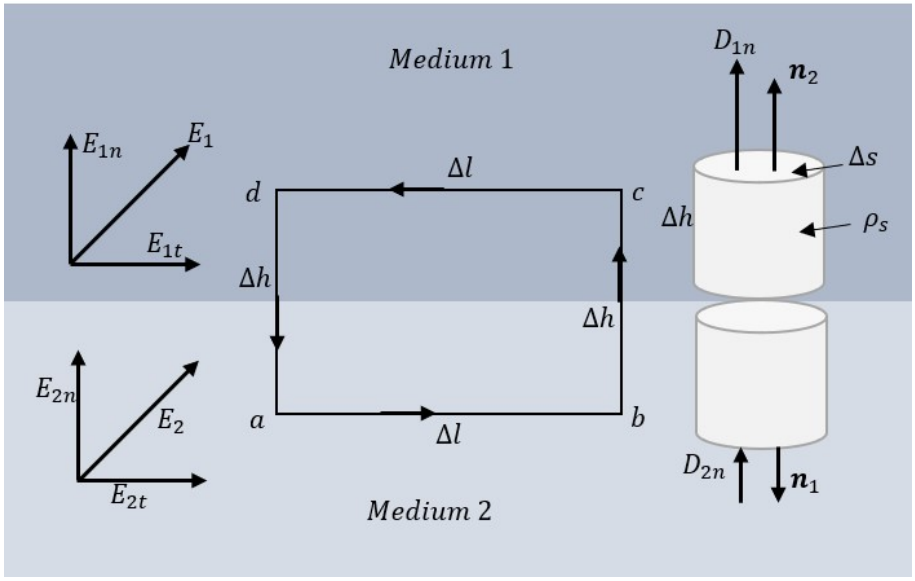

Figure 2.1: Boundary conditions at the interface of two materials having permittivites ε_1,ε_2, and permeabilities μ_1,μ_2, respectively. The upper portion is the medium 1 of refractive index n_1 and and the lower portion represents the medium 2 of refractive index n_2.

$$E_{2t}\Delta l + E_{2n}\frac{\Delta h}{2} + E_{1n}\frac{\Delta h}{2} + E_{1t}(-\Delta l) + E_{1n}\left(-\frac{\Delta h}{2}\right) + E_{2n}\left(-\frac{\Delta h}{2}\right) = -\frac{\partial B_\perp}{\partial t}\Delta h \Delta l, \qquad (2.14)$$

where $B_\perp$ is the component of magnetic field perpendicular to the loop *abcd*. When $\Delta h \to 0$, Eq.2.14 reduces to

$$E_{2t}\Delta l + E_{1t}\left(-\Delta l\right) = 0. \qquad (2.15)$$

which gives the the continuity condition for tangential component of the electric field at the interface between the two media.

$$\mathbf{E}_{2t} = \mathbf{E}_{1t}. \qquad (2.16)$$

The tangential component of the electric field, **E** is continuous across the boundary between the two media. This is the first boundary condition for Maxwell's equation.

Third Boundary Condition: The tangential component of the magnetic field, **H** is continuous across the boundary between two media.

To find the tangential component of H, we apply Ampere's law, Eq.2.5, to the loop *abcda*.

At $\Delta h \to 0$, components of $\mathbf{H}$ around the loop gives the equation

$$\begin{aligned} H_{2t}\Delta l + H_{1t}(-\Delta l) &= J_s \Delta l \\ \text{or} \quad H_{2t} - H_{1t} &= J_s \end{aligned} \tag{2.17}$$

where H_{1t} and H_{2t} are the tangential components of $\mathbf{H}$ along the long arms of the loop and J_s is the magnitude of the surface current density normal to the loop. Eq.2.17 can be written as

$$\mathbf{n}_2 \times (\mathbf{H}_1 - \mathbf{H}_2) = \mathbf{J}_s. \tag{2.18}$$

where $\mathbf{n}_2$ is the unit vector normal to the surface of the cylinder. In the absence of surface current density J_s, Eq.2.17 can be written as

$$H_{2t} = H_{1t} \tag{2.19}$$

The tangential component of the magnetic field, $\mathbf{H}$ is continuous across the boundary between the two media. This is the third boundary condition for Maxwell's equation.

Fourth Boundary Condition: The normal component of magnetic flux density, $\mathbf{B}$ is continuous across the boundary between the two media. By applying Gauss' law, Eq.2.7, to the loop *abcda* yields

$$\begin{aligned} \mathbf{n} \cdot (\mathbf{B}_1 - \mathbf{B}_2) &= 0, \\ \text{or,} \quad B_{2n} &= B_{1n}. \end{aligned} \tag{2.20}$$

In this case, the normal component of the magnetic field $\mathbf{B}$ is continuous across the boundary between the two media.

2.3 Propagation of EM Wave in a Homogeneous Medium

We assume that a plane electromagnetic wave is incident at the interface between the two media of refractive index n_1 and n_2. The permittivity and permeability of the media are ε_1, ε_2,

and μ_1, μ_2, respectively. In linear, homogeneous, and isotropic medium, Maxwell's equations are written as

$$\nabla \cdot \mathbf{D} = 0, \tag{2.21}$$

$$\nabla \cdot \mathbf{B} = 0, \tag{2.22}$$

$$\nabla \times \mathbf{E} = -\frac{\partial \mathbf{B}}{\partial t}, \tag{2.23}$$

$$\nabla \times \mathbf{H} = \frac{\partial \mathbf{D}}{\partial t}, \tag{2.24}$$

where $\mathbf{D} = \varepsilon \mathbf{E}$ and $\mathbf{B} = \mu \mathbf{H}$. Here $\varepsilon = \varepsilon_0 \varepsilon_r$ and $\mu = \mu_0 \mu_r$. From Eq.2.23

$$\begin{aligned} -i\mathbf{k} \times \mathbf{E} &= -\mu i \omega \mathbf{H}, \\ \mathbf{H} &= \frac{1}{\mu \omega} \mathbf{k} \times \mathbf{E}. \end{aligned} \tag{2.25}$$

We assume the fields associated with the incident plane wave are

$$\mathbf{E} = \mathbf{E}_0 e^{i(\omega t - \mathbf{k} \cdot \mathbf{r})}. \tag{2.26a}$$

$$\mathbf{B} = \mathbf{B}_0 e^{i(\omega t - \mathbf{k} \cdot \mathbf{r})}. \tag{2.26b}$$

$$\mathbf{H} = \mathbf{H}_0 e^{i(\omega t - \mathbf{k} \cdot \mathbf{r})}. \tag{2.26c}$$

In the first medium, the incident plane wave is written as

$$\mathbf{E}_1 = \mathbf{E}_i e^{i(\omega t - \mathbf{k}_i \cdot \mathbf{r})}. \tag{2.27}$$

Similarly, the reflected plane wave can be written as

$$\mathbf{E}_2 = \mathbf{E}_r e^{i(\omega t - \mathbf{k}_r \cdot \mathbf{r})}. \tag{2.28}$$

and the transmitted wave is

$$\mathbf{E}_3 = \mathbf{E}_t e^{i(\omega t - \mathbf{k}_t \cdot \mathbf{r})}. \tag{2.29}$$

The plane wave incident at the interface between the media has two type of polarization-

Transverse Electric (TE): the incident **E**-field is perpendicular to the plane of incidence and

Transverse Magnetic (TM): the incident **H**-field is perpendicular to the plane of incidence.

TE Polarization

For TE-polarization, $\mathbf{E} = E_y \hat{y}$. The component of electric field E_y is continuous across the boundary and component of magnetic field H_x is continuous across the boundary.

In the first medium, total field

$$E_{1y} = E_{iy} e^{i(\omega t - \mathbf{k}_i \cdot \mathbf{r})} + E_{ry} e^{i(\omega t - \mathbf{k}_r \cdot \mathbf{r})}. \tag{2.30}$$

For simplicity, we will omit the subscript y from the field.

$$E_1 = E_i e^{i(\omega t - \mathbf{k}_i \cdot \mathbf{r})} + E_r e^{i(\omega t - \mathbf{k}_r \cdot \mathbf{r})}. \tag{2.31}$$

In the second medium, transmitted field is written as

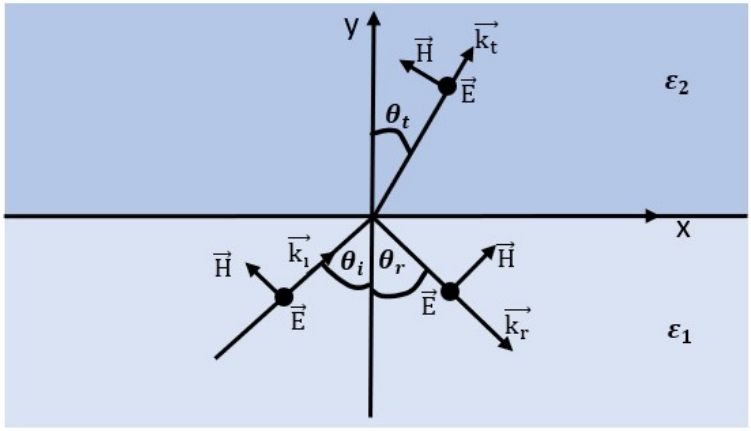

Figure 2.2: A plane electromagnetic wave is propagating through the two media of dielectric constant ε_1 and ε_2, respectively. For TE-polarization, the direction of electric field is into the page, $\mathbf{E} = E_y \hat{y}$

$$E_2 = E_t e^{i(\omega t - \mathbf{k}_t \cdot \mathbf{r})}. \tag{2.32}$$

Now, applying boundary conditions at the interface ($z = 0$). The tangential component of the electric field **E** is continuous across the boundary

$$\begin{aligned} E_1(z=0) &= E_2(z=0), \\ E_i e^{i(\omega t - k_{ix} x)} + E_r e^{i(\omega t - k_{rx} x)} &= E_t e^{i(\omega t - k_{tx} x)}. \end{aligned} \tag{2.33}$$

The component of k-vectors tangential to the interface of the two media are identical, that means $k_{ix} = k_{rx} = k_{tx}$. The Eq.2.33 yields

$$E_i + E_r = E_t. \tag{2.34}$$

From Eq.2.25, the incident **H**-field

$$\mathbf{H}_i = \frac{1}{\mu_1 \omega} \mathbf{k} \times \mathbf{E}_i. \tag{2.35}$$

since E_y and H_x component are continuous across the boundary, we can write the incident field as

$$\mathbf{H}_i = \frac{E_i e^{i(\omega t - \mathbf{k} \cdot \mathbf{r})}}{\mu_1 \omega} (k_{ix} \hat{z} - k_{iz} \hat{x}). \tag{2.36}$$

Similarly, reflected **H**-field is written as

$$\mathbf{H}_r = \frac{E_r e^{i(\omega t - \mathbf{k} \cdot \mathbf{r})}}{\mu_1 \omega} (k_{rx} \hat{z} - k_{rz} \hat{x}). \tag{2.37}$$

and transmitted field **H**-field is written as

$$\mathbf{H}_t = \frac{E_t e^{i(\omega t - \mathbf{k} \cdot \mathbf{r})}}{\mu_2 \omega} (k_{tx} \hat{z} - k_{tz} \hat{x}). \tag{2.38}$$

Applying boundary condition, the tangential component of **H**- field is continuous. Here H_x compo-

nents are continuous across the boundary.

$$\frac{E_i e^{i(\omega t-\mathbf{k}\cdot\mathbf{r})}}{\mu_1\omega}(-k_{iz})+\frac{E_t e^{i(\omega t-\mathbf{k}\cdot\mathbf{r})}}{\mu_1\omega}(-k_{rz})=\frac{E_t e^{i(\omega t-\mathbf{k}\cdot\mathbf{r})}}{\mu_2\omega}(-k_{tz}). \tag{2.39}$$

at $z=0$

$$\begin{aligned}\frac{E_i k_{iz}}{\mu_1}+\frac{E_r k_{rz}}{\mu_1}&=\frac{E_t k_{tz}}{\mu_2},\\ \frac{E_i k_{iz}}{\mu_1}-\frac{E_r k_{iz}}{\mu_1}&=\frac{E_t k_{tz}}{\mu_2}.\end{aligned} \tag{2.40}$$

since $k_{rz}=-k_{iz}$. From Eq.2.34 and Eq.2.40

$$\frac{E_r}{E_i}=\frac{\mu_2 k_{iz}-\mu_1 k_{tz}}{\mu_2 k_{iz}+\mu_1 k_{tz}}. \tag{2.41}$$

$$r_{TE}=\frac{E_r}{E_i}. \tag{2.42}$$

Here, r_{TE} is called the coefficient of reflection.

Similarly, from Eq.2.34 and Eq.2.40

$$\frac{E_t}{E_i}=\frac{2\mu_2 k_{iz}}{\mu_2 k_{iz}+\mu_1 k_{tz}} \tag{2.43}$$

$$t_{TE}=\frac{E_t}{E_i}. \tag{2.44}$$

Here, t_{TE} is called the coefficient of transmission of the medium.

TM Polarization

For TM-polarization, the **H**-field is along y-direction, $\mathbf{H}=H_y\hat{y}$. Now H_y and E_x components are continuous across the boundary. Similarly, using the boundary condition at the interface ($z=0$) we get

$$H_i+H_r=H_t. \tag{2.45}$$

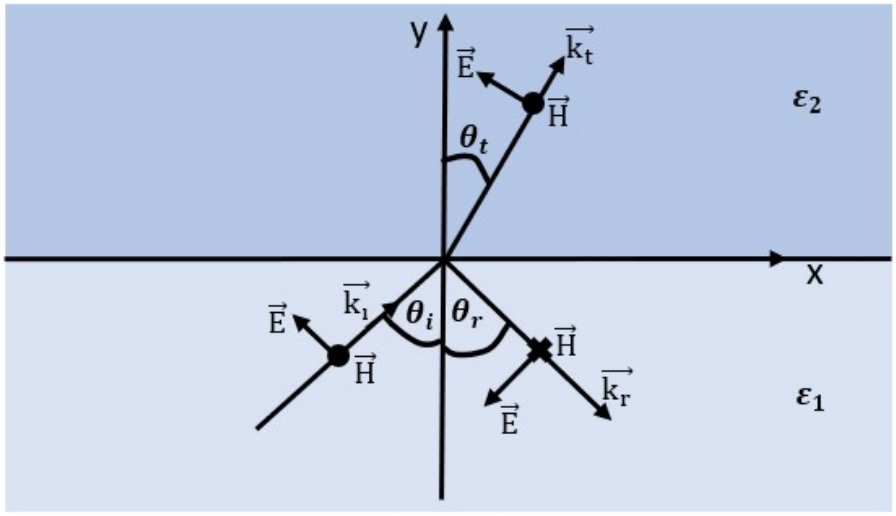

Figure 2.3: A plane electromagnetic wave is propagating through the two media of dielectric constant ε_1 and ε_2, respectively. For TM-polarization, the direction of magnetic field is into the page, $\mathbf{H} = H_y\hat{y}$

and

$$\frac{k_{iz}}{\varepsilon_1}H_i + \frac{k_{rz}}{\varepsilon_1}H_r = \frac{k_{tz}}{\varepsilon_2}H_t. \tag{2.46}$$

From Eq.2.45 and Eq.2.46, we get

$$\frac{H_r}{H_i} = \frac{\varepsilon_2 k_{iz} - \varepsilon_1 k_{tz}}{\varepsilon_2 k_{iz} + \varepsilon_1 k_{tz}}. \tag{2.47}$$

and

$$r_{TM} = \frac{H_r}{H_i}. \tag{2.48}$$

Here, r_{TM} is called the coefficient of reflection.

$$t_{TM} = \frac{2\varepsilon_2 k_{iz}}{\varepsilon_2 k_{iz} + \varepsilon_1 k_{tz}}. \tag{2.49}$$

and

$$t_{TM} = \frac{H_t}{H_i}. \tag{2.50}$$

Here, t_{TM} is called coefficient of transmission.

2.4 Fresnel's Equations

We assume that θ_i is the angle of incidence, θ_r is the angle of reflection, and θ_t is the angle of transmission. From Fig.2.2, the components of k-vector yields

$$k_{ix} = k_{rx} = k_{tx},$$

$$k_{ix} = k_i \sin\theta_i = \frac{\omega}{c} n_1 \sin\theta_i. \tag{2.51}$$

$$k_{iz} = k_i \cos\theta = \frac{\omega}{c} n_1 \cos\theta_i. \tag{2.52}$$

$$k_{rz} = -k_{iz} = -\frac{\omega}{c} n_1 \cos\theta_i. \tag{2.53}$$

The transmitted k-vector has two components, k_{tz} and k_{tx}.The component of k-vector k_{tz} is found by using Pythagorean theorem.

$$\begin{aligned} k_t^2 &= k_{tz}^2 + k_{tx}^2, \\ k_{tz} &= \sqrt{k_z^2 - k_{tx}^2}, \\ &= \sqrt{(\frac{\omega}{c} n_2)^2 - (\frac{\omega}{c} n_1)^2 \sin^2\theta_i}, \\ &= \frac{\omega}{c}\sqrt{n_2^2 - n_1^2 \sin^2\theta_i}. \end{aligned} \tag{2.54}$$

From Snell's law

$$n_1 \sin\theta_i = n_2 \sin\theta_t. \tag{2.55}$$

From Eq.2.54 and Eq.2.55

$$\begin{aligned} k_{tz} &= \frac{\omega}{c}\sqrt{n_2^2 - n_2^2 \sin^2\theta_t}, \\ k_{tz} &= \frac{\omega}{c} n_2 \cos\theta_t. \end{aligned} \tag{2.56}$$

By substituting the values of k_{ix}, k_{iz}, k_{rz}, and k_{tz} in Eq.2.41, Eq.2.43, Eq.2.47, and Eq.2.49, and taking the the values of $\mu_1 = \mu_2 = 1$, and $n = \sqrt{\varepsilon}$ yields

$$r_{TE} = \frac{n_1 \cos\theta_i - \sqrt{n_2^2 - n_1^2 \sin^2\theta_i}}{n_1 \cos\theta_i + \sqrt{n_2^2 - n_1^2 \sin^2\theta_i}}. \tag{2.57}$$

$$t_{TE} = \frac{2n_1 \cos\theta_i}{n_1 \cos\theta_i + \sqrt{n_2^2 - n_1^2 \sin^2\theta_i}}. \tag{2.58}$$

$$r_{TM} = \frac{n_2^2 \cos\theta_i - n_1\sqrt{n_2^2 - n_1^2 \sin\theta_i}}{n_2^2 \cos\theta_i + n_1\sqrt{n_2^2 - n_1^2 \sin\theta_i}}. \tag{2.59}$$

$$t_{TM} = \frac{2n_2^2 \cos\theta_i}{n_2^2 \cos\theta_i + n_1\sqrt{n_2^2 - n_1^2 \sin\theta_i}}. \tag{2.60}$$

This set of equations is called Fresnel's law. The coefficient of reflection and transmission for typical air-glass interface are shown in Fig.2.4 and Fig.2.5. The red line represents the TE-polarization and blue line represents the TM-polarization. For TM-polarization, the reflection becomes zero for the particular angle of incidence. This angle is called *Brewster angle*,θ_B.

$$\theta_B = \arctan\left(\frac{n_2}{n_1}\right). \tag{2.61}$$

For glass of index 1.5, we have external reflection from air to glass and $\theta_B = 56.31^\circ$. For internal

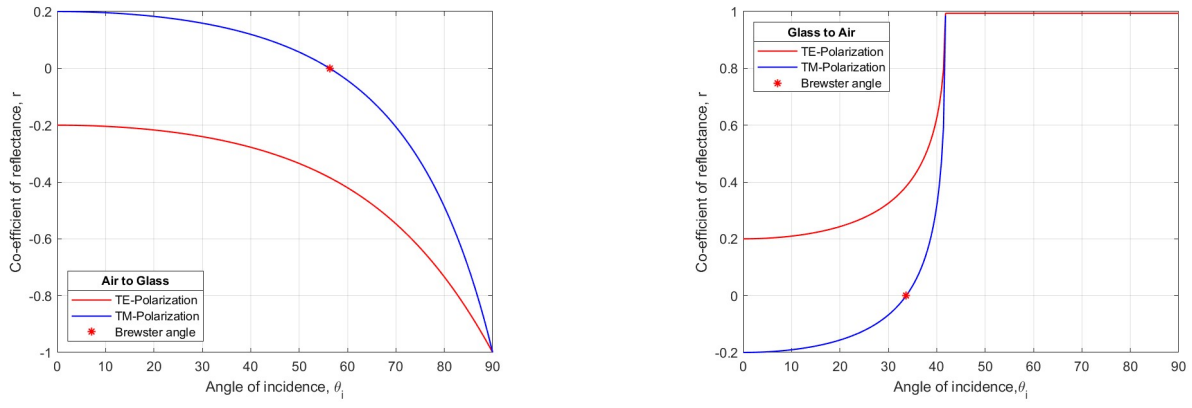

(a) (b)

Figure 2.4: The coefficient of reflection, (a) for air to glass and (b) for glass to air materials.

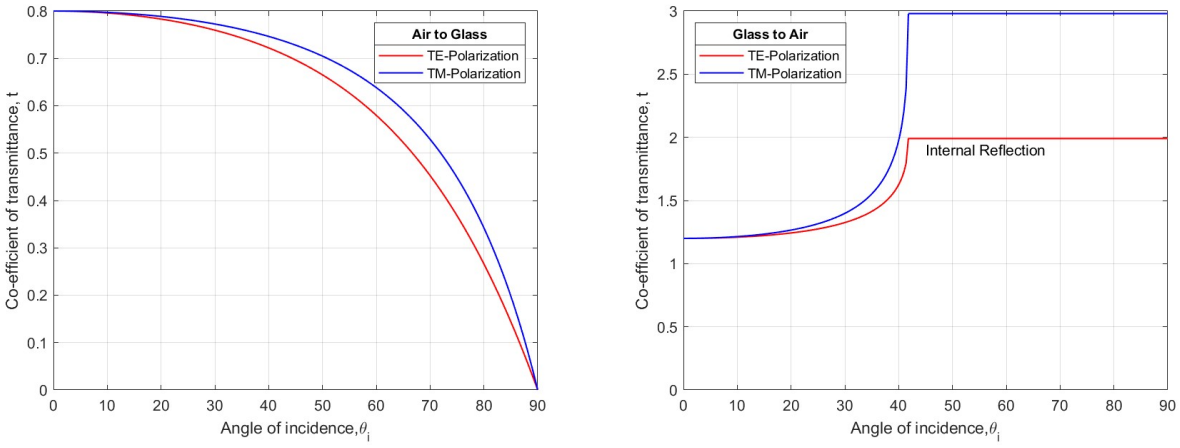

(a) (b)

Figure 2.5: The coefficient of transmittance, (a) for air to glass and (b) for glass to air materials.

reflection, from glass to air, $\theta_B = 33.69°$. The *Brewster angle* for TM-polarization is shown in Fig.2.4a and Fig.2.4b. The critical angle for glass to air medium is $41.81°$ as show in Fig.2.4b and Fig.2.5b.

Total Internal Reflection

For total internal reflection, let us consider two cases- $n_2 \geq n_1$ and $n_2 < n_1$.

In the case of $n_2 \geq n_1$, it is called external reflection. From Eq.2.54

$$k_{tz} = \frac{\omega}{c}\sqrt{n_2^2 - n_1^2 \sin^2\theta_i},$$
$$k_{tz} > 0. \tag{2.62}$$

k_{tz} is always positive, real.

In the case of $n_1 \geq n_2$, it is called internal reflection.

k_{tz} is real if $\theta_i \in [0, \theta_{max}]$

$$n_2^2 = n_1^2 \sin^2\theta_{cr},$$
$$\sin\theta_{max} = \frac{n_2}{n_1}. \tag{2.63}$$

Here, the maximum angle, θ_{max} is called the critical angle θ_{cr}. We will find total internal reflection if the angle of incidence is equal to or greater than the critical angle.

For $\theta_i > \theta_{cr}$

$$\begin{aligned} k_{tz} &= -i\beta, \\ \beta &= \frac{\omega}{c}\sqrt{n_1^2 \sin^2\theta_i - n_2^2}. \end{aligned} \tag{2.64}$$

Here, β is real.

Now

$$\begin{aligned} k_t^2 &= k_{tz}^2 + k_{tx}^2, \\ k_t^2 &= k_{ix}^2 - \beta^2, \\ \beta^2 &= k_i^2 - k_{iz}^2 - k_t^2, \\ \beta &= \sqrt{\frac{\omega^2}{c^2}(n_1^2 - n_2^2) - k_{iz}^2}. \end{aligned} \tag{2.65}$$

If $\mu_1 = \mu_2 = 1$, the coefficient of reflection is written as

$$\begin{aligned} \frac{E_r}{E_i} &= \frac{k_{iz} - k_{tz}}{k_{iz} + k_{tz}}, \\ \frac{E_r}{E_i} &= \frac{k_{iz} + i\beta}{k_{iz} - i\beta}, \\ E_r &= E_i e^{2i\phi}, \end{aligned} \tag{2.66}$$

where $e^{-2i\phi}$ is the phase factor. The phase angle is given by

$$\tan\phi = \frac{\beta}{k_{iz}}. \tag{2.67}$$

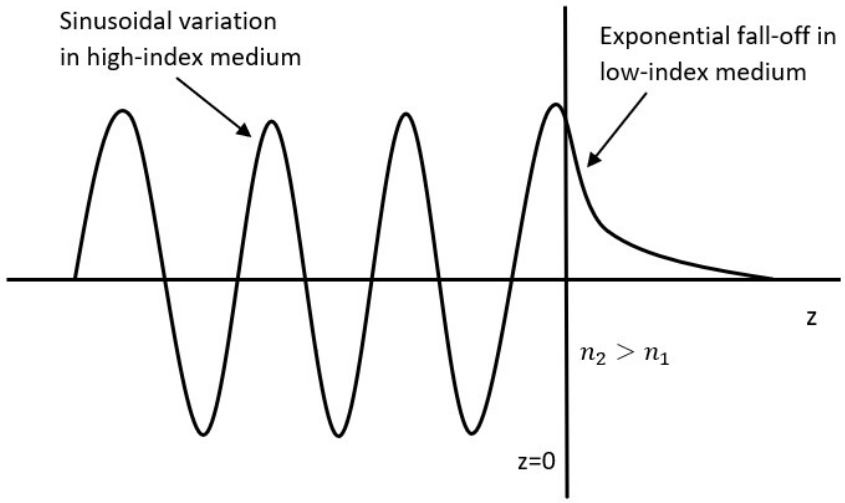

Figure 2.6: Amplitude of the electric field corresponding to TE wave undergoing total internal reflection at the a dielectric boundary.

Inserting the values of k_{iz} from Eq.2.52 and β from Eq.2.64 in Eq.2.67 yields

$$\begin{aligned}\tan\phi &= \frac{\frac{\omega}{c}\sqrt{n_1^2\sin^2\theta_i - n_2^2}}{\frac{\omega}{c}n_1\cos\theta_i},\\ &= \frac{n_2}{n_1}\sqrt{\frac{\tan^2\theta_i}{\tan^2\theta_{cr}} - 1}. \end{aligned} \tag{2.68}$$

Now, the total field in the first medium is

$$\begin{aligned} E_1 + E_2 &= E_i e^{i(\omega t - \mathbf{k}_i\cdot\mathbf{r})} + E_r e^{i(\omega t - \mathbf{k}_r\cdot\mathbf{r})},\\ &= E_i e^{i(\omega t - \mathbf{k}_i\cdot\mathbf{r})} + E_i e^{2i\phi} e^{i(\omega t - \mathbf{k}_r\cdot\mathbf{r})},\\ &= \left[e^{ik_{iz}z} + e^{2i\phi}e^{-ik_{iz}z}\right] E_i e^{i(\omega t - k_{ix}x)},\\ &= E_i e^{i(\omega t - k_{ix}x)} e^{i\phi}\left[e^{-i\phi}e^{ik_{iz}z} + e^{i\phi}e^{-ik_{iz}z}\right],\\ &= E_i e^{i(\omega t - k_{ix}x + \phi)} 2\cos(k_{iz}z + \phi),\\ E_1 + E_2 &= 2E_i e^{i\phi}\cos(k_{iz}z + \phi) e^{i(\omega t - k_{ix}x)}. \end{aligned} \tag{2.69}$$

The phase factor $e^{i\phi}$ can be absorbed in the field amplitude E_i. So, the total field in the high-index material $(z \leq 0)$ is

$$E_{tot} = 2E_i \cos(k_{iz}z + \phi)e^{i(\omega t - k_{ix}x)}. \tag{2.70}$$

In the low-index medium $(z > 0)$ the field decays exponentially in the z-direction

$$E_3 = 2E_i \cos(\phi)e^{i(\omega t - k_{ix}x)}e^{-\beta z}. \tag{2.71}$$

Eq.2.70 and Eq.2.71 are equation of fields for a single boundary at separation $z = 0$. Applying boundary condition at the dielectric boundary at $z = 0$

$$\begin{aligned}
&\frac{\partial E_{tot}}{\partial z}|_{z=0} = \frac{\partial E_3}{\partial z}|_{z=0}. \\
&2E_i(-\sin\phi)k_z e^{i(\omega t - k_{ix}x)} = 2E_i \cos\phi(-\beta)e^{i(\omega t - k_{ix}x)}. \\
&\tan\phi = \frac{\beta}{k_{iz}}.
\end{aligned} \tag{2.72}$$

The Eq.2.72 is equal to the Eq.2.67. In other words,

$$\frac{\partial E_{tot}}{\partial z}|_{z=0} = \frac{\partial E_1}{\partial z}|_{z=0}. \tag{2.73}$$

Which means the field is continuous at the dielectric boundary.

CHAPTER III

PHOTONIC CRYSTALS

3.1 Periodic Dielectric Structures

The fundamental concept of a periodic crystalline structure is described by the *Bravais* lattice. A Bravais lattice is an infinite discrete points of array arranged periodically in space and looks the same from whichever of the points the array is viewed. A *Bravais* lattice is a set of discrete points of the array in which repeated units of crystals are arranged periodically in space [26]. The repeated units can be single atoms, a group of atoms, molecules, ions, etc. A Bravais lattice in two dimension can be written as

$$\mathbf{R} = l\mathbf{a}_1 + m\mathbf{a}_2. \tag{3.1}$$

where *l,m,* and *n* are constants and $\mathbf{a}_1$ and $\mathbf{a}_2$ are *primitive lattice vectors*. The lattice vector $\mathbf{R}$ is also called a *translation vector*. For any given Bravais lattice, the set of primitive vectors is not

Figure 3.1: Primitive lattice vectors for (a) square and (b) oblique lattice in two dimension.

unique. Because there are infinitely many choices of pairs of primitive vectors, all of those do not make a periodic crystal structure.

3.2 Primitive Unit Cell

A volume of space filled up by the translation vector in a Bravais lattice without either overlapping itself or leaving a void is called a primitive unit cell of a lattice. The *unit cell* is any region of space filled up by the translation operation of every *lattice vectors*. A *primitive unit cell* is a minimum-volume unit cell. The number of points (atoms) in a lattice is always the same for a given crystal. A primitive cell always has one lattice point per unit cell. There is no unique way of choosing a primitive unit cell for a given Bravais lattice. There are many ways to choose a *primitive unit cell* for a given lattice.

The primitive unit cell has disadvantages since it does not show the complete symmetry of the Bravais lattice. This problem can be solved in two ways, such as using *unit cells* (or *conventional unit cells*) and *Wigner-Seitz unit cells*, Fig.3.2. A unit cell (or conventional unit cell) is a region of space filled up without overlapping by the translation of a subset of vectors of the Bravais lattice. Typically, the conventional unit cell is chosen to be bigger than the primitive cells and has the

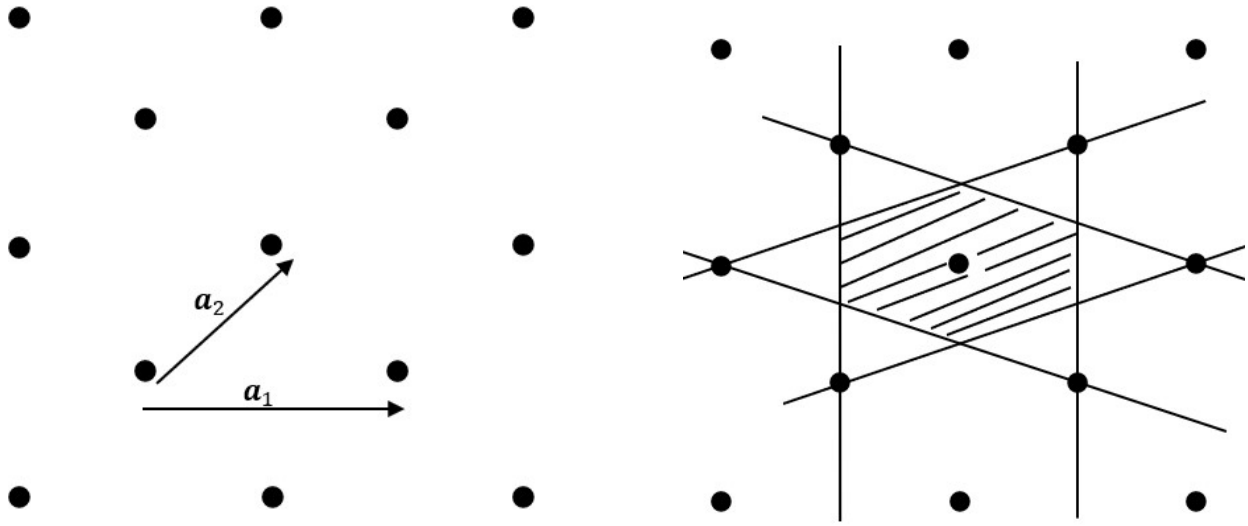

(a) Triangular lattice (b) Wigner-Seitz cell

Figure 3.2: (a) Two-dimensional triangular lattice with primitive vectors $\mathbf{a}_1$ and $\mathbf{a}_2$ (b) Wigner-Seitz primitive unit cell.

required symmetry. Another way of choosing a primitive cell with complete symmetry of the Bravais lattice is *Wigner-Seitz* unit cells. Wigner-Seitz cell is a region of space translated through

all lattice vectors without overlapping. The six sides of the cells construct the Wigner-Seitz unit cell and bisect the lines joining the central points to its six nearest neighboring points.

3.3 Reciprocal Lattice

Let us consider a set of points **R** constituting a *Bravais* lattice and a plane wave $e^{i\mathbf{k}\cdot\mathbf{r}}$. The set of all wave vectors **G** that yield plane waves with the periodicity of a given **Bravais** lattice is known as its *reciprocal lattice*. In three-dimensional photonic crystals, the dielectric constant can be written as

$$\varepsilon(\mathbf{r}) = \sum_{G} \varepsilon(\mathbf{G}) e^{i\mathbf{G}\cdot\mathbf{r}}. \tag{3.2}$$

Where **G** is an infinite set of vectors in *k-space* that defines the frequencies contributing to the plane wave expansion. Since the photonic crystal is periodic, Eq.3.2 must satisfy the following equation for all **r**, and for all **R**

$$\varepsilon(\mathbf{r}+\mathbf{R}) = \sum_{G} \varepsilon(\mathbf{G}) e^{i\mathbf{G}\cdot\mathbf{r}} e^{i\mathbf{G}\cdot\mathbf{R}} = \varepsilon(\mathbf{r}). \tag{3.3}$$

This implies that $e^{i\mathbf{G}\cdot\mathbf{R}} = 1$, and therefore $\mathbf{G}\cdot\mathbf{R} = 2\pi n$, where m is an integer. We assume the lattice vector, **R**

$$\mathbf{R} = n_1\mathbf{a}_1 + n_2\mathbf{a}_2 + n_3\mathbf{a}_3. \tag{3.4}$$

where n_1, n_2, and n_3 are integers. The Eq.3.3 can be satisfied by the following relation

$$\mathbf{G} = m_1\mathbf{b}_1 + m_2\mathbf{b}_2 + m_3\mathbf{b}_3. \tag{3.5}$$

where m_1, m_2, and m_3 are integers. The fundamental vectors **b** and **a** must satisfy the relation

$$\mathbf{b}_i \cdot \mathbf{a}_j = 2\pi\delta_{ij}. \tag{3.6}$$

where δ_{ij} is *Kronecker* delta

$$\delta_{ij} = 0, \qquad i \neq j,$$
$$\delta_{ij} = 1, \qquad i = j. \tag{3.7}$$

The vectors **b** that satisfy the relation

$$\mathbf{b}_1 = 2\pi \frac{\mathbf{a}_2 \times \mathbf{a}_3}{\mathbf{a}_1 \cdot (\mathbf{a}_2 \times \mathbf{a}_3)},$$
$$\mathbf{b}_2 = 2\pi \frac{\mathbf{a}_3 \times \mathbf{a}_1}{\mathbf{a}_1 \cdot (\mathbf{a}_2 \times \mathbf{a}_3)}, \tag{3.8}$$
$$\mathbf{b}_3 = 2\pi \frac{\mathbf{a}_1 \times \mathbf{a}_2}{\mathbf{a}_1 \cdot (\mathbf{a}_2 \times \mathbf{a}_3)}.$$

This set of equations of **b** is called the *reciprocal lattice* vectors in *k-space*. The volume of the reciprocal lattice is $\frac{2\pi}{V^3}$. The vectors **G** are called the reciprocal lattice vectors in *k-space* that contribute to the Fourier expansion in periodic dielectric structures.

Every lattice in real space has a corresponding lattice reciprocal space (or *k-space*). From Eq.3.8, we can make the few assumptions: The reciprocal lattice of the simple cubic (SC) real-space lattice is a simple cubic in *k-space*, the reciprocal of body-centered-cubic (BCC) real-space lattice is a face-centered-cubic (FCC) lattice in *k-space*, and the reciprocal lattice of face-centered-cubic real-space is a face-centered-cubic lattice in *k-space*.

Let us consider a square lattice of lattice vectors $\mathbf{a}_1 = a\hat{\mathbf{x}}$, $\mathbf{a}_2 = a\hat{\mathbf{y}}$, and arbitrary length in the $\hat{\mathbf{z}}$-direction, since the crystal is homogeneous along this direction. The corresponding reciprocal lattice of square lattice is found by using Eq.3.8 in two-dimension as

$$\mathbf{b}_1 = \frac{2\pi}{a}\hat{\mathbf{x}}, \tag{3.9}$$
$$\mathbf{b}_2 = \frac{2\pi}{a}\hat{\mathbf{y}}. \tag{3.10}$$

The reciprocal lattice is also a square lattice, but spacing $2\pi/a$ instead of a.

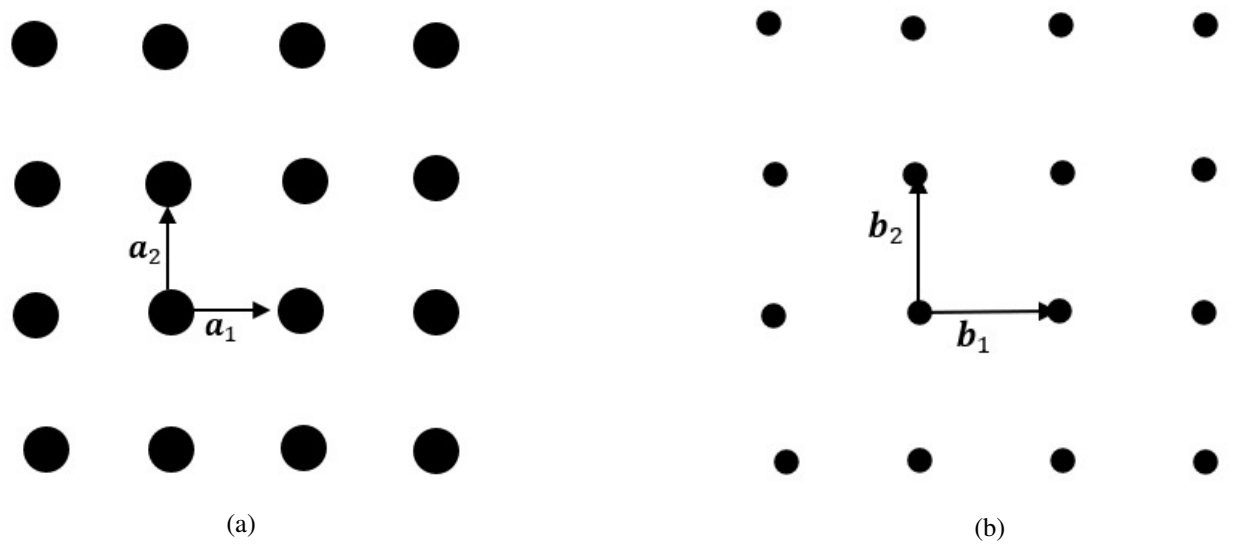

(a) (b)

Figure 3.3: (a) The square lattice in real space. Here $\mathbf{a}_1$ and $\mathbf{a}_2$ are lattice vector in real space (b) Reciprocal lattice of square lattice in reciprocal space. Here $\mathbf{b}_1$ and $\mathbf{b}_2$ are lattice vectors in reciprocal space.

3.4 Brillouin Zone

The Wigner-Seitz primitive cell in a reciprocal lattice is known as the Brillouin zone. The Brillouin zone gives a geometrical interpretation of the diffraction condition in the crystal structure. If $\mathbf{k}$ is the wave vector and $\mathbf{G}$ is the reciprocal lattice vector of a lattice, then the Bragg diffraction condition is given by

$$\begin{aligned} 2\mathbf{k}\cdot\mathbf{G} &= G^2, \\ \mathbf{k}\cdot\left(\frac{1}{2}\mathbf{G}\right) &= \left(\frac{1}{2}G\right)^2. \end{aligned} \tag{3.11}$$

The Brillouin zone is constructed in reciprocal space, the space of $\mathbf{k}$'s and $\mathbf{G}$'s. At first, we select a reciprocal lattice vector $\mathbf{G}$ from the origin to a reciprocal lattice point. Then we construct a plane perpendicular bisector of the reciprocal vector $\mathbf{G}$. This plane gives a part of the Brillouin zone boundary. In Fig.3.4, the reciprocal lattice vector G_C connects the point OC; and G_D connects the OD. Two perpendicular planes AB and $A'B'$ are perpendicular bisectors of G_D and G_C, respectively. Any vector from the origin of reciprocal lattice vector to the plane AB will satisfy the diffraction

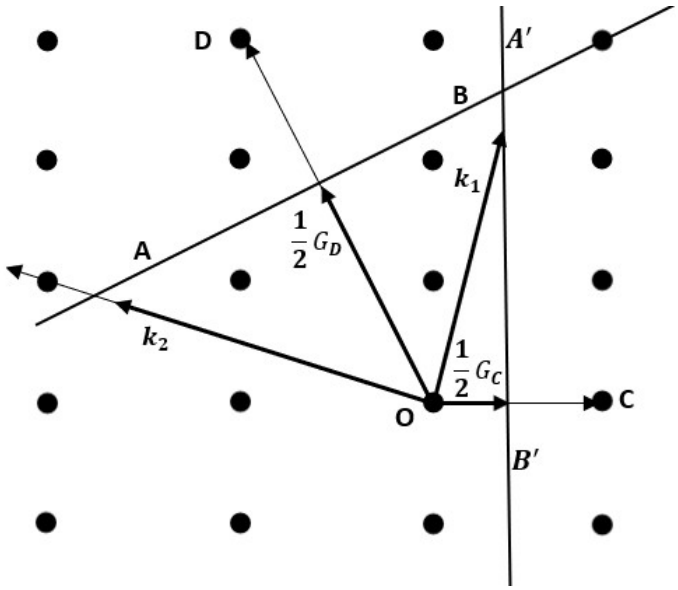

Figure 3.4: The reciprocal lattice points near the origin O of the reciprocal lattice. The reciprocal lattice vector G_C connects OC and G_D connects OD. The plane AB and $A'B'$ are perpendicular bisectors of the reciprocal lattice vectors OC and OD. These two planes form a part of the Brillouin zone.

condition $\mathbf{k}_2 \cdot (\frac{1}{2}\mathbf{G}_D) = (\frac{1}{2}G_D)^2$. Similarly, any vector from the origin to the plane $A'B'$ will satisfy the diffraction condition $\mathbf{k}_1 \cdot (\frac{1}{2}\mathbf{G}_D) = (\frac{1}{2}G_D)^2$.

The square reciprocal lattice with reciprocal lattice vectors is shown in the bold black lines in Fig.3.4. We take the perpendicular bisectors of the line joining the origin of the reciprocal lattice to the nearest reciprocal lattice points. The lines AB, BC, CD, and DA in the central square are the perpendicular bisectors of the reciprocal lattice vectors that form a Brillouin zone. This zone is called the *first Brillouin zone* in the reciprocal lattice. The first Brillouin zone is the smallest volume entirely enclosed by planes perpendicular bisectors of the reciprocal lattice vectors drawn from the origin, as shown in Fig.3.5.

We can construct a *Wigner-Seitz* unit cell in *k-space*. This cell has special significance, and the Wigner-Seitz cell in reciprocal space is known as the first *Brillouin zone* (FBZ). Due to the periodicity of the crystals, all points in *k-space* are equivalent to the points within the FBZ, which differ by a reciprocal lattice vector. Conventionally, specific high-symmetry directions associated with each lattice are labeled by Greek letters $\Gamma, X, M, K, etc.$, as shown in Fig.3.5. These points

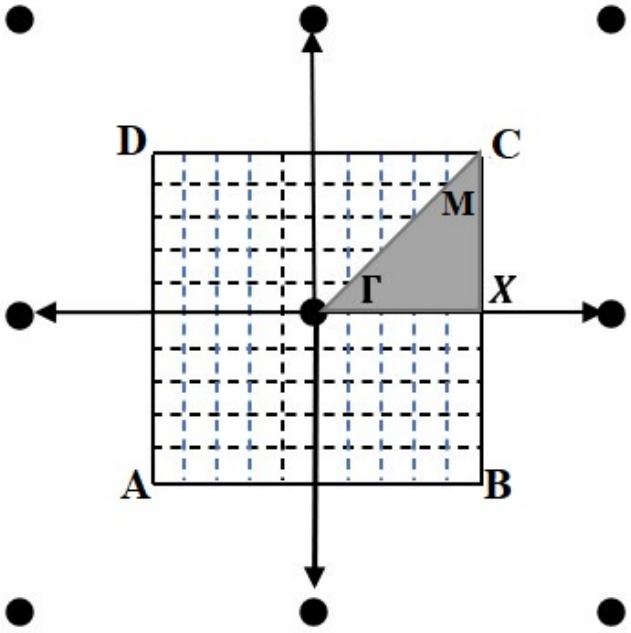

Figure 3.5: Two dimensional square reciprocal lattice with reciprocal lattice vectors. The lines AB, BC, CD, and DA are the perpendicular bisector of the reciprocal lattice vectors and form *first Brillouin zone*. Higher-symmetry directions associated with lattice in k-space is represented by Γ, X, M, and K. Here Γ is the origin of the k-space.

represent the *k-vectors* corresponding to the point on the surfaces of FBZs in particular directions. Here Γ is the center of the k-space. In Fig.3.5, the triangular gray region $\Gamma - X - M - \Gamma$ is called the irreducible Brillouin zone (IBZ).

3.5 Master Equation for Photonic Crystals

Let us assume the dielectric function,$\varepsilon_r(\mathbf{r})$ is invariant under translational symmetry and $\varepsilon_r(\mathbf{r}) = \varepsilon_r(\mathbf{r}+\mathbf{R})$, $\mathbf{R}$ is any vector. For most dielectric materials relative magnetic permeability, μ_r is close to unity and $\mu(\mathbf{r}) = \mu_0\mu_r(\mathbf{r}) = \mu_0$. The propagation of electromagnetic wave through a periodic dielectric crystals is described by Maxwell's equations.

$$\nabla \cdot [\varepsilon_r(\mathbf{r})\mathbf{E}(\mathbf{r},t)] = 0. \tag{3.12a}$$

$$\nabla \cdot \mathbf{H}(\mathbf{r},t) = 0. \tag{3.12b}$$

$$\nabla \times \mathbf{E}(\mathbf{r},t) = -\mu_0 \frac{\partial \mathbf{H}(\mathbf{r},t)}{\partial t}. \tag{3.12c}$$

$$\nabla \times \mathbf{H}(\mathbf{r},t) = \varepsilon_0\varepsilon_r(\mathbf{r}) \frac{\partial \mathbf{E}(\mathbf{r},t)}{\partial t}. \tag{3.12d}$$

Let us consider the modes or state of the photonic crystals are

$$\mathbf{E}(\mathbf{r},t) = \mathbf{E}(\mathbf{r})e^{-i\omega t}. \tag{3.13a}$$

$$\mathbf{H}(\mathbf{r},t) = \mathbf{H}(\mathbf{r})e^{-i\omega t}. \tag{3.13b}$$

Inserting Eq.3.13a in Eq.3.12a and Eq.3.13b in Eq.3.12b the divergence equations gives the conditions

$$\nabla \cdot [\varepsilon_r(\mathbf{r})\mathbf{E}(\mathbf{r})] = 0. \tag{3.14a}$$

$$\nabla \cdot \mathbf{H}(\mathbf{r}) = 0. \tag{3.14b}$$

Inserting Eq.3.13a in Eq.3.12c and Eq.3.13b in Eq.3.12d, two curl equations becomes

$$\nabla \times \mathbf{E}(\mathbf{r}) = i\omega\mu_0\mathbf{H}(\mathbf{r}). \tag{3.15a}$$

$$\nabla \times \mathbf{H}(\mathbf{r}) = -i\omega\varepsilon_0\varepsilon_r(\mathbf{r})\mathbf{E}(\mathbf{r}). \tag{3.15b}$$

Taking curl in both side of Eq.3.15a and using the value of Eq.3.15b to eliminate $\mathbf{H}(\mathbf{r})$ yields

$$\nabla \times [\nabla \times \mathbf{E}(\mathbf{r})] = \omega^2 \mu_0 \varepsilon(\mathbf{r}) \mathbf{E}(\mathbf{r}). \tag{3.16}$$

Again taking the curl in both side of Eq.3.15b and using the value of Eq.3.15a to eliminate $\mathbf{E}(\mathbf{r})$, we get

$$\nabla \times \left[\frac{1}{\varepsilon_r(\mathbf{r})} \nabla \times \mathbf{H}(\mathbf{r}) \right] = \left(\frac{\omega}{c} \right)^2 \mathbf{H}(\mathbf{r}). \tag{3.17}$$

This equation is called the Master equation for photonic crystals. Here $c = \frac{1}{\sqrt{\varepsilon_0 \mu_0}}$.

Using the value of $\mathbf{H}(\mathbf{r})$ in Eq.3.15b, we find the mode $\mathbf{E}(\mathbf{r})$

$$\mathbf{E}(\mathbf{r}) = \frac{i}{\omega \varepsilon_0 \varepsilon_r(\mathbf{r})} \nabla \times \mathbf{H}(\mathbf{r}). \tag{3.18}$$

Eq.3.18 gives the $\mathbf{E}$-mode in terms of magnetic field.

The Eq.3.17 is the eigenvalue equation and $\mathbf{H}(\mathbf{r})$ is the eigenfunction. The term $\nabla \times \frac{1}{\varepsilon_r(\mathbf{r})} \nabla$ is an operator, called Hermitian operator which have real eigenvalues. The multiplicative term of $\mathbf{H}(\mathbf{r})$ on the right-hand side of the Eq.3.17 is called the eigenvalue.

CHAPTER IV

FINITE-DIFFERENCE TIME-DOMAIN MODEL

4.1 Maxwell's Equations in Two Dimensions

In linear, isotropic, and nondispersive materials, four Maxwell's equation from Chapter.II can be written as

$$\nabla \cdot \mathbf{D} = 0. \tag{4.1a}$$

$$\nabla \cdot \mathbf{B} = 0. \tag{4.1b}$$

$$\nabla \times \mathbf{E} = -\frac{\partial \mathbf{B}}{\partial t}. \tag{4.1c}$$

$$\nabla \times \mathbf{H} = \frac{\partial \mathbf{D}}{\partial t}. \tag{4.1d}$$

We assumed that the current density, $\mathbf{J} = 0$ and charge density in free space, $\rho = 0$.

We assume the electric field- $\mathbf{E}$ and magnetic field - $\mathbf{H}$ are

$$\mathbf{E} = \mathbf{E}(x, y, z, t). \tag{4.2a}$$

$$\mathbf{H} = \mathbf{H}(x, y, z, t). \tag{4.2b}$$

The $\mathbf{E}$- field and $\mathbf{H}$- field is in the xy-plane and they do not depend on z- axis. From Eq.4.1c, we get,

$$\frac{\partial \mathbf{H}}{\partial t} = -\frac{1}{\mu} \nabla \times \mathbf{E}. \tag{4.3}$$

and from Eq.4.1d

$$\frac{\partial \mathbf{E}}{\partial t} = \frac{1}{\varepsilon} \nabla \times \mathbf{H}. \tag{4.4}$$

Let us consider that the wave is confined in xy- plane then the partial derivative with respect z component is zero. Separating **H**-field in x, and y- components

$$\frac{\partial H_x}{\partial t} = -\frac{1}{\mu}\frac{\partial E_z}{\partial y}. \tag{4.5a}$$

$$\frac{\partial H_y}{\partial t} = \frac{1}{\mu}\frac{\partial E_z}{\partial x}. \tag{4.5b}$$

$$\frac{\partial H_z}{\partial t} = \frac{1}{\mu}\left(\frac{\partial E_y}{\partial x} - \frac{\partial E_x}{\partial y}\right). \tag{4.5c}$$

Similarly, separating **E**-field into x and y-components

$$\frac{\partial E_x}{\partial t} = \frac{1}{\varepsilon}\frac{\partial H_z}{\partial y}. \tag{4.6a}$$

$$\frac{\partial E_y}{\partial t} = -\frac{1}{\varepsilon}\frac{\partial H_z}{\partial x}. \tag{4.6b}$$

$$\frac{\partial E_z}{\partial t} = \frac{1}{\varepsilon}\left(\frac{\partial H_y}{\partial x} - \frac{\partial H_x}{\partial y}\right). \tag{4.6c}$$

The electric field is in z-direction, $\mathbf{E} = E_z\hat{z}$.Then, the magnetic field, $\mathbf{H} = H_x\hat{x} + H_y\hat{y}$. The components of H_x, H_y, and E_z are

$$\frac{\partial H_x}{\partial t} = -\frac{1}{\mu}\frac{\partial E_z}{\partial y}. \tag{4.7a}$$

$$\frac{\partial H_y}{\partial t} = \frac{1}{\mu}\frac{\partial E_z}{\partial x}. \tag{4.7b}$$

$$\frac{\partial E_z}{\partial t} = \frac{1}{\varepsilon}\left(\frac{\partial H_y}{\partial x} - \frac{\partial H_x}{\partial y}\right). \tag{4.7c}$$

The three components, H_x, H_y, and E_z constitute a *transverse magnetic* (TM) mode with respect to z-direction.

Now, the magnetic field **H** is in z-direction, $\mathbf{H} = H_z\hat{z}$. Then, the electric field, $\mathbf{E} = E_x\hat{x} + E_y\hat{y}$. The

components of E_x, E_y, and H_z are

$$\frac{\partial E_x}{\partial t} = \frac{1}{\varepsilon}\frac{\partial H_z}{\partial y}. \tag{4.8a}$$

$$\frac{\partial E_y}{\partial t} = -\frac{1}{\varepsilon}\frac{\partial H_z}{\partial x}. \tag{4.8b}$$

$$\frac{\partial H_z}{\partial t} = \frac{1}{\mu}\left(\frac{\partial E_y}{\partial x} - \frac{\partial E_x}{\partial y}\right). \tag{4.8c}$$

In this case, these three components, E_x, E_y, and H_z constitute a *transverse electric* (TE) mode with respect to the z-direction.

4.2 Yee's Grid

Solving time-dependent Maxwell's is difficult due to the imposition of boundary conditions. In 1966, Kane Yee proposed the finite-difference method to solve time-dependent Maxwell's equation [25]. Yee used the central difference expression for both space and time derivatives and second-order accuracy in the space and time increments. Hence the method is named as finite-difference. The Yee algorithm solves Maxwell's curl equations for the electric and magnetic fields

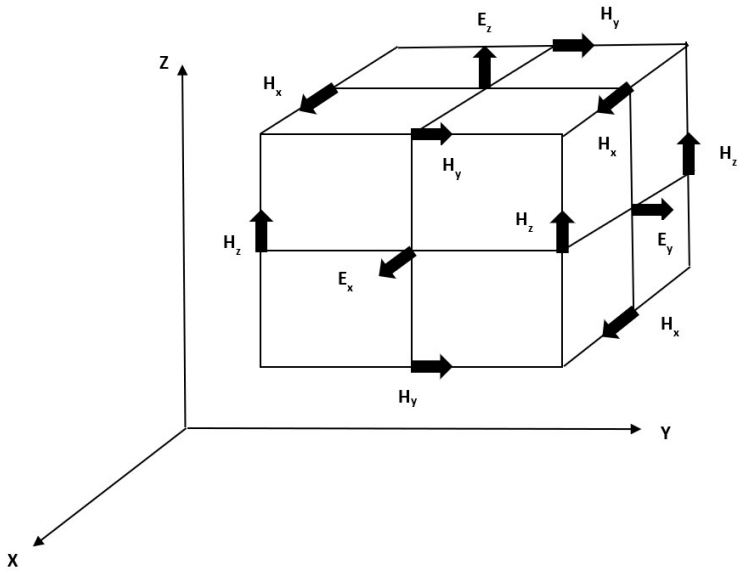

Figure 4.1: The components of **E** field and and **H** field in a cubic unit cell of the Yee's grid. Yee's algorithm centers its components of **E**-field and **H** -field in the cubic unit cell so that the every components of **E**-field is surrounded by the four circulating **H**-field and vice-versa.

in the same time and space rather than solving wave equations alone. In Yee's cubic unit cell, one magnetic field component **H** is surrounded by the four electric field components **E**. Similarly, one component **E**-fields is surrounded by four **H**-field components, as shown in Fig.4.1. The Yee's algorithm centers its components of **E**-field and **H**-field in the three-dimensional space so that every **E** component is surrounded by four circulating **H** components. Every **H** component is surrounded by four circulating **E** components. This circulating **E**-field satisfies Faraday's curl law, and the circulating **H**-field satisfies Ampere's curl law. Another advantage of using the Yee grid is we do not need another set of equations for different materials. The position of **E**-field or **H**-field could be in different unit cells. And this automatically satisfies the boundary conditions for **E**-field and **H**-field

The two-dimensional Yee's grid is shown in Fig.4.2. For TE polarization or $\mathbf{E}_z$-mode, the electric field is in z-direction; it has a circulating magnetic field along the xy-plane. Similarly, for TM polarization or $\mathbf{H}_z$-mode, the magnetic field is in z-direction; it has a circulating electric field in xy-plane.

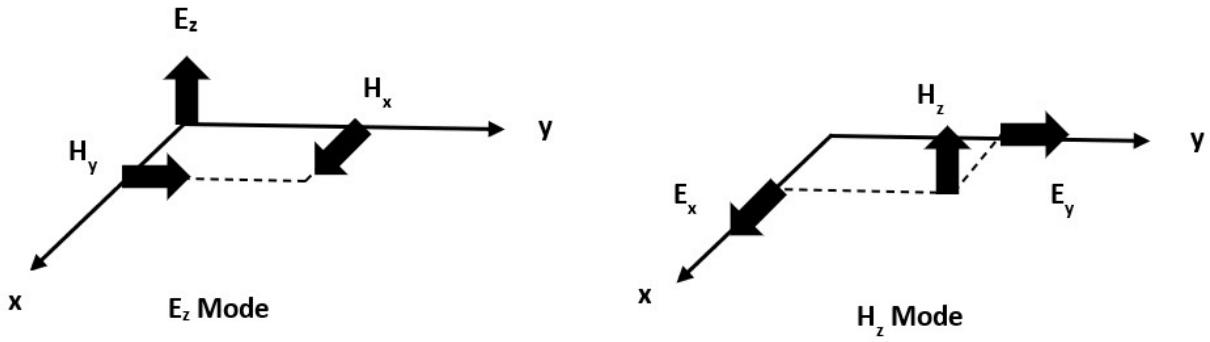

Figure 4.2: Two dimensional Yee's grid. When **E**-field is in z direction, its components are $\mathbf{E}(0,0,E_z)$ and $\mathbf{H}(H_x,H_y,0)$. This is called TE -mode. When **H**-field is in z-direction, its components are $\mathbf{H}(0,0,H_z)$ and $\mathbf{E}(E_x,E_y,0)$. This is called TM-mode.

4.3 The Finite-Difference Expression for Maxwell's Equations

Let us consider a function $u(x,t_n)$, here x is the space point and t_n is the temporal coordinates. For fixed t_n, from the point x to $x+\Delta x$, the Taylor's series expansion of the function $u(x,t_n)$ is written as,

$$u(x_i+\Delta x)|_{t_n} = u|_{x_i,t_n} + \Delta x.\frac{\partial u}{\partial x}|_{x_i,t_n} + \frac{(\Delta x)^2}{2}.\frac{\partial^2 u}{\partial x^2}|_{x_i,t_n} + \frac{(\Delta x)^3}{6}.\frac{\partial^3 u}{\partial x^3}|_{x_i,t_n} + \frac{(\Delta x)^4}{24}.\frac{\partial^4 u}{\partial x^4}|_{\xi_1,t_n}. \quad (4.9)$$

The last term is the remainder term, and ξ_1 is a space point located between x_i and $x+\Delta x$.
Similarly, the Taylor's series in the space point $(x_i-\Delta x)$ at fixed t_n is written as

$$u(x_i-\Delta x)|_{t_n} = u|_{x_i,t_n} - \Delta x.\frac{\partial u}{\partial x}|_{x_i,t_n} + \frac{(\Delta x)^2}{2}.\frac{\partial^2 u}{\partial x^2}|_{x_i,t_n} - \frac{(\Delta x)^3}{6}.\frac{\partial^3 u}{\partial x^3}|_{x_i,t_n} + \frac{(\Delta x)^4}{24}.\frac{\partial^4 u}{\partial x^4}|_{\xi_2,t_n}. \quad (4.10)$$

In the remainder term, ξ_2 is a space point located between x_i and $x-\Delta x$. Subtracting Eq.4.10 from Eq.4.9 and rearranging yield

$$\frac{\partial u}{\partial x}|_{x_i,t_n} = \left[\frac{u(x_i+\Delta x)|_{t_n} - u(x_i-\Delta x)|_{t_n}}{\Delta x}\right]_{t_n} + O[(\Delta x)^2]. \quad (4.11)$$

Where $O[(\Delta x)^2]$ represents the remainder term, which approaches zero as the square of the space increment. The Eq.4.11 is called central-difference approximation to the first-order partial derivative of u and second-order accurate in space and time increments.
Let us represent the space point in a uniform, rectangular lattice as

$$(i,j,k) = (i\Delta x, j\Delta y, k\Delta z). \quad (4.12)$$

Here $\Delta x, \Delta y$, and Δz are the lattice space increments in x, y, and z directions, respectively, and i, j, and k are integers. Further, we denote the function $u(x,t)$ evaluated at a discrete point in the grid

and at a discrete point in time as,

$$u(i\Delta x, j\Delta y, k\Delta z, n\Delta t) = u^n_{i,j,k}. \tag{4.13}$$

Here, Δt is the time increment and n is the integer. Rewriting Eq.4.11 in the x-direction, evaluated at the fixed time, $t_n = n\Delta t$,

$$\frac{\partial u}{\partial x}(i\Delta x, j\Delta y, k\Delta z, n\Delta t) = \frac{u^n_{i+1/2,j,k} - u^n_{i-1/2,j,k}}{\Delta x} + O[(\Delta x)^2]. \tag{4.14}$$

Here we note the $\pm 1/2$ increment in the x-coordinate (i-subscript) of function u, represents the finite-difference over $\pm 1/2\Delta x$. Similarly, the first-order partial derivative of y and z can be found by taking the finite-difference $\pm 1/2\Delta y$, and $\pm 1/2\Delta z$, respectively.

The first-order partial time derivative of the function u, evaluated at the fixed space (i, j, k) is written as according the Eq.4.14 as

$$\frac{\partial u}{\partial t}(i\Delta x, j\Delta y, k\Delta z, n\Delta t) = \frac{u^{n+1/2}_{i,j,k} - u^{n-1/2}_{i,j,k}}{\Delta t} + O[(\Delta t)^2]. \tag{4.15}$$

Here $\pm 1/2$ increment is in the time coordinate (n-superscript) of the function u, denoting a finite-difference in time over $\pm 1/2\Delta t$.

Using Finite-Difference (central-difference) Maxwell's curl equations in one-dimension can be written as

$$\frac{H_x(x,y,t+\frac{\Delta t}{2}) - H_x(x,y,t-\frac{\Delta t}{2})}{\Delta t} = -\frac{1}{\mu}\left(\frac{E_z(x,y+\frac{\Delta y}{2},t) - E_z(x,y-\frac{\Delta y}{2},t)}{\Delta y}\right). \tag{4.16a}$$

$$\frac{H_y(x,y,t+\frac{\Delta t}{2}) - H_y(x,y,t-\frac{\Delta t}{2})}{\Delta t} = \frac{1}{\mu}\left(\frac{E_z(x+\frac{\Delta x}{2},y,t) - E_z(x-\frac{\Delta x}{2},y,t)}{\Delta x}\right). \tag{4.16b}$$

$$\begin{aligned}\frac{E_z(x,y,t+\frac{\Delta t}{2}) - E_z(x,y,t-\frac{\Delta t}{2})}{\Delta t} = &\frac{1}{\varepsilon}\left(\frac{H_y(x+\frac{\Delta x}{2},y,t) - H_y(x-\frac{\Delta x}{2},y,t)}{\Delta x}\right). \\ &-\frac{1}{\varepsilon}\left(\frac{H_x(x,y+\frac{\Delta y}{2},t) - H_x(x,y-\frac{\Delta y}{2},t)}{\Delta y}\right).\end{aligned} \tag{4.16c}$$

At space-step y$\rightarrow y+\frac{\Delta y}{2}$, Eq.4.16a can be written as

$$H_x\left(x,y+\frac{\Delta y}{2},t+\frac{\Delta t}{2}\right)=H_x\left(x,y+\frac{\Delta y}{2},t-\frac{\Delta t}{2}\right)-\frac{\Delta t}{\mu\Delta y}\left[E_z(x,y+\Delta y,t)-E_z(x,y,t)\right]. \tag{4.17}$$

Similarly, for y-component Eq.4.16b becomes

$$H_y\left(x+\frac{\Delta x}{2},y,t+\frac{\Delta t}{2}\right)=H_Y\left(x+\frac{\Delta x}{2},y,t-\frac{\Delta t}{2}\right)+\frac{\Delta t}{\mu\Delta x}\left[E_z(x+\Delta x,y,t)-E_z(x,y,t)\right]. \tag{4.18}$$

From Eq.4.16c

$$\begin{aligned}E_z(x,y,t+\Delta t)=E_z(x,y,t)&+\frac{\Delta t}{\varepsilon\Delta x}\left(H_y(x+\frac{\Delta x}{2},y,t+\frac{\Delta t}{2})-H_y(x-\frac{\Delta x}{2},y,t-\frac{\Delta t}{2})\right)\\&-\frac{\Delta t}{\varepsilon\Delta y}\left(H_x(x,y+\frac{\Delta y}{2},t+\frac{\Delta t}{2})-H_x(x,y-\frac{\Delta y}{2},t-\frac{\Delta t}{2})\right).\end{aligned} \tag{4.19}$$

Now, we introduce new notation

$$\begin{aligned}H_x(x,y+\frac{\Delta y}{2},t+\frac{\Delta t}{2})&\cong\sqrt{\frac{\varepsilon}{\mu}}\tilde{H}_x(x,y,t).\\H_y(x+\frac{\Delta x}{2},y,t+\frac{\Delta t}{2})&\cong\sqrt{\frac{\varepsilon}{\mu}}\tilde{H}_y(x,y,t).\end{aligned} \tag{4.20}$$

Using notation from Eq.4.20 in Eq.4.17, Eq.4.18, and Eq.4.19

$$\sqrt{\frac{\varepsilon}{\mu}}\tilde{H}_x(x,y,t)=\sqrt{\frac{\varepsilon}{\mu}}\tilde{H}_y(x,y,t-\Delta t)-\frac{\Delta t}{\mu\Delta y}\left[E_z(x,y+\Delta y,t)-E_z(x,y,t)\right]. \tag{4.21a}$$

$$\sqrt{\frac{\varepsilon}{\mu}}\tilde{H}_y(x,y,t)=\sqrt{\frac{\varepsilon}{\mu}}\tilde{H}_y(x,y,t-\Delta t)+\frac{\Delta t}{\mu\Delta x}\left[E_z(x+\Delta x,y,t)-E_z(x,y,t)\right]. \tag{4.21b}$$

$$\begin{aligned}E_z(x,y,t+\Delta t)&=E_z(x,y,t)+\frac{\Delta t}{\varepsilon\Delta x}\sqrt{\frac{\varepsilon}{\mu}}\left[\tilde{H}_y(x,y,t)-\tilde{H}_y(x-\Delta x,y,t)\right]\\&-\frac{\Delta t}{\varepsilon\Delta y}\sqrt{\frac{\varepsilon}{\mu}}\left[\tilde{H}_x(x,y,t)-\tilde{H}_x(x,y-\Delta y,t)\right].\end{aligned} \tag{4.21c}$$

by simplifying

$$\tilde{H}_x(x,y,t) = \tilde{H}_y(x,y,t-\Delta t) - \frac{\Delta t}{\sqrt{\varepsilon\mu}\Delta y}\left[E_z(x,y+\Delta y,t) - E_z(x,y,t)\right]. \tag{4.22a}$$

$$\tilde{H}_y(x,y,t) = \tilde{H}_y(x,y,t-\Delta t) + \frac{\Delta t}{\sqrt{\varepsilon\mu}\Delta x}\left[E_z(x+\Delta x,y,t) - E_z(x,y,t)\right]. \tag{4.22b}$$

$$\begin{aligned} E_z(x,y,t+\Delta t) = E_z(x,y,t) &+ \frac{\Delta t}{\sqrt{\varepsilon\mu}\Delta x}\left[\tilde{H}_y(x,y,t) - \tilde{H}_y(x-\Delta x,y,t)\right] \\ &- \frac{\Delta t}{\sqrt{\varepsilon\mu}\Delta y}\left[\tilde{H}_x(x,y,t) - \tilde{H}_x(x,y-\Delta y,t)\right]. \end{aligned} \tag{4.22c}$$

Here $\tilde{H}(x,y,t)$ = H-field at the present time and space

$\tilde{H}(x-\Delta x,y,t)$ = H-field in the previous step

$\tilde{H}(x,y,t-\Delta t)$ = H-field in the past time

$E(x,y,t)$ = E-field at the present time and space

$E(x,y,t+\Delta t)$ = E-field in the updated time

$E(x+\Delta x,y,t)$ = E-field in the updated step or position

and $\frac{\Delta t}{\sqrt{\varepsilon\mu}\Delta y}$ = updated co-efficient.

Let us define $x = i\Delta x$, $y = j\Delta y$, and $\frac{1}{\sqrt{\varepsilon\mu}} = v$ in Eq.4.22

$$\tilde{H}_x(i,j) = \tilde{H}_x(i,j) - \frac{v\Delta t}{\Delta y}\left[E_z(i,j+1) - E_z(i,j)\right]. \tag{4.23a}$$

$$\tilde{H}_y(i,j) = \tilde{H}_y(i,j) + \frac{v\Delta t}{\Delta x}\left[E_z(i+1,j) - E_z(i,j)\right]. \tag{4.23b}$$

$$\begin{aligned} E_z(i,j) = E_z(i,j) &+ \frac{v\Delta t}{\Delta x}\left[\tilde{H}_y(i,j) - \tilde{H}_y(i-1,j)\right]. \\ &- \frac{v\Delta t}{\Delta y}\left[\tilde{H}_x(i,j) - \tilde{H}_x(i,j-1)\right]. \end{aligned} \tag{4.23c}$$

Eq.4.23a, Eq.4.23b, and Eq.4.23c are update equations in time and space. The left-hand side of Eq.4.23a-Eq.4.23c represent the field at the next time step and the first term of the right-hand side represent the field at previous time step, and the second term represents the other field at intermediate time steps. Here $\frac{v\Delta t}{\Delta y}$ and $\frac{v\Delta t}{\Delta x}$ are the update coefficients.

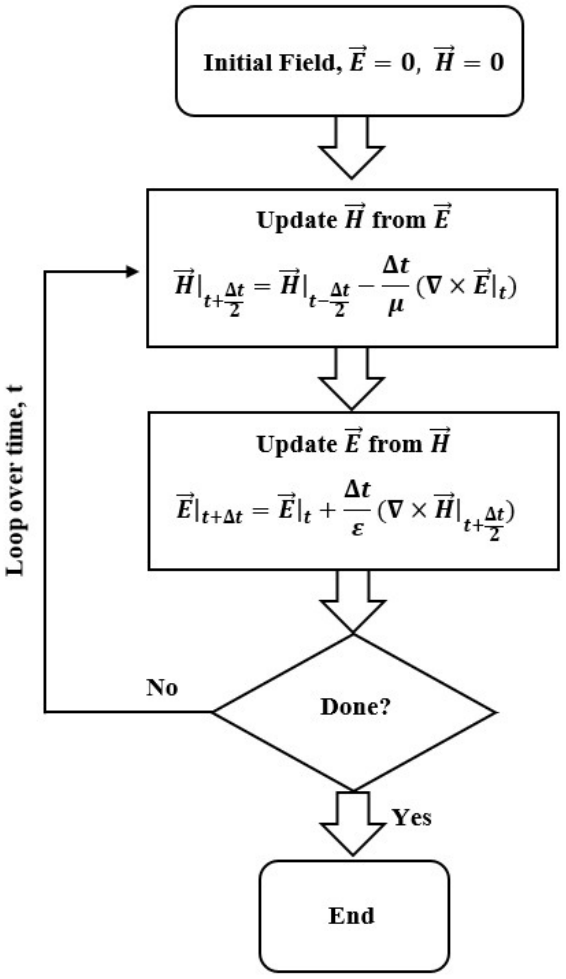

Figure 4.3: The Finite-Difference Time-Domain method flowchart. At first the algorithm is initialized by setting the fields **E**, and **H** are equal to zero. Then, the **H** field is updated from **E**, and vice-versa until the convergence criterion are met.

The finite-difference time-domain method is sometimes called the leapfrog algorithm. Fig.4.3 shows a basic flowchart of the FDTD computational method. The FDTD begins by defining a grid in the computational region and the properties such as permittivity, permeability, and conductivity to each initial field at time step $n = 0$. Then the new values of electric and magnetic fields are calculated. The magnetic field, **H** is calculated from the **E** field by using the updated equation, and update **E** field from the **H**-field until the convergence criteria are met. The calculation ends when the convergence criteria are fulfilled.

4.4 The Perfectly Matched Layer (PML)

The Finite-Difference Time-Domain (FDTD) method is widely used for computing Maxwell's electromagnetic wave equations. One of the inconveniences of the FDTD method is wave equations have to be solved in the discretized domain, and the domain size needs to be finite. Free-space problems can be solved theoretically using special boundary conditions on the computational domain. But the difficulty arises in solving field problems when the scattering field is open, i.e., the computational domain in which the field has to be computed is unbounded. The computer cannot store unlimited data for open boundary calculations. It is necessary to restrain the computational domain in which the field has to be computed. It is done by limiting the mesh grid size, but large enough to contain all the information related to the field and by using boundary conditions outside the mesh grid. These boundary conditions are called Absorbing Boundary Conditions.

Several methods are available for absorbing the outgoing electromagnetic waves in the FDTD method [27, 28, 29, 30]. A new technique, Perfectly Matched Layer (PML), has been widely used for solving free-space outgoing electromagnetic waves [31]. In PML, the layer surrounding boundaries absorbs the outgoing waves towards the boundary without reflection.

Consider a TE electromagnetic plane wave in the xy-plane. The components of an electric field in the x and y-directions are E_x and E_y, respectively. The component of a magnetic field in the z-direction is H_z. Maxwell's equations in a medium having electric conductivity σ, and magnetic conductivity σ^* are written as

$$\varepsilon_0 \frac{\partial E_x}{\partial t} + \sigma E_x = \frac{\partial H_z}{\partial y}. \tag{4.24a}$$

$$\varepsilon_0 \frac{\partial E_y}{\partial t} + \sigma E_y = -\frac{\partial H_z}{\partial x}. \tag{4.24b}$$

$$\mu_0 \frac{\partial H_z}{\partial t} + \sigma^* H_z = \frac{\partial E_x}{\partial y} - \frac{\partial E_y}{\partial x}. \tag{4.24c}$$

Furthermore,

$$\frac{\sigma}{\varepsilon_0} = \frac{\sigma^*}{\mu_0}. \tag{4.25}$$

This is the condition for impedance matching. Suppose the condition (Eq.4.25) is satisfied. In that case, the impedance of the medium (4.24) is equal to the impedance of the vacuum. No reflection will occur if a plane wave propagates across the vacuum-medium interface.

Let us define the PML medium in the case of TE polarization. In PML medium, the z-component of the magnetic field H_z is decomposed into two components such as H_zx and H_zy, and $H_z = H_{zx} + H_{zy}$. PML medium has four components for TE polarization: E_x,E_y H_{zx}, and H_{zy}.

$$\varepsilon_0 \frac{\partial E_x}{\partial t} + \sigma_y E_x = \frac{\partial (H_{zx} + H_{zy})}{\partial y}. \tag{4.26a}$$

$$\varepsilon_0 \frac{\partial E_y}{\partial t} + \sigma_x E_y = -\frac{\partial (H_{zx} + H_{zy})}{\partial x}. \tag{4.26b}$$

$$\mu_0 \frac{\partial H_{zx}}{\partial t} + \sigma_x^* H_{zx} = -\frac{\partial E_y}{\partial x}. \tag{4.26c}$$

$$\mu_0 \frac{\partial H_{zy}}{\partial t} + \sigma_y^* H_{zy} = -\frac{\partial E_x}{\partial y}. \tag{4.26d}$$

where the parameters $(\sigma_x, \sigma_x^*, \sigma_y, \sigma_y^*)$ are homogeneous to electric and magnetic conductivities. From the set of equations in Eq.4.26 it can be said that-

i If $\sigma_x^* = \sigma_y^*$, then Eq.4.26c and Eq.4.26d merge, and Eq.4.26 becomes a set of three equations containing components E_x, E_y, H_{zx}, and H_{zy} only. So, the PML medium holds as particular cases for all media.

ii If $\sigma_x = \sigma_x^* = \sigma_y = \sigma_y^* = 0$, then Eq.4.26 reduces to the Maxwell's equations for vacuum.

iii If $\sigma_x = \sigma_y$ and $\sigma_x^* = \sigma_y^* = 0$, then Eq.4.26 reduces to the Maxwell's equation for conductive medium.

iv if $\sigma_x = \sigma_y$ and $\sigma_x^* = \sigma_y^*$, Eq.4.26 reduces to the equation for absorbing medium.

v If $\sigma_y = \sigma_y^* = 0$, then the PML medium absorbs the plane wave propagating along x-direction, but it does not absorb the waves propagating along y-direction. And if $\sigma_x = \sigma_x^* = 0$, it absorbs waves propagating along y-direction, but it does not absorb waves propagating along x-direction.

Let us consider a plane EM wave makes an angle ϕ with the y-axis and propagating in the PML medium. The components of fields are

$$E_x = -E_0 \sin\phi e^{i\omega(t-\alpha x-\beta y)}. \tag{4.27a}$$

$$E_y = E_0 \cos\phi e^{i\omega(t-\alpha x-\beta y)}. \tag{4.27b}$$

$$H_{zx} = H_{zx0} e^{i\omega(t-\alpha x-\beta y)}. \tag{4.27c}$$

$$H_{zy} = H_{zy0} e^{i\omega(t-\alpha x-\beta y)}. \tag{4.27d}$$

where ω is the angular frequency of the wave, t is the time of propagation, α and β are complex constants. The Eq.4.27 have four unknowns,α,β, H_{zx0}, and H_{zy0}. These unknown can be determined by using PML equations form Eq.4.26.

$$\varepsilon_0 E_0 \sin\phi - i\frac{\sigma_y}{\omega} E_0 \sin\phi = \beta(H_{zx0} + H_{zy0}). \tag{4.28a}$$

$$\varepsilon_0 E_0 \cos\phi - i\frac{\sigma_x}{\omega} E_0 \cos\phi = \alpha(H_{zx0} + H_{zy0}). \tag{4.28b}$$

$$\mu_0 H_{zx0} - i\frac{\sigma_x^*}{\omega} H_{zx0} = \alpha E_0 \cos\phi. \tag{4.28c}$$

$$\mu_0 H_{zy0} - i\frac{\sigma_y^*}{\omega} H_{zy0} = \beta E_0 \sin\phi. \tag{4.28d}$$

From Eq.4.28c and Eq.4.28d

$$H_{zx0} = \frac{\alpha E_0 \cos\phi}{\mu_0 - i\frac{\sigma_x^*}{\omega}}. \tag{4.29a}$$

$$H_{zy0} = \frac{\beta E_0 \sin\phi}{\mu_0 - i\frac{\sigma_y^*}{\omega}}. \tag{4.29b}$$

Using Eq.4.29 in Eq.4.28a and Eq.4.28b, respectively, yield

$$\varepsilon_0\mu_0(1-i\frac{\sigma_y}{\varepsilon_0\omega})\sin\phi = \beta\left(\frac{\alpha\cos\phi}{(1-i\frac{\sigma_x^*}{\omega\mu_0})}+\frac{\beta\sin\phi}{(1-i\frac{\sigma_y^*}{\omega\mu_0})}\right). \tag{4.30a}$$

$$\varepsilon_0\mu_0(1-i\frac{\sigma_y}{\varepsilon_0\omega})\cos\phi = \alpha\left(\frac{\alpha\cos\phi}{(1-i\frac{\sigma_x^*}{\omega\mu_0})}+\frac{\beta\sin\phi}{(1-i\frac{\sigma_y^*}{\omega\mu_0})}\right). \tag{4.30b}$$

Dividing Eq.4.30a by Eq.4.30b yields

$$\frac{\beta}{\alpha} = \frac{\sin\phi}{\cos\phi}\frac{1-i\frac{\sigma_y}{\varepsilon_0\omega}}{1-i\frac{\sigma_x}{\varepsilon_0\omega}}. \tag{4.31}$$

Substituting Eq.4.31 in Eq.4.30 results

$$\alpha = \frac{\sqrt{\varepsilon_0\mu_0}}{G}\left(1-i\frac{\sigma_x}{\varepsilon_0\omega}\right)\cos\phi. \tag{4.32a}$$

$$\beta = \frac{\sqrt{\varepsilon_0\mu_0}}{G}\left(1-i\frac{\sigma_y}{\varepsilon_0\omega}\right)\sin\phi. \tag{4.32b}$$

where

$$G = \sqrt{w_x\cos^2\phi + w_y\sin^2\phi}. \tag{4.33}$$

$$w_x = \frac{1-i\frac{\sigma_x}{\varepsilon_0\omega}}{1-i\frac{\sigma_x^*}{\mu_0\omega}}. \tag{4.34a}$$

$$w_y = \frac{1-i\frac{\sigma_y}{\varepsilon_0\omega}}{1-i\frac{\sigma_y^*}{\mu_0\omega}}. \tag{4.34b}$$

Denoting Ψ as the component of field, ψ_0 is the magnitude of the field, and $c = \frac{1}{\sqrt{\varepsilon_0\mu_0}}$ is the speed of light, using the values of Eq.4.32 and Eq.4.33 in Eq.4.27 yield

$$\Psi = \psi_0 e^{i\omega(t-(x\cos\phi+y\sin\phi)/cG)}e^{(\sigma_x\cos\phi/\varepsilon_0cG)x}e^{(\sigma_y\sin\phi/\varepsilon_0cG)y}. \tag{4.35}$$

Substituting Eq.4.32a in Eq.4.29a, and Eq.4.32b in Eq.4.29b yields

$$H_{zx0} = \frac{E_0\sqrt{\varepsilon_0/\mu_0}}{G} w_x \cos^2\phi. \tag{4.36a}$$

$$H_{zy0} = \frac{E_0\sqrt{\varepsilon_0/\mu_0}}{G} w_y \sin^2\phi. \tag{4.36b}$$

Adding Eq.4.36a and Eq.4.36b yields

$$H_0 = E_0 G\sqrt{\varepsilon_0/\mu_0}. \tag{4.37}$$

Impedance is the ratio of the magnitude of electric field E_0 to that of magnetic field H_0,

$$Z = \frac{E_0}{H_0} = \frac{\sqrt{(\mu_0/\varepsilon_0)}}{G}. \tag{4.38}$$

If (σ_x, σ_x^*) and (σ_y, σ_y^*) satisfy the condition $\frac{\sigma}{\varepsilon_0} = \frac{\sigma*}{\mu_0}$, then the quantities w_x, w_y, and G equal to unity at any frequencies. Finally, the expression for field and impedance become

$$\Psi = \psi_0 e^{i\omega(t-(x\cos\phi+y\sin\phi)/c)} e^{(\sigma_x\cos\phi/\varepsilon_0 c)x} e^{(\sigma_y\sin\phi/\varepsilon_0 c)y}. \tag{4.39}$$

$$Z = \sqrt{\mu_0/\varepsilon_0}. \tag{4.40}$$

The first exponential of Eq.4.39 represents the wave phase that propagates normally to the electric field at the speed of light c. The last two exponentials represent the wave decreasing exponentially in the x and y-directions. And Eq.4.40 represents the impedance matching condition for the vacuum-medium interface. From Eq.4.35, or Eq.4.39, it can be concluded that if $\sigma_y = \sigma_y^* = 0$ it is not absorbed along y-direction and if $\cos\pi = 0$ the wave propagates along y-direction. For matched media, Eq.4.39 is the function of the x coordinate only.

Let us consider a plane wave incident at an angle of θ_i at a PML interface. Fig.4.4 shows the interface between two PML media. The interface is infinitely long, and the incident wave is a plane wave. The angle θ has been taken to the y-axis. The angle of reflection and transmission to

the PML interface is θ_r and θ_t, respectively.

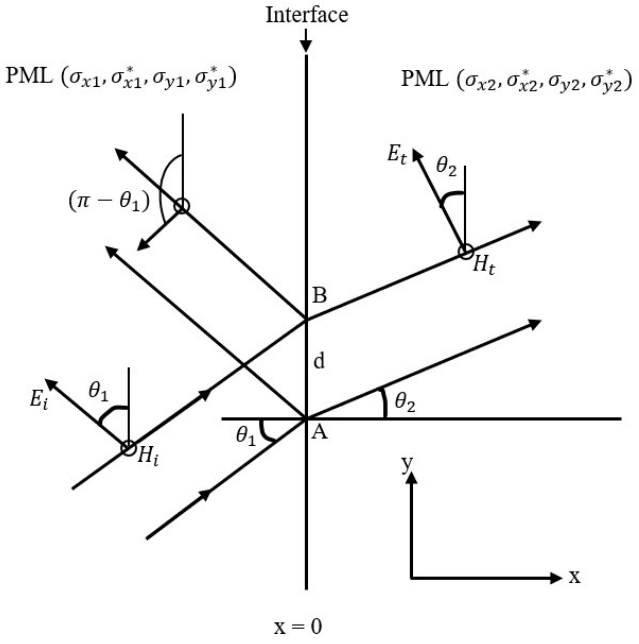

Figure 4.4: Interface lying between two Perfectly matched layer media

We assume the incident, reflected, and transmitted electric fields are E_i, E_r, and E_t, respectively. For any component Ψ of the incident and transmitted plane wave at point A and B of the interface can be written as

$$\frac{\psi_t(B)}{\psi_i(B)} = \frac{\psi_t(A)}{\psi_i(A)}. \tag{4.41}$$

Let the distance between the points A and B is d, and G_1 and G_2 are quantities of each media, then we can write incident and transmitted fields as

$$\psi_i(B) = \psi_i(A) e^{-i\omega(d\sin\theta_1/cG_1) - (\sigma_{y1}\sin\theta_1/c\varepsilon_0 G_1)d}. \tag{4.42a}$$

$$\psi_t(B) = \psi_t(A) e^{-i\omega(d\sin\theta_2/cG_2) - (\sigma_{y2}\sin\theta_2/c\varepsilon_0 G_2)d}. \tag{4.42b}$$

From Eq.4.41 and Eq.4.42, we get

$$\left(1 - i\frac{\sigma_{y1}}{\varepsilon_0\omega}\right)\frac{\sin\theta_1}{G_1} = \left(1 - i\frac{\sigma_{y2}}{\varepsilon_0\omega}\right)\frac{\sin\theta_2}{G_2}. \tag{4.43}$$

here

$$G_k = \sqrt{w_{xk}\cos^2\theta_k + w_{yk}\sin^2\theta_k} \qquad \text{(for k = 1, 2).} \tag{4.44}$$

The Eq.4.43 is the Snell-Descartes law which connects the incident and transmitted angles at an interface normal to x, (Fig.4.4), lying between the two PML media.

Let us consider the incident, reflected, transmitted electric fields are E_i, E_r, E_t and magnetic fields H are H_i, H_r, H_t, respectively.

$$E_i = E_{i0}e^{-i\omega(y\sin\theta_1/cG_1)(1-i(\sigma_{y1}/\varepsilon_0\omega))}e^{i\omega t}. \tag{4.45a}$$

$$E_r = E_{r0}e^{-i\omega(y\sin\theta_1/cG_1)(1-i(\sigma_{y1}/\varepsilon_0\omega))}e^{i\omega t}. \tag{4.45b}$$

$$E_t = E_{t0}e^{-i\omega(y\sin\theta_1/cG_1)(1-i(\sigma_{y1}/\varepsilon_0\omega))}e^{i\omega t}. \tag{4.45c}$$

$$H_i = E_i/Z_1. \tag{4.45d}$$

$$H_r = E_r/Z_1. \tag{4.45e}$$

$$H_t = E_t/Z_2. \tag{4.45f}$$

From Eq.4.43, according to the Snell's law, the three exponential terms of Eq.4.45a, Eq.4.45b, and Eq.4.45c on space are equal. Using the boundary conditions, the electric fields are continuous along the y-axis, we get

$$E_i\cos\theta_1 - E_r\cos\theta_1 = E_t\cos\theta_2. \tag{4.46a}$$

$$H_i + H_r = H_t. \tag{4.46b}$$

From Eq.4.45 and Eq.4.46, we get

$$E_{i0}\cos\theta_1 - E_{r0}\cos\theta_1 = E_{t0}\cos\theta_2. \tag{4.47a}$$

$$\frac{E_{i0}}{Z_1} + \frac{E_{r0}}{Z_1} = \frac{E_{t0}}{Z_2}. \tag{4.47b}$$

Solving Eq.4.47a and Eq.4.47b we get the coefficient of reflectance r_p and r_t,

$$r_p = \frac{Z_2 \cos\theta_2 - Z_1 \cos\theta_1}{Z_1 \cos\theta_1 + Z_2 \cos\theta_2}. \tag{4.48a}$$

$$r_t = \frac{2Z_2 \cos\theta_2}{Z_1 \cos\theta_1 + Z_2 \cos\theta_2}. \tag{4.48b}$$

Using the value of $Z = \sqrt{\mu_0 \varepsilon_0}\frac{1}{G}$ in Eq.4.48 we get

$$r_p = \frac{G_1 \cos\theta_2 - G_2 \cos\theta_1}{G_1 \cos\theta_1 + G_2 \cos\theta_2}. \tag{4.49a}$$

$$r_t = \frac{2G_2 \cos\theta_2}{G_1 \cos\theta_1 + G_2 \cos\theta_2}. \tag{4.49b}$$

where G_1 and G_2 are functions of θ_1 and θ_2 through Eq.4.44. Let us consider an interface lying between two PML media having conductivities σ_y and σ_y^*. For conductivities $(\sigma_{x1}, \sigma_{x1}^*, \sigma_y, \sigma_y^*)$ and $(\sigma_{x2}, \sigma_{x2}^*, \sigma_y, \sigma_y^x)$, Snell's law Eq.4.43 yields

$$\frac{\sin\theta_1}{G_1} = \frac{\sin\theta_2}{G_2}. \tag{4.50}$$

If the two media are matched ones, $(\sigma_{x1}, \sigma_{x1}^*)$, $(\sigma_{x2}, \sigma_{x2}^*)$, and (σ_y, σ_y^*) satisfy Eq.4.25 and we have $G_1 = G_2 = 1$, and Eq.4.50 becomes

$$\theta_1 = \theta_2. \tag{4.51}$$

and the coefficient of reflectance becomes

$$r_p = 0. \tag{4.52}$$

So, at an interface normal to x between two matched PML media having conductivities (σ_y, σ_y^*), a plane wave is transmitted through the medium without reflection at any incident angles and frequencies. This also applies if the first medium is a vacuum and the second medium has conductivity $(\sigma_x, \sigma_x^*, 0, 0)$ because the vacuum medium can be seen as a $(0,0,0,0)$ medium.

For unmatched medium having the same conductivities (σ_y, σ_y^*), the equation can be found by substituting Eq.4.50 into Eq.4.48a as

$$r_p = \frac{\sin\theta_1 \cos\theta_2 - \sin\theta_2 \cos\theta_1}{\sin\theta_1 \cos\theta_2 + \sin\theta_2 \cos\theta_1}. \tag{4.53}$$

Taking into account $w_{y1} = w_{y2}$, from Eq.4.44 and Eq.4.50 we get

$$\sqrt{w_{x2}} \sin\theta_1 \cos\theta_2 = \sqrt{w_{x1}} \sin\theta_2 \cos\theta_1. \tag{4.54}$$

and from Eq.4.53 and Eq.4.54, the coefficient of reflectance becomes

$$r_p = \frac{\sqrt{w_{x1}} - \sqrt{w_{x2}}}{\sqrt{w_{x1}} + \sqrt{w_{x2}}}. \tag{4.55}$$

From Eq.4.55, it is seen that for unmatched media, the reflection does not depend on the incident angles. It depends only on the frequency through the Eq.4.32. For matched media $w_{x1} = w_{x2} = 1$ and Eq.4.55 reduces to the Eq.4.52, i.e., $r_p = 0$.

At an interface normal to x between to PML media whose conductivities σ_y and σ_y^* are the same and satisfy Eq.4.25, the coefficient of reflectance r_p is null. Similarly, at an interface normal to y having the same conductivities σ_x and σ_x^*, the coefficient of reflectance is null.

4.5 Plane Wave Expansion Method

The Plane-Wave Expansion Method (PWEM) is a full vectorial simulation tools used to calculate the photonic band structure [32]. The PWEM depends on the Fourier representation of the periodic $\mathbf{E_k}$ and $\mathbf{H_k}$ fields in terms of periodic harmonic function. The reciprocal lattice vector defines the period harmonic function.

Let us consider a two-dimensional periodic structure defined by the set of lattice vectors $\mathbf{R}$.

$$\mathbf{R} = m\mathbf{a}_1 + n\mathbf{a}_2. \tag{4.56}$$

Here, a_1 and a_2 are primitive lattice vectors, m and n are integers. The reciprocal lattice is formed by a set of vectors **G** is

$$e^{i\mathbf{G}\cdot\mathbf{R}} = 1. \tag{4.57}$$

for all **R**. The Eq.4.57 can be written as

$$\mathbf{G}\cdot\mathbf{R} = 2\pi l. \tag{4.58}$$

Here l is an integer. The reciprocal lattice vector **G** is generated by vectors $\mathbf{g}_1$ and $\mathbf{g}_2$ is

$$\mathbf{G} = m'\mathbf{g}_1 + n'\mathbf{g}_2. \tag{4.59}$$

here m', n' are integers, and $\mathbf{g}_1$ and $\mathbf{g}_2$ are primitive lattice vectors defined by the *Kronecker delta*,

$$\delta_{ij} = \begin{cases} 1, & i = j \\ 0, & i \neq j. \end{cases} \tag{4.60}$$

The primitive lattice vectors can be written as, (Fig.4.5a)

$$\begin{aligned} \mathbf{a}_1 &= a\hat{\mathbf{x}}, \\ \mathbf{a}_2 &= a\hat{\mathbf{y}}. \end{aligned} \tag{4.61}$$

The reciprocal lattice vectors of square lattice can be found as (Fig.4.5b)

$$\begin{aligned} \mathbf{g}_1 &= \left(\frac{2\pi}{a}\right)\hat{\mathbf{x}}, \\ \mathbf{g}_2 &= \left(\frac{2\pi}{a}\right)\hat{\mathbf{y}}. \end{aligned} \tag{4.62}$$

Let us consider the dielectric function $\varepsilon_r(\mathbf{r})$ is periodic in 2D, i.e., it satisfies the relation $\varepsilon_r(\mathbf{r}+\mathbf{R}) =$

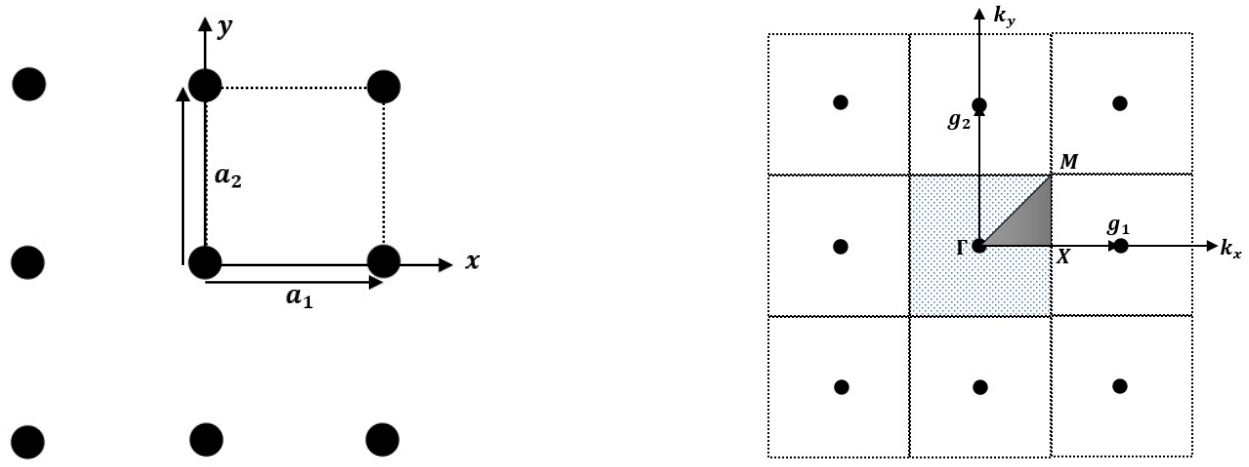

(a) (b)

Figure 4.5: Square lattice (a) Real-space generated by primitive vectors $\mathbf{a}_1$ and $\mathbf{a}_2$. (b) Reciprocal-space with primitive vectors $\mathbf{g}_1$ and $\mathbf{g}_2$; the shaded region is the first Brillouin zone and grey right triangle $\triangle\Gamma XM$ is the irreducible Brillouin zone.

$\varepsilon_r(\mathbf{r})$. Then, the reciprocal of the dielectric function, $\varepsilon_r^{-1}(\mathbf{r}+\mathbf{R}) = \varepsilon_r^{-1}(\mathbf{r})$. The reciprocal of dielectric function in Fourier series can be written as

$$\varepsilon_r^{-1} = \sum_{G'} \kappa(\mathbf{G}') e^{i(\mathbf{G}'\cdot\mathbf{r})}. \tag{4.63}$$

where $\kappa(\mathbf{G}')$ is the Fourier coefficient, written as

$$\kappa(\mathbf{G}) = \frac{1}{S}\int_S \varepsilon_r^{-1}(\mathbf{r}) e^{-i\mathbf{G}\cdot\mathbf{r}} ds. \tag{4.64}$$

here S is the area of the unit cell. If $\mathbf{G} = m_1\mathbf{g}_1 + m_2\mathbf{g}_2$, putting this value in Eq.4.64 yields

$$\begin{aligned}
\kappa(m_1,m_2) &= \frac{1}{S}\int_0^{a_1}\int_0^{a_2} \frac{1}{\varepsilon_r(\xi,\eta)} e^{-i[m_1\mathbf{g}_1+m_2\mathbf{g}_2]\left[\xi\frac{\mathbf{a}_1}{a_1}+\eta\frac{\mathbf{a}_2}{a_2}\right]} \sin\theta d\xi d\eta \\
&= \frac{1}{S}\int_0^{a_1}\int_0^{a_2} \frac{1}{\varepsilon_r(\xi,\eta)} e^{-2\pi\left[\xi\frac{m_1 n_1}{N_1}+\eta\frac{m_2 n_2}{N_2}\right]} \sin\theta d\xi d\eta \\
&\approx \frac{1}{N_1 N_2}\sum_{n_1}\sum_{n_2} \frac{1}{\varepsilon_r(n_1,n_2)} e^{-2\pi\left[\xi\frac{m_1 n_1}{N_1}+\eta\frac{m_2 n_2}{N_2}\right]}.
\end{aligned} \tag{4.65}$$

Here, in the last step, the integrals are approximated by discrete sums. The Fourier coefficients

$\kappa(m_1, m_2)$ can be obtained by using the Fast Fourier Transform (FFT).

Let us consider a circular rod of radius r and dielectric constant ε_a embedded in a background of dielectric constant ε_b, the Fourier coefficients can be calculated as

$$\kappa(\mathbf{G}) = \begin{cases} \frac{1}{\varepsilon_a} + \frac{1}{\varepsilon_b}(1-f), & |\mathbf{G}| = 0 \\ \left(\frac{1}{\varepsilon_a} - \frac{1}{\varepsilon_b}\right) f \frac{J_1(|\mathbf{G}|R)}{|\mathbf{G}|R}, & |\mathbf{G}| \neq 0. \end{cases} \tag{4.66}$$

Here, $f = \pi r^2/(a^2 \sin\theta)$ is the *fill factor* and $J_1(x)$ is the first-order Bessel function.

Let us calculate the band structure for electromagnetic waves propagating perpendicular to a periodic dielectric structure of rods. The rods are homogeneous along z-direction, i.e., $\frac{\partial}{\partial z} = 0$. Maxwell equations in x and y directions can be written as

$$\frac{\partial H_z}{\partial x} = -i\omega\varepsilon_0\varepsilon_r E_y. \tag{4.67a}$$

$$\frac{\partial H_z}{\partial y} = i\omega\varepsilon_0\varepsilon_r E_x. \tag{4.67b}$$

$$\frac{\partial E_x}{\partial y} - \frac{\partial E_y}{\partial x} = i\omega\mu_0 H_z. \tag{4.67c}$$

$$\frac{\partial E_z}{\partial x} = i\omega\mu_0 H_y. \tag{4.67d}$$

$$\frac{\partial E_z}{\partial y} = -i\omega\mu_0 H_x. \tag{4.67e}$$

$$\frac{\partial H_y}{\partial x} - \frac{\partial H_x}{\partial y} = i\omega\varepsilon_0\varepsilon_r E_z. \tag{4.67f}$$

This first set of equations, Eq.4.67a-Eq.4.67c is called the *transverse-electric mode* with respect to z (TE_z) in two-dimensions. The second set of equations, Eq.4.67d-Eq.4.67f is called the *transverse-magnetic mode* with respect to z (TM_z) in two-dimensions.

By eliminating the electric field components E_x and E_y from the Eq.4.67a-Eq.4.67c we get the wave equation for the magnetic field H_z component for the *TE* mode

$$\frac{\partial}{\partial x}\left(\frac{1}{\varepsilon(\mathbf{r})}\frac{\partial}{\partial x}H_z(\mathbf{r})\right) + \frac{\partial}{\partial y}\left(\frac{1}{\varepsilon(\mathbf{r})}\frac{\partial}{\partial y}H_z(\mathbf{r})\right) + \left(\frac{\omega}{c}\right)^2 H_z(\mathbf{r}) = 0. \tag{4.68}$$

Similarly, from Eq.4.67d-Eq.4.67f we get the component of electric field E_z for TM_z mode

$$\frac{1}{\varepsilon(\mathbf{r})}\left[\frac{\partial^2}{\partial x^2}+\frac{\partial^2}{\partial y^2}\right]E_z(\mathbf{r})+\left(\frac{\omega}{c}\right)^2 E_z(\mathbf{r})=0. \tag{4.69}$$

The solution of the Eq.4.68 and Eq.4.69 is Bloch wave, the component of magnetic field is given by

$$H_z(\mathbf{r})=u(\mathbf{k},\mathbf{r})e^{i(\mathbf{k}\cdot\mathbf{r})}. \tag{4.70}$$

Here, $u(\mathbf{k},\mathbf{r})$ is the periodic function and $u(\mathbf{k},\mathbf{r}+\mathbf{R})=u(\mathbf{k},\mathbf{r})$. The Fourier series of H_z is

$$H_z(\mathbf{r})=\sum_G h(\mathbf{k},\mathbf{G})e^{i(\mathbf{k}+\mathbf{G})\cdot\mathbf{r}}. \tag{4.71}$$

Here, $\mathbf{k}=k_x\hat{\mathbf{x}}+k_y\hat{\mathbf{y}}$ is the wave vector in two dimension.

Substituting Eq.4.63 and Eq.4.71 in Eq.4.68 yields

$$\sum_{\mathbf{G},\mathbf{G}''}(\mathbf{k}+\mathbf{G})\cdot(\mathbf{k}+\mathbf{G}'')\kappa(\mathbf{G}''-\mathbf{G})h(\mathbf{k},\mathbf{G})e^{i(\mathbf{k}+\mathbf{G}'')\cdot\mathbf{r}}=\frac{\omega^2}{c^2}\sum_G h(\mathbf{k},\mathbf{G})e^{i(\mathbf{k}+\mathbf{G}'')\cdot\mathbf{r}}. \tag{4.72}$$

Here, $\mathbf{G}''=\mathbf{G}+\mathbf{G}'$.

Let us consider the testing function is the same as the expansion basis function, and taking the dot product of each sides of the testing function yields

$$\sum_{\mathbf{G},\mathbf{G}''}(\mathbf{k}+\mathbf{G})\cdot(\mathbf{k}+\mathbf{G}'')\kappa(\mathbf{G}''-\mathbf{G})h(\mathbf{k},\mathbf{G})\int_S e^{i(\mathbf{G}''-\mathbf{G}')\cdot\mathbf{r}}ds=\frac{\omega^2}{c^2}\sum_G h(\mathbf{k},\mathbf{G})\int_S e^{i(\mathbf{G}-\mathbf{G}')\cdot\mathbf{r}}ds. \tag{4.73}$$

The integral over unit cell can be carried out as

$$\int_S e^{i(\mathbf{G}''-\mathbf{G}')\cdot\mathbf{r}}ds=\begin{cases}S, & \mathbf{G}''=\mathbf{G}'\\ 0, & \mathbf{G}''\neq\mathbf{G}'.\end{cases} \tag{4.74}$$

The Eq.4.74 leads the standard eigenvalue problem,

$$\sum_{\mathbf{G}}(\mathbf{k}+\mathbf{G})\cdot(\mathbf{k}+\mathbf{G}')\kappa(\mathbf{G}'-\mathbf{G})h(\mathbf{k},\mathbf{G}) = \frac{\omega^2}{c^2}h(\mathbf{k},\mathbf{G}'). \tag{4.75}$$

or standard eigenvalue equation

$$\mathbf{A}\mathbf{h} = \lambda\mathbf{h}. \tag{4.76}$$

Comparing Eq.4.75 and Eq.4.76, we get the eigenvalue, $\lambda = \frac{\omega^2}{c^2}$. Here the matrix $\mathbf{A}$ is self-adjoint, that means the eigenvalues of the Eq.4.76 are real.

Similarly, the component of electric field $E_z(\mathbf{r})$ in TM mode is given by

$$E_z(\mathbf{r}) = \sum_{G}\eta(\mathbf{k},\mathbf{G})e^{i(\mathbf{k}+\mathbf{G})\cdot\mathbf{r}}. \tag{4.77}$$

Substituting the value of Eq.4.77 in Eq.4.69 yields

$$\sum_{G}|\mathbf{k}+\mathbf{G}'|\kappa(\mathbf{G}'-\mathbf{G})|\mathbf{k}+\mathbf{G}|b(\mathbf{k},\mathbf{G}) = \frac{\omega^2}{c^2}b(\mathbf{k},\mathbf{G}'). \tag{4.78}$$

The Eq.4.78 can also be written in matrix form,

$$\mathbf{A}\mathbf{b} = \lambda\mathbf{b}. \tag{4.79}$$

here, the eigenvalue is again, $\lambda = \frac{\omega^2}{c^2}$.

In both equations Eq.4.75 and Eq.4.78, the reciprocal lattice sum is truncated to obtain a numerical solution to the eigenvalue problem. These two equations have been solved for both the eigenvalues $\lambda = \frac{\omega^2}{c^2}$ and the eigenvalues $h(\mathbf{k},\mathbf{G})$ and $b(\mathbf{k},\mathbf{G}')$, respectively. The electric and magnetic field that corresponds to a given eigenfrequency $\omega(\mathbf{k})$ can be found by solving Eq.4.75 and Eq.4.78.

4.6 Photonic Band Structure

The most commonly used method is the plane-wave expansion method [32], which expands the magnetic and dielectric function on the basis of a plane wave. The Eq.4.75 and Eq.4.78 can be reduced to a matrix equation which gives a series of solutions in the form of a function $\omega_n(k)$, n = 1, 2, 3,.., . These series of functions form a band called photonic bands. This band structure gives all frequencies in which the optical modes are allowed for a given wave vector k. A photonic bandgap is a range of frequencies, ω, for no eigenolutions for any wavevector k.

A two-dimensional photonic crystal made of a square lattice of circular dielectric rods ($\varepsilon = 13$) embedded in air background is shown in Fig.4.6a. The radius of the circular rod is $r = 0.3a$; here a is the lattice parameter. The Brillouin zone of the square lattice is shown in Fig.4.6b. The band structure calculation for this 2D photonic crystals has been done in RSoft CAD using the BandSOLVE package with PWE method [32] provided by the synopsis photonic solutions group [33]. The band structures for TE and TM polarization are shown in Fig.4.7 and Fig.4.8, respectively. The horizontal axis represents the higher symmetry points in the k-space. The vertical

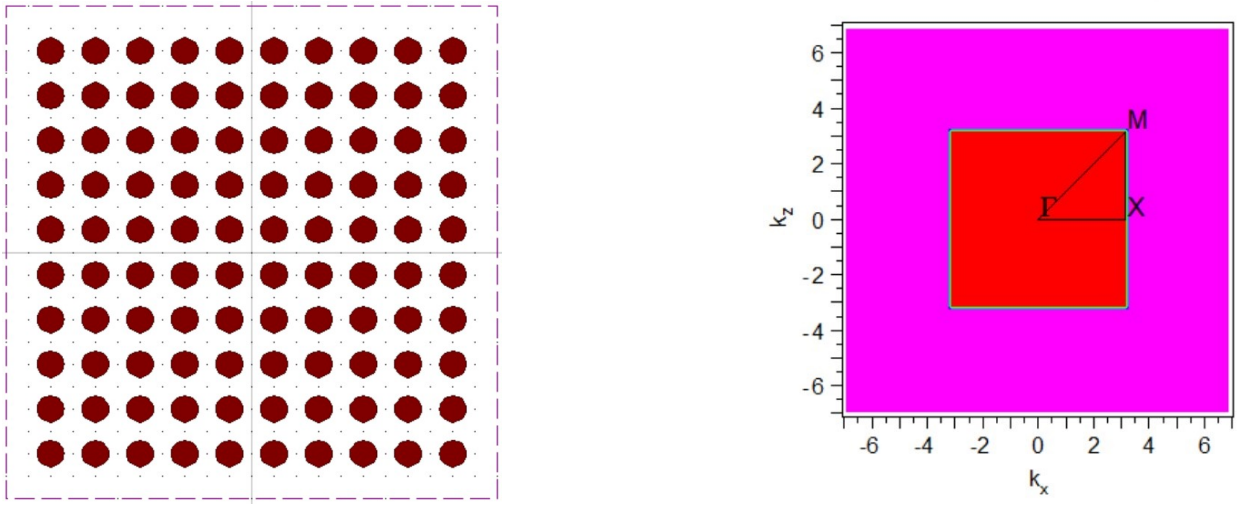

(a) 2D Square lattice

(b) Brillouin zone

Figure 4.6: (a) A 2D photonic crystal made of square lattice of dielectric rods ($\varepsilon = 13$) in air background (RSof CAD interface). (b) The first Brillouin zone. Here Γ, X and M represent the higher symmetry points. Γ is the center of the BZ, X is the center of the edge, and M is the corner point.

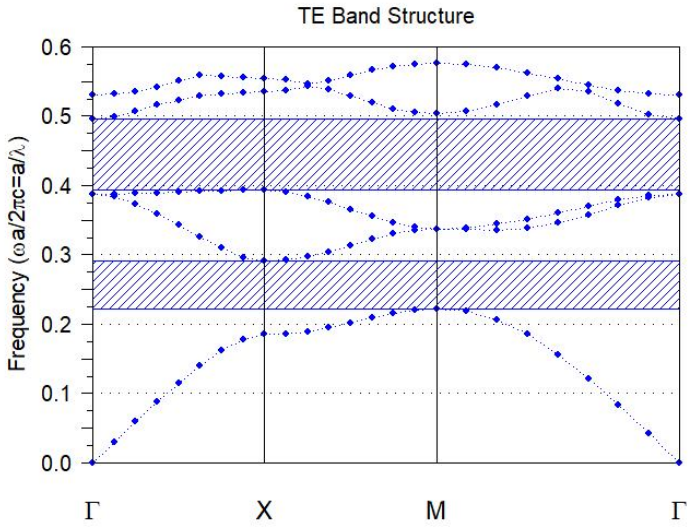

Figure 4.7: Band structure of 2D photonic crystals for TE polarization

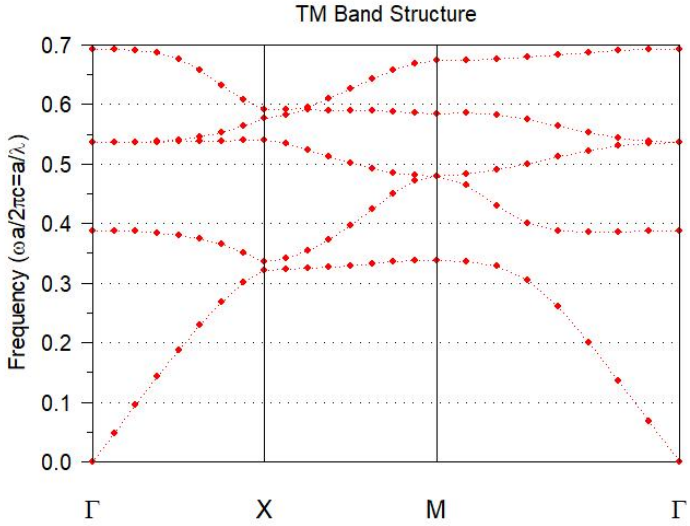

Figure 4.8: Band structure of 2D photonic crystals for TM polarization.

axis represents the dimensionless normalized frequency, $\omega a/2\pi c = a/\lambda$. We have calculated the first five band structures for both TE and TM polarization. For TE polarization, the photonic crystals shows two band gaps, as shown in the shaded region of Fig.4.7. On the other hand, the photonic crystals does not have band gap for TM polarization, Fig.4.8. The photonic crystals have partial band gap near X point.

CHAPTER V

APPLICATION OF 2D FAST FOURIER TRANSFORM

5.1 Single Boundary Interface between Two Materials

A homogeneous dielectric medium of the air-dielectric system in an air background has been considered to determine the angle of refraction in PhC. The refractive index of the dielectric medium is $n_2 = 1.52$. Fig.5.1 shows the 2D homogeneous dielectric material in an air background ($n_1 = 1.0$) in RSoft CAD [34] interface. The lower rectangle (gray color) represents the air medium, and the upper rectangle (magenta color) represents the second dielectric medium. The FDTD method [27] with FullWave [34] package has been used to model the propagation of a plane EM wave through the dielectric material. A plane EM wave was sent from the air to the 2D homogeneous dielectric material at various angles of incidence.

Figure 5.1: Two dimensional homogeneous dielectric medium. The lower rectangle (gray color) is the first dielectric medium, $n_1 = 1.0$ and upper rectangle (magenta color) represents the second dielectric medium, $n_2 = 1.52$.

The plane EM wave at various angles of incidence such as 10°, 15°, 20°, 25°, 30°, 35°, and 40° as shown in Fig.5.2 and Fig.5.3. The propagation of EM waves through the homogeneous medium can be separated into two possible polarizations: TE and TM polarization. Since it is a homogeneous dielectric material, we considered TE polarization only. The electric field is perpendicular to the plane of incidence for TE polarization. The direction of the electric field is perpendicular to the *xz*- plane, along the *y*-direction (into the page). The EM wave propagation through the dielectric medium at normal incidence is shown in Fig.5.2a. The lower region shows the amplitude of the incident and reflected EM wave, and the upper part shows the amplitude of the transmitted wave.

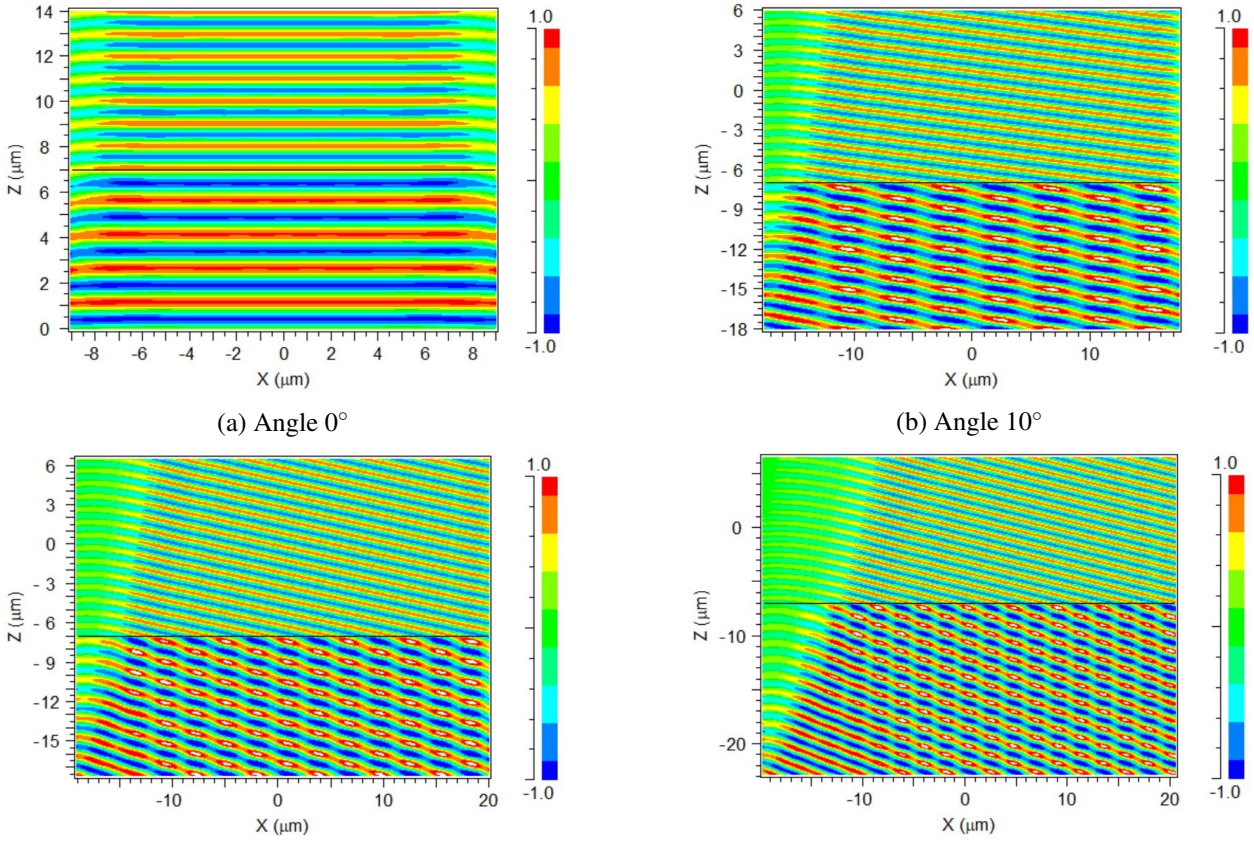

(a) Angle 0°

(b) Angle 10°

(c) Angle 15°

(d) Angle 20°

Figure 5.2: The color map of electric field for TE polarization. A plane EM wave passing through the first medium to the second medium making an angle of (a) 0° (b) 10° (c) 15° and (d) 20° with the normal of the boundary.

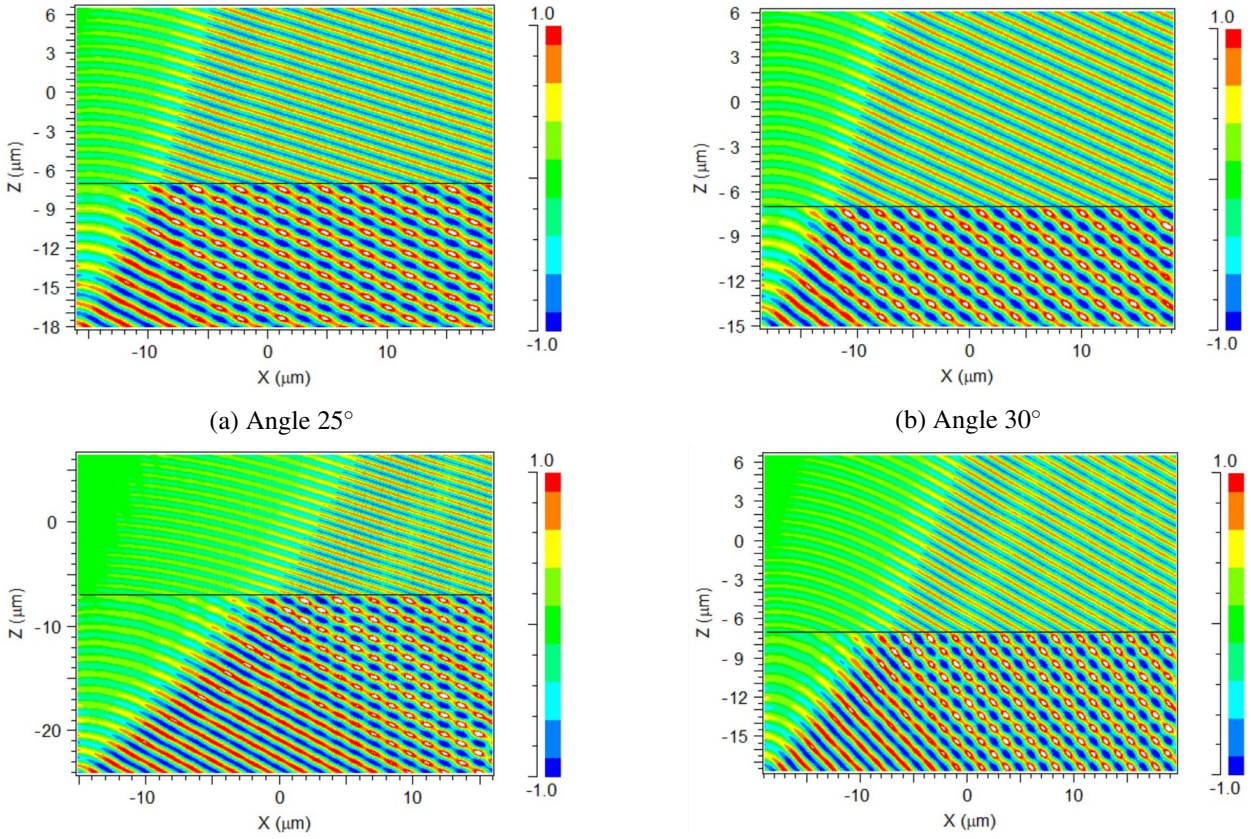

(a) Angle 25°

(b) Angle 30°

(c) Angle 35°

(d) Angle 40°

Figure 5.3: The color map of electric field for TE polarization. A plane EM wave passing through the first medium to the second medium making an angle of (a) 25° (b) 30° (c)35° (d) 40° with the normal of the boundary.

In the lower region, the incident and reflected EM wave make superposition constructively or destructively. The constructive superposition increases the intensity of the electric field (the white color in the red background). In contrast, destructive superposition decreases the intensity of the electric field (blue region) in the lower part of the air-dielectric system. In the upper region, the amplitude of the transmitted wave passes through the dielectric medium without making superposition since it is a single transmitted wave only.

5.2 Determination of Wave Vectors

5.2.1 Wave Vectors of E-Field in Fourier Domain

The output results of the FDTD method have been imported from the FullWave to MATLAB to determine the angle of incident and the angle of refraction in the air-dielectric system. In MATLAB, the propagation vector **k** has been separated from the plane wave by using the two-dimensional *Fast-Fourier Transformation (FFT2)*. The coordinates of the wave vector **k** in the Fourier domain give the angle of incident or the angle of refraction in the air-dielectric system. The

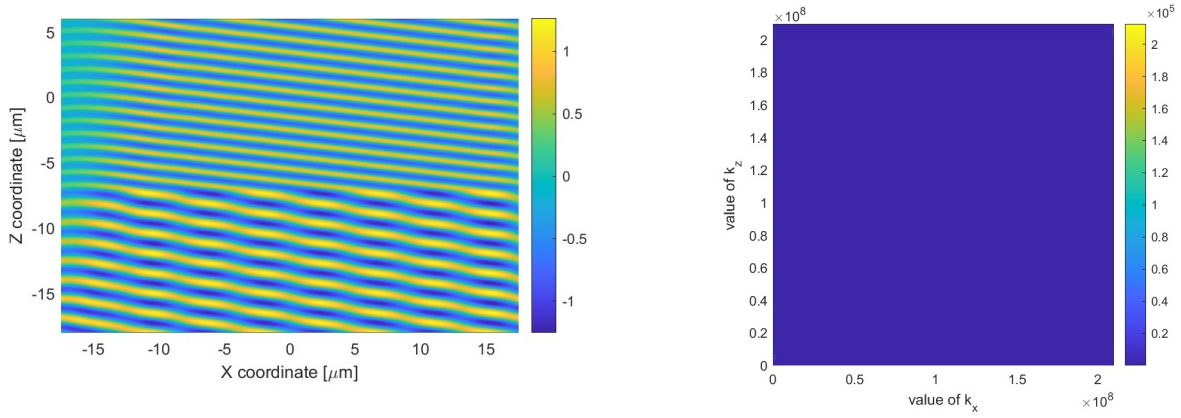

Figure 5.4: The color map of E-field reproduced in MATLAB (left) and the Fast-Fourier Transformation of E-field (right).

imported results from the FullWave have been reproduced in MATLAB. This output result contains the amplitude of the incident, reflected, and transmitted wave, Fig.5.4 (left). This whole region of the electric field is transformed into the Fourier domain by using *FFT2* tool, as shown in Fig.5.4 (right). The output of the Fast-Fourier Transformation gives the magnitude of the E-field in Fourier domain. The magnitude of the E-field in the Fourier domain is symmetric. So, we took only the lower part (Fig.5.5a) and ignored the upper part (Fig.5.5b).

In the Fourier domain, we found two bright peaks surrounded by secondary bright peaks in the first quadrants. The first bright peak represents the wave vector **k** for the incident field, and the second bright peak represents the wave vector **k** for the refracted field. The Fourier domain of the E -field contains wave vector **k** of the incident and refracted waves. To determine the angle of

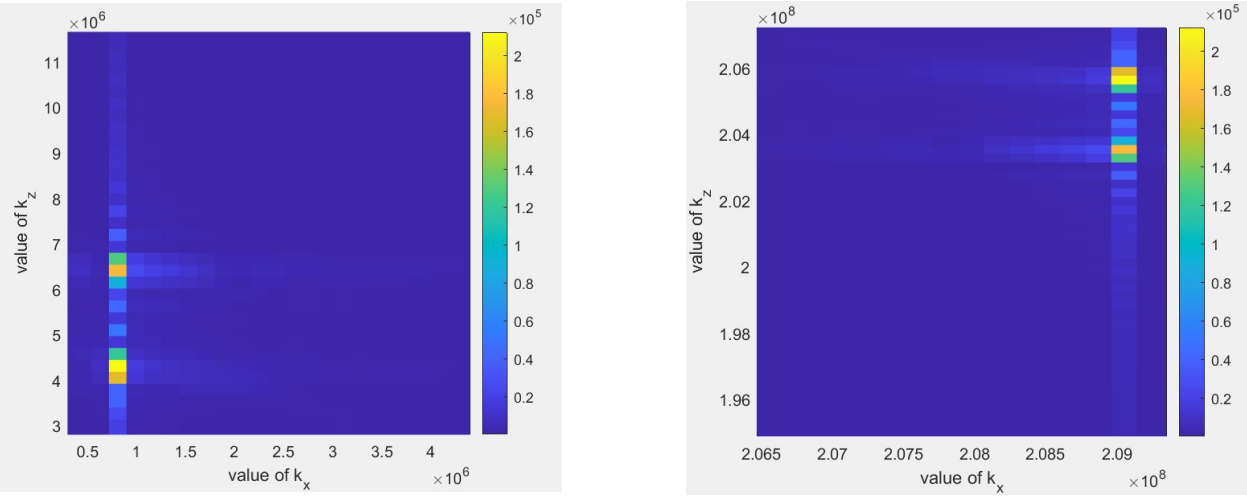

(a) (b)

Figure 5.5: The magnitude of the E-field in Fourier domain. The images (a) and (b) are symmetric.

incident and the angle of refraction separately, we divided the output of the electric field into two parts: one is for the incident field, and another is for the refracted field. Then we determined their corresponding wave vector **k**.

We set up a boundary for incident waves in the region containing both the incident, reflected, and refracted waves as shown in Fig.5.1. Then, we cut a region containing the incident wave only, Fig.5.6a. To find the wave vector **k** of the incident plane wave, we used the *FFT2* tool. The *FFT2* tool gives the wave vector **k** of the incident electric field in the Fourier domain. The corresponding

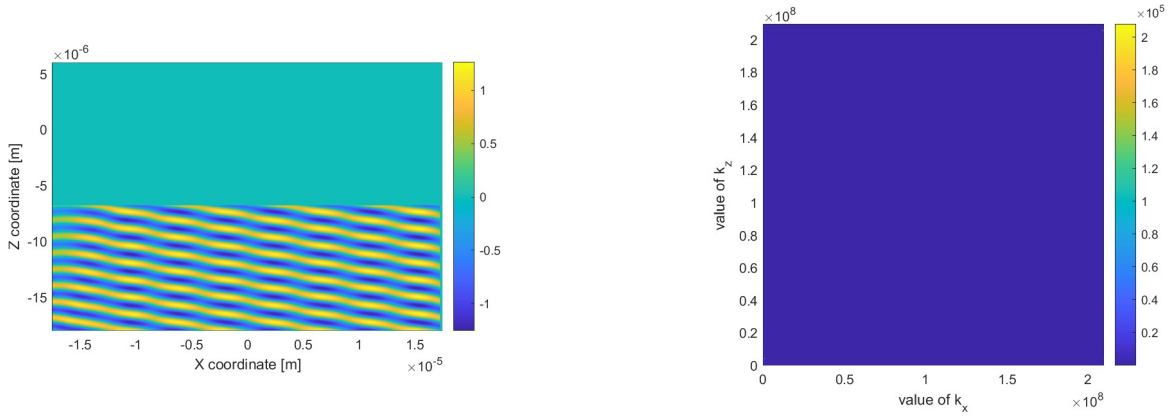

(a) (b)

Figure 5.6: (a) A region of the incident wave reproduced in MATLAB. (b) The wave vector **k** in the Fourier domain of the incident field.

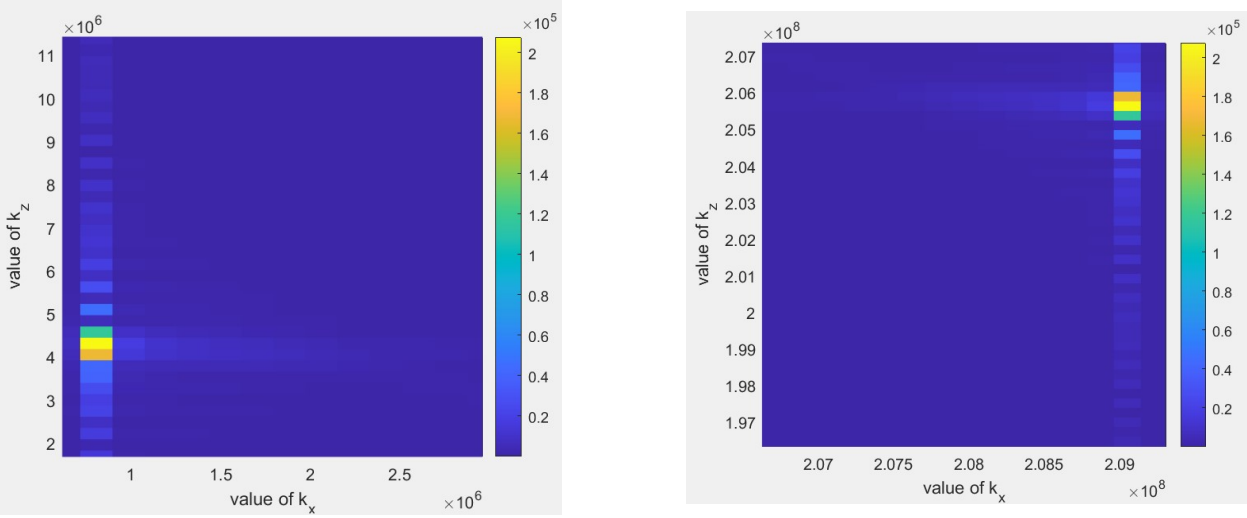

(a) (b)

Figure 5.7: The magnitude of the E-field in Fourier domain. The image (a) and (b) are symmetric.

Fourier domain of the incident wave is shown in Fig.5.6b. The Fast-Fourier Transformation gives symmetric images of the E-field, as shown in Fig.5.7. These symmetric images can be found by zooming Fig.5.6b. Since the images are symmetric, we took only one image, the lower one, as shown in Fig.5.7a. There are several bright peaks can be found in the Fourier domain. Among those bright peaks, only one point has the maximum magnitude of the E-field.

We separated the symmetric images in the Fourier domain and kept only the lower part for calculation. In the lower part of the Fourier domain (Fig.5.8a), we searched for the maximum value of the E- field. This brightest peak in the Fourier domain is visible after zooming in on the lower part, as shown in Fig.5.8b. We selected the brightest peaks in the Fourier domain. A few secondary bright peaks surround this brightest peak in the Fourier domain. We ignored the secondary bright peaks in the Fourier domain. The brightest peak represents the maximum magnitude of the plane EM wave in the Fourier domain. The coordinates of this brightest peak give the desired angle.

5.2.2 Determination of the Angle from Wave Vector

The brightest peak in the Fourier domain represents the wave vector **k** of the plane EM wave. This brightest peak has two components: x-component of wave vector **k** along the interface between air-dielectric; and z-component of wave vector **k** along the z-axis (perpendicular to the air-dielectric

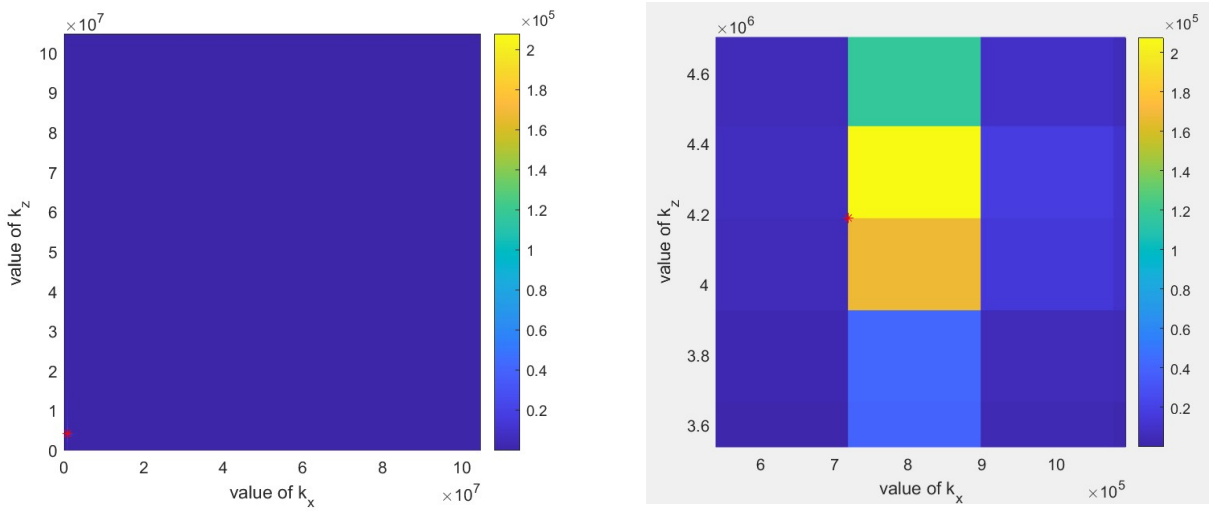

(a) (b)

Figure 5.8: (a) The maximum magnitude of E-field in the lower part of Fourier domain. (b) The maximum magnitude of E -value after zooming in. The red star represents the position of the wave vector **k** in Fourier domain.

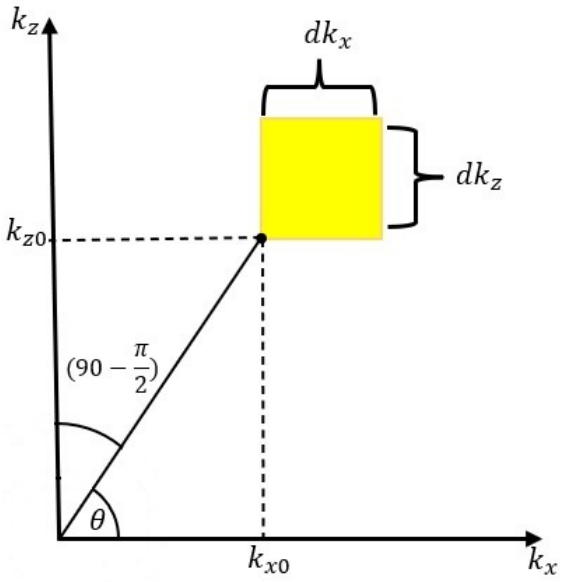

Figure 5.9: Wave vector representation for determining the angle of incidence or the angle of refraction. The yellow area represents the brightest **k**-point.

interface). The wave vector **k** representation is shown in Fig.5.9.

The x-component of the wave vector **k** is k_{x0} and the z-component of the wave vector **k** is

k_{z0}. The tangent between k_{x0} and k_{z0} is

$$\tan\theta = \frac{k_{z0}}{k_{x0}}. \tag{5.1}$$

But the wave vector **k** makes an angle θ_i with the normal of the boundary. The angle of incidence, θ_i is given by

$$\theta_i = \frac{\pi}{2} - \theta. \tag{5.2}$$

Using Eq.5.2, we calculated the angle of incidence in first dielectric (air) medium. The data for different angle of incidence is reported in the Table.5.1.

Table 5.1: The data for the angle of incident in homogeneous air ($n_1 = 1.0$) and dielectric ($n_2 = 1.52$) media. The angle of incident, θ_i is in degree.

No.	θ_i (Theoretical)	(Numerical)
1.	10	9.73
2.	15	15.13
3.	20	19.98
4.	25	25.21
5.	30	30.01
6.	35	34.87
7.	40	40.00

Following a similar approach, as we did for the incident wave, we separated the refracted part from the incident part, as shown in Fig.5.10. Then, we used *FFT2* tool in the refracted region to transform the components of the electric field into the Fourier domain. Again, we divided the symmetric image and kept only the lower part of the Fourier domain in a similar way we did for the incident wave. In the real part, we searched for the brightest k-point. the corresponding x and y-component of the k-vector have used in Eq.5.3, to determine the angle of refraction. The angle of refraction, θ_r is given by

$$\theta_r = \frac{\pi}{2} - \arctan\left(\frac{k_{z0}}{k_{x0}}\right). \tag{5.3}$$

The data for the angle of refraction for different angle of incidence is reported in the Table.5.2.

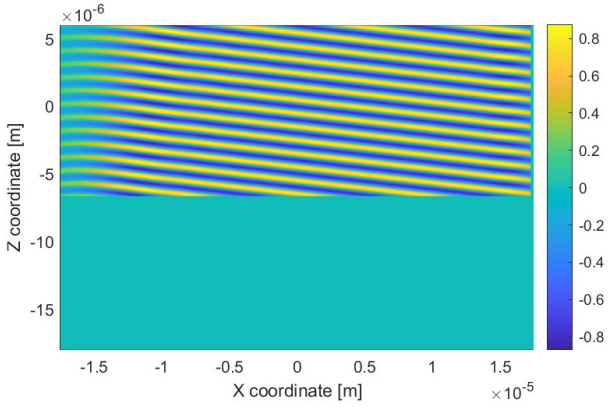

Figure 5.10: The electric field of a separated portion of the refracted wave.

Table 5.2: The data for the angle of refraction in homogeneous air-dielectric medium. The angle of incidence,θ_i and the angle of refraction, θ_r are in degrees.

No.	θ_i	θ_r
1.	10	6.52
2.	15	10.21
3.	20	12.71
4.	25	16.39
5.	30	19.12
6.	35	22.22
7.	40	24.60

5.3 Determination of Index of Refraction

We determined the angle of incidence and the angle of refraction from the k-vector using Snell's law. For air-dielectric system, the index of refraction of the dielectric medium can be found by Snell's law,

$$n_2 = \frac{n_1 \sin\theta_i}{\sin\theta_r}. \tag{5.4}$$

The index of refraction of air is $n = 1.0$. Using the values of the angle of incidence and the angle of refraction from Table.5.1 and Table.5.2, we have determined the index of refraction of the dielectric material. The theoretical value of the index of refraction for the dielectric material is $n_2 = 1.52$. The numerical calculation is shown in Table.5.3. The comparison between the index of refraction

and angle of incidence is given in Fig.5.10.

Table 5.3: The data for refractive index and angle of incident in homogeneous air ($n_1 = 1.0$) and dielectric (n_2) media. The angle of incident, θ_i and refracted angle, θ_r are in degree and refractive index, n_2 is dimensionless. The theoretical value of index of refraction is 1.52.

No.	θ_i		θ_r	n_2
	Theoretical	Numerical		
1.	10	9.73	6.52	1.49
2.	15	15.13	10.21	1.47
3.	20	19.98	12.71	1.55
4.	25	25.21	16.39	1.51
5.	30	30.01	19.12	1.53
6.	35	34.87	22.22	1.51
7.	40	40.00	24.60	1.54

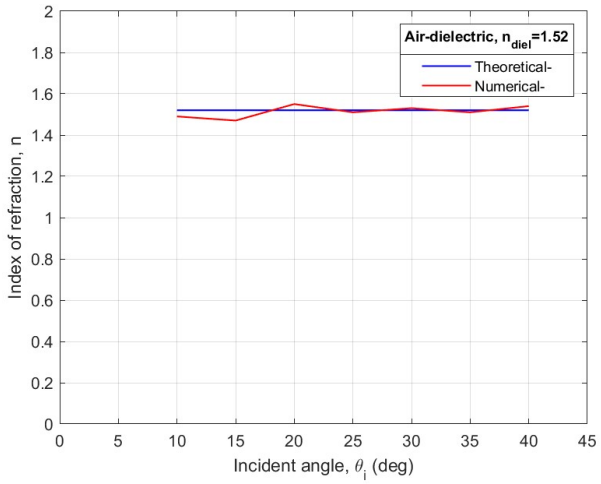

Figure 5.11: The index of refraction for various angle of incidence in homogeneous air-dielectric media. Here the refractive index for air is $n_1 = 1.0$ and for dielectric, $n_2 = 1.52$. The red line represents the theoretical value and blue line represents the numerical value of refractive index of the dielectric material.

5.4 Analysis of Resolution of FFT

The propagation vector **k** of the plane EM wave has a finite size in the Fourier domain. The number of pixels primarily affects the measurement of the angle of incidence or refraction. In the calculation, we selected a corner point of the **k**-point grid as a reference point, as shown in Fig. 5.12. The coordinate of the corner point A is k_{x0} and k_{z0}. Taking this point as a reference point, the

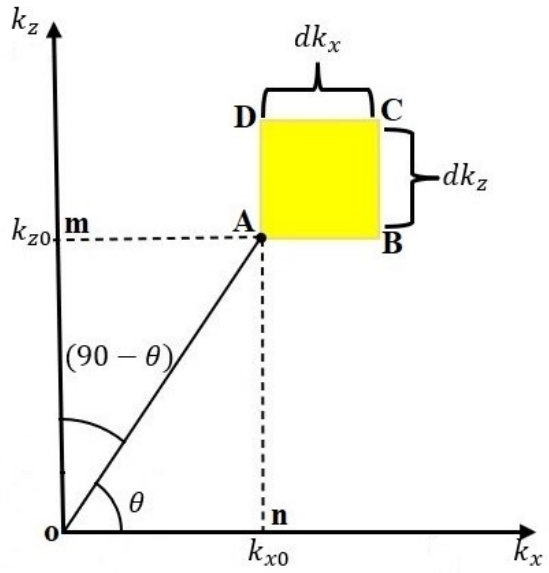

Figure 5.12: The pixel grid in Fourier domain. The size of the grid is dK.

angle of incidence can be written as, Eq.5.1

$$\theta_0 = \arctan\left(\frac{k_{z0}}{k_{x0}}\right). \tag{5.5}$$

But the angle of incidence with the normal of the boundary is

$$\theta = \frac{\pi}{2} - \theta_0. \tag{5.6}$$

We assume $u = \frac{k_{z0}}{k_{x0}}$. From Eq.5.5

$$\frac{d}{du}\arctan(u) = \left(\frac{1}{1+u^2}\right). \tag{5.7}$$

Let us take the derivative of $\arctan(u)$ in the x and z-directions, respectively.

$$\frac{d}{dk_{x0}}\arctan(u) = -\frac{1}{1+u^2}\frac{u}{k_{x0}^2}. \tag{5.8}$$

$$\frac{d}{dk_{z0}}\arctan(u) = \frac{1}{1+u^2}\frac{u}{k_{z0}}. \tag{5.9}$$

The Eq.5.8 gives the analytical error in x-direction and Eq.5.9 gives the analytical error in z-directions.

Let us consider the size of the pixel is dK. The size of the wave vector $\mathbf{k}$ pixel in x-direction is dk_x. and the size of the wave vector k pixel in the z-direction is dk_z.

But the numerical errors in finite differences for left and right side of point A are

$$x_1 = \arctan\left(\frac{k_{z0}}{k_{x0}+dK_x}\right) - \arctan\left(\frac{k_{z0}}{k_{x0}}\right). \tag{5.10}$$

$$x_2 = \arctan\left(\frac{k_{z0}}{k_{x0}-dK_x}\right) - \arctan\left(\frac{k_{z0}}{k_{x0}}\right). \tag{5.11}$$

The numerical errors in up and down of the reference point A are

$$y_1 = \arctan\left(\frac{k_{z0}+dK_z}{k_{x0}}\right) - \arctan\left(\frac{k_{z0}}{k_{x0}}\right). \tag{5.12}$$

$$y_2 = \arctan\left(\frac{k_{z0}-dK_z}{k_{x0}}\right) - \arctan\left(\frac{k_{z0}}{k_{x0}}\right). \tag{5.13}$$

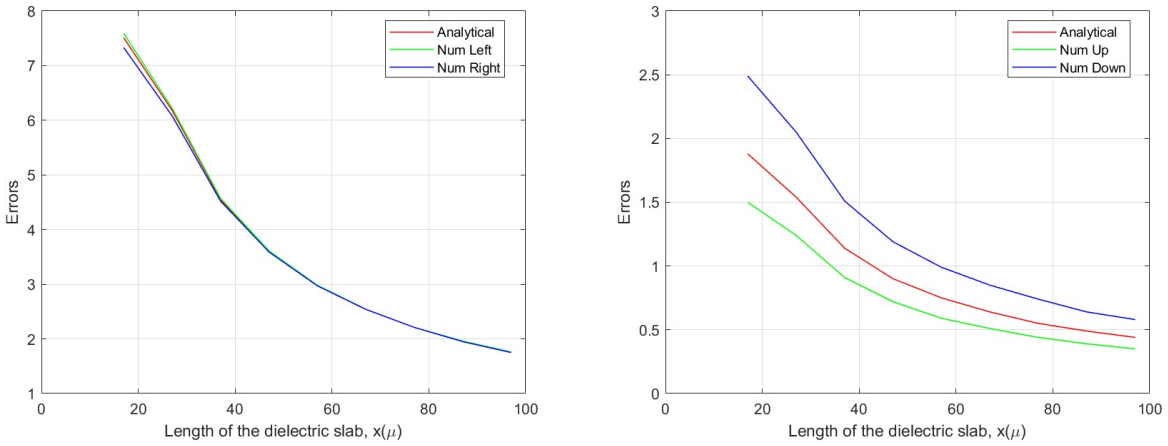

(a) (b)

Figure 5.13: Comparison between analytical error and numerical error. (a) Error to left and right side of the reference point and (b) Error to the up and down of the reference point with increasing length of the dielectric material.

Fig.5.13 shows the variation of errors with increasing the length of the dielectric material. The errors in the left and right side of the reference point A are decreasing with the increasing of the length of the dielectric medium, Fig.5.13a. The red line represents the analytical error, the blue line represents the error on the right side of the reference point A, and the green line represents the error on the left side of the reference point A. The analytical and numerical error converges after $40\mu m$. The variation of the error on the upper and lower ends of the reference point A are shown in Fig.5.13b. The red line represents the analytical error, and the blue line represents the error one step below the reference point A, and the green line represents the error one step above the reference point A. The analytical and numerical errors follow the same trendline, and a longer dielectric medium is needed for convergence.

CHAPTER VI

NUMERICAL ANALYSIS OF 2D PHOTONIC CRYSTALS

6.1 Design of Photonic Crystals

A 2D photonic crystals is made of a square lattice of circular dielectric rods in air. The permittivity of the circular rods is $\varepsilon = 8.9$, and the radius of the rods is $r = 0.35a$; here a is the lattice parameter. We considered the permeability of the dielectric rods $\mu = 1.0$. The PhC is extended on the xz-plane, as shown in Fig.6.1. The dark blue dielectric circles represent the dielectric materials. The structure has been drawn in RSoft CAD [34]. The Fig.6.1 shows the square dielectric crystals in the RSoft CAD interface.

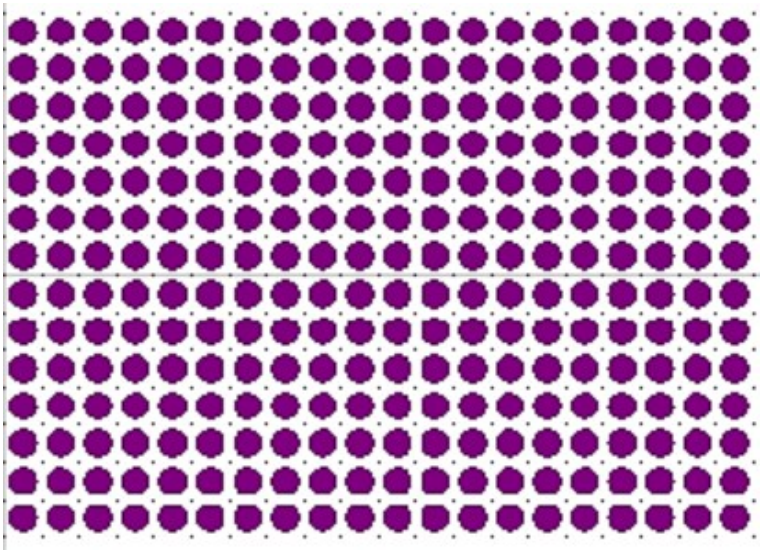

Figure 6.1: (a) Two-dimensional photonic crystals made from a square lattice of dielectric rods of $\varepsilon = 8.9$ embedded in air background. The radius of the rods, $r = 0.35a$, where a is the lattice parameter.

6.2 Reflection and Refraction in Photonic Crystals

The Finite-Difference Time-Domain (FDTD) [27] method included in FullWave package [34] is used to model the propagation of a plane electromagnetic (EM) wave through the 2D PhC. The simulation has been done in Yee's mesh grid [25] to compute the **E** and **H** field components at a point on the grid. The size of grid points is 0.01 in x and z-directions, and 10 grid points-per-wavelength (PPW) was taken for the calculation. To absorb the outgoing energy without reflections, the perfectly matched layer (PML) [31] boundary condition was used in x and $z-$ directions. The time step is selected as the Courant condition, which relates temporal and spatial step size, to obtain a stable simulation. The Courant condition is given by

$$c\Delta t < \frac{1}{\sqrt{1/\Delta x^2 + 1/\Delta y^2 + 1/\Delta z^2}}. \tag{6.1}$$

A plane EM wave has been sent from medium 1 (air) to medium 2 (2D PhC) at an angle with the normal incidence. The schematic diagram of the numerical simulation is shown in Fig.6.2. There are two types of polarizations are considered - *Transverse Electric* (TE) and *Transverse Magnetic* (TM). In the case of TE, the electric field (**E**) of the incident wave is perpendicular to the plane of incidence. For TM, the magnetic field (**H**) of the incident wave is perpendicular to the plane of incidence.

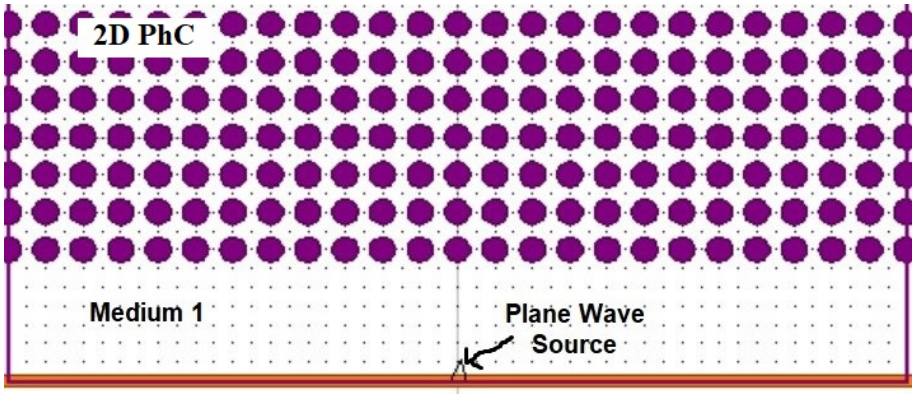

Figure 6.2: Two-dimensional photonic crystals made of square lattice of dielectric rods having dielectric $\varepsilon = 8.9$ in air background (RSoft CAD interface). The radius of the rods is $r = 0.35a$.

Depending upon the frequency of the incident wave, periodicity and band structure, a finite number of phenomena such as reflection, refraction, or Bragg-diffraction could happen in the photonic crystals [35]. With these phenomena, additional diffractive reflection and refraction could have occurred. All these phenomena can be explained with the help of wave vector **k**.

Suppose that the periodicity parallel to the interface is a, and the components of incident wave vectors $\mathbf{k}_{\parallel}, \mathbf{k}_{\perp}$, and frequency ω. For any integer m,

$$\frac{n_i^2\omega^2}{c^2} = k_{\perp}^2 + \left(m\frac{2\pi}{a}\right)^2. \tag{6.2}$$

Here, n_i is the index of refraction of the incident medium, $k_{\parallel}$ and $k_{\perp}$ are the components of wave vector **k** parallel and perpendicular to the interface, respectively. And a is the periodicity of the crystals. For m=0, Eq.6.2 yields

$$\frac{n_i^2\omega^2}{c^2} = k_i^2 = k_{\parallel}^2 + k_{\perp}^2. \tag{6.3}$$

For reflected wave

$$k_r^2 = k_{\parallel}^2 + (k'_{\perp})^2. \tag{6.4}$$

Applying the law of reflection, Eq.6.2 and Eq.6.3 yields

$$k'_{\perp} = \pm k_{\perp}. \tag{6.5}$$

But the reflected wave must be propagate away from the interface. So, the refracted wave vector **k** will be, $k'_{\perp} = -k_{\perp}$.

$$k'_{\perp} = -k_{\perp}.$$
$$\text{or}, k'_{\perp} = -\sqrt{\frac{n_i^2\omega^2}{c^2} - k_{\parallel}^2}. \tag{6.6}$$

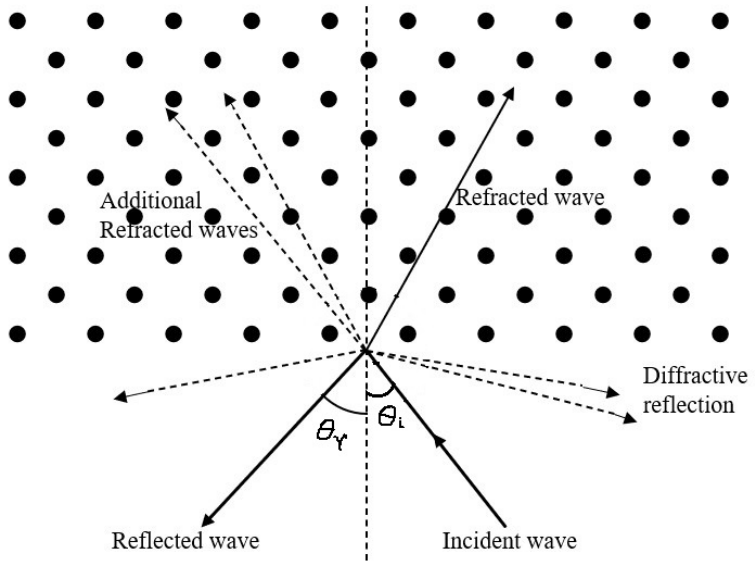

Figure 6.3: Reflection, refraction, and diffraction phenomena in photonic crystals.

For the diffractive reflection, $m \neq 0$. From Eq.6.2 and Eq.6.6 we can write,

$$k'_{\perp} = -\sqrt{\frac{n_i^2\omega^2}{c^2} - \left(k_{\parallel} + m\frac{2\pi}{a}\right)^2}. \tag{6.7}$$

When ω is too small, or if m is too large, then Eq.6.7 will be *imaginary*, corresponding to an evanescent field that decays exponentially away from the interface.

The non-evanescent diffractive reflection will occur at m, when

$$\omega > \frac{c}{n_i}\left|k_{\parallel} + \frac{2\pi m}{a}\right|. \tag{6.8}$$

If θ_i is the angle of incidence, then

$$k_i = \frac{\omega}{c}\sin\theta_i. \tag{6.9}$$

Here $\theta_i \geq 0$. The first diffractive reflection will occur at $m = -1$, and

$$\frac{\omega a}{2\pi c} = \frac{a}{\lambda} > \frac{1}{n_i(1+\sin\theta_i)}. \tag{6.10}$$

Here ω is the angular frequency, λ is the free space wavelength, n_i is the refractive index of the

incident medium, and θ_i is the angle of incidence.

The reflection of light in PhC can explain the refraction phenomenon. In the case of refraction, the information of the waves propagating in the crystals, the component of **k** vector parallel to the interface, $k_{\|} + 2\pi m/a$, and the direction of the group velocity, $v_g = \nabla_k \omega$ are required. The EFS contour gives the available state of $\omega(\mathbf{k})$. The group velocity $v_g = \nabla_k \omega$ is perpendicular to the ω contour and points toward increasing ω for the positive index of refraction materials.

According to the conservation law, the wave vectors **k** parallel to the interface between two media (air-PhC) are conserved.

$$k_i = k_{\|} + \frac{2\pi m}{a}. \tag{6.11}$$

For refraction, using $m = 0$ in Eq.6.11 and the conservation of wave vector **k** gives,

$$k_i = k_{\|}. \tag{6.12}$$

Now, putting the components of k_i and k_r in Eq.6.12 yields

$$\frac{n_i \omega}{c} \sin\theta_i = \frac{n_{\text{eff}} \omega}{c} \sin\theta_r. \tag{6.13}$$

From Eq.6.13, the effective index of refraction of the photonic crystals is given by

$$n_{\text{eff}} = \frac{n_i \sin\theta_i}{\sin\theta_r}. \tag{6.14}$$

Here n_i is the refractive index of the incident medium, θ_i is the angle of incidence, θ_r is the angle of refraction, and n_{eff} is the effective index of refraction of the PhC.

6.3 Band Structure of Photonic Crystals

We need band structures to study the propagation of EM waves in the PhC. We used Plane Wave Expansion Method (PWEM) [32] embedded in the BandSOLVE package [33] to obtain the band structure of 2D PhC. We calculated the first 4 bands of both TE and TM polarization. The

eigenvalue tolerance was set to 1.0×10^{-8} for the best optimal resolution and accuracy of the results. The first Brillouin (FBZ) zone of the 2D photonic crystals is shown in Fig.6.4. The FBZ is the region in a reciprocal space consisting of all points closer to the origin than any other reciprocal lattice vectors. The symbols Γ, X, and M represent the higher symmetry directions of the square lattice, which represent the wave vectors $\mathbf{k}$ that correspond to the point on the FBZ surface along that particular direction. In the FBZ, Γ represents the center of the FBZ, X is the center of the edge, and M is the corner point. The region $\Gamma - X - M - \Gamma$ is called the irreducible Brillouin zone (IBZ). All points within the FBZ can be mapped to on points within the IBZ by symmetry operations. The

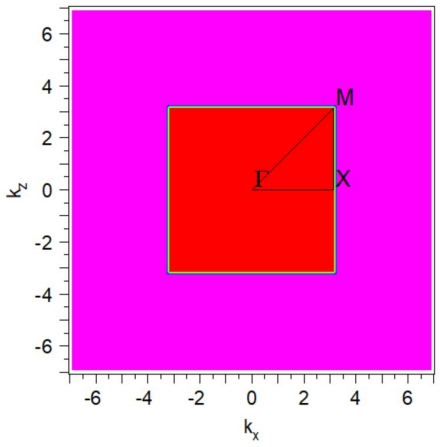

Figure 6.4: The first Brillouin zone, a region in a reciprocal space consisting of all points closer to the origin than to any other reciprocal lattice vector. Here, Γ represents the center of the FBZ, X is the center of the edge, and M is the corner point. The region $\Gamma - X - M - \Gamma$ is called the irreducible Brillouin zone.

first four band structure of TE and TM polarization is shown in Fig.6.5. The vertical axis of the band structure represents the normalized frequency $\omega a/2\pi c = a/\lambda$ which is dimensionless. The horizontal axis represents the higher symmetry points in the FBZ. In this case of TE, the band gap was found in the range normalized frequencies $\Omega = 0.42 - 0.49$ and $\Omega = 0.24 - 0.29$. On the other hand, the band gap was not found in TM polarization, Fig.6.5b. The iso-surface for the TE and TM polarization is shown in Fig.6.6.

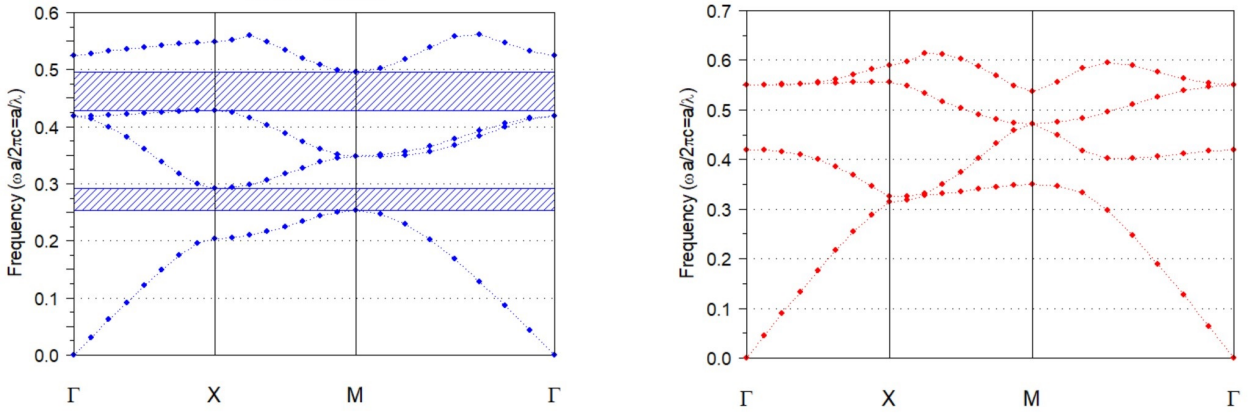

Figure 6.5: Band structure for (a) TE and (b) TM polarization in the PhC. The dielectric constant of the square lattice is 8.9 embedded in air background. The radius of the rods is $r = 0.35a$. The vertical axis is the dimensionless normalized frequency $(\omega a/2\pi c = a/\lambda)$ and horizontal axis is the higher symmetry point in the first Brillouin zone.

6.4 Equifrequency Surfaces and their Cross-Sections

To study the refraction properties of the light through PhC, the proposed structure's EFS diagram is obtained using the PWE method. The dispersion diagram of 2D PhC is show in Fig.6.6, Fig.6.7a, and Fig.6.8. Each diagram consists of several surfaces stacked vertically in the ω direction. That means the dispersion diagram for 2D PhC consists of a family of surfaces that represent the multivalued function $\omega = \omega(\mathbf{k})$, where the intersections of a constant k-line with different surfaces corresponds to particular modes at different frequencies within the lattice. The dispersion diagram of the first four bands of a square lattice is shown in Fig.6.6. For comparison, we have calculated the first four bands of the PhC and the first four EFS diagrams of TE and TM polarization are shown in Fig.6.7 and Fig.6.8. The EFS contours give the allowed frequency for light propagation through the photonic crystals. From the band diagram (Fig.6.5a) and EFS plots (Fig.6.7), it is clear that the range of frequencies $0.24-0.29$, and $0.42-0.49$ in 2D PhC give the forbidden mode for light propagation.

We can determine the direction of propagation of the incident wave in the PhC using contour maps. The direction of propagation of the incident wave coincides with the direction of the group

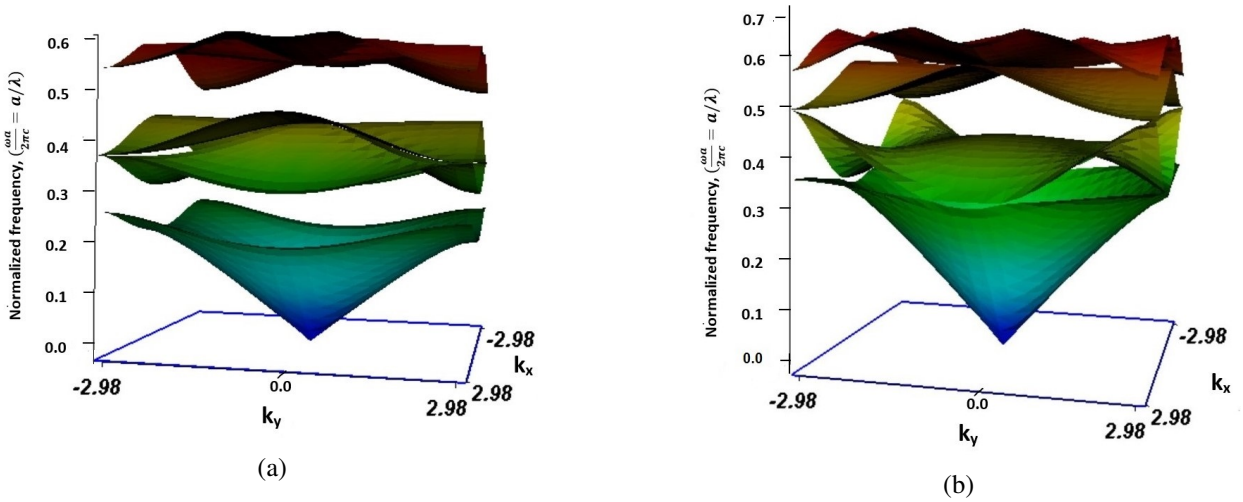

Figure 6.6: The dispersion surface diagram for (a) TE and (b) TM polarization in the PhC. The dielectric constant of the square lattice is 8.9 embedded in air background. The radius of the rods is $r = 0.35a$. The vertical axis is the dimensionless normalized frequency $(\omega a/2\pi c = a/\lambda)$ and horizontal axis is the higher symmetry point in the first Brillouin zone. The dispersion surfaces show the relation $\omega = \omega(\mathbf{k})$ in the 2D PhC.

velocity, $\mathbf{v}_g$. The group velocity, $\mathbf{v}_g = \nabla\omega_k$, for a given Bloch mode is characterized by wave vector $\mathbf{k}$ is parallel to the EFS normal at this $\mathbf{k}$ point. So, with increasing outward frequency, $\mathbf{v}_g \cdot \mathbf{k} > 0$ and the direction of v_g is outward along ΓX direction, corresponding to the positive index for 2D PhC. For the rest of the bands of TE (Fig.6.7b-Fig.6.7d) and TM (Fig.6.8b-Fig.6.8d) polarization, the EFS contour lines are moving outward with increasing normalized frequencies. In that case, $\mathbf{v}_g \cdot \mathbf{k} < 0$, the group velocity, $\mathbf{v}_g$ is anti-parallel to wave vector $\mathbf{k}$, corresponding to the negative index of refraction.

The EFS contours are centered around ΓX line in the FBZ. In the case of TE (Fig.6.7a) and TM (Fig.6.8a) polarization for band 0, all the EFS contour lines are circular and moving outward from the center with increasing normalized frequencies. In this case, the PhC behaves like a homogeneous one, and its effective index is positive. Beyond the first band, the PhC is not homogeneous, and light scatters for the allowed frequency bands.

6.5 Modeling of EM Waves in Photonic Crystals

We have used the FDTD method [27] to model the propagation of a plane EM wave through the PhC with a Perfectly Matched Layer (PML) [29] to absorb the outgoing waves. We chose

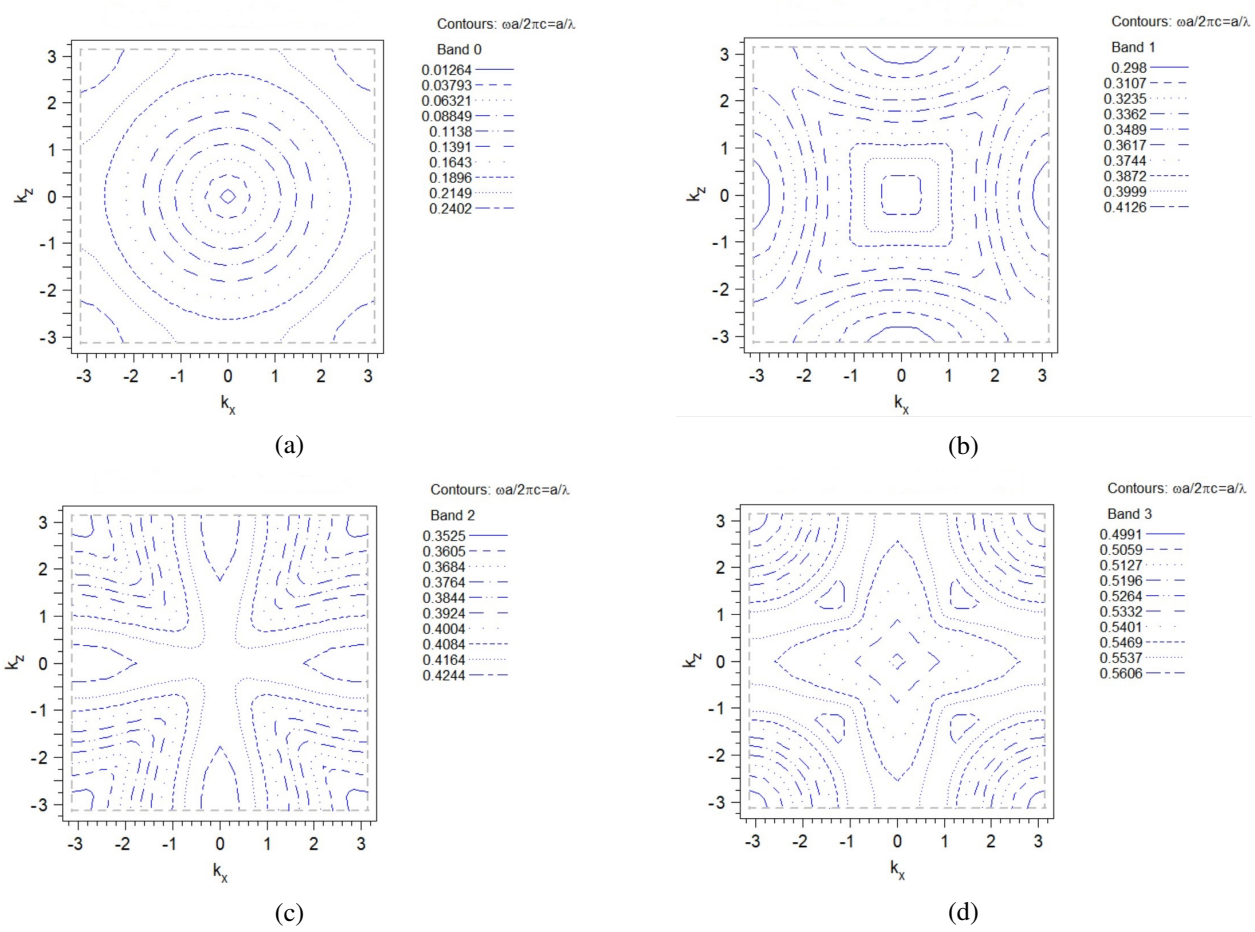

Figure 6.7: The first four EFS contours of TE polarization. The EFS contours can be found by intersecting constant frequency plane with the dispersion surface.

the normalized frequency (wavelength) of the plane EM wave from the cross-sections of the EFS contours. The plane EM wave was sent at an angle of 10°, 15°, 20°, 25°, 30°, 35°, 40°, and 45° degrees with respect to the normal of incidence of the air-PhC. We took the same values of angle of incidence for both TE and TM polarization.

At first, we studied the diffractive reflection in air-PhC for both TE and TM polarization using the Eq.6.10. The index of refraction for air, $n_i = 1.0$. For angle of incidence $\theta_i = 10$, a/λ is

$$\frac{a}{\lambda} = \frac{1}{n_i(1+\sin 10^\circ)} = 0.85 \tag{6.15}$$

But the normalized frequency $\frac{\omega a}{2\pi c} = 0.16$. From Eq.6.15, *normalized frequency*< 0.85. Similarly,

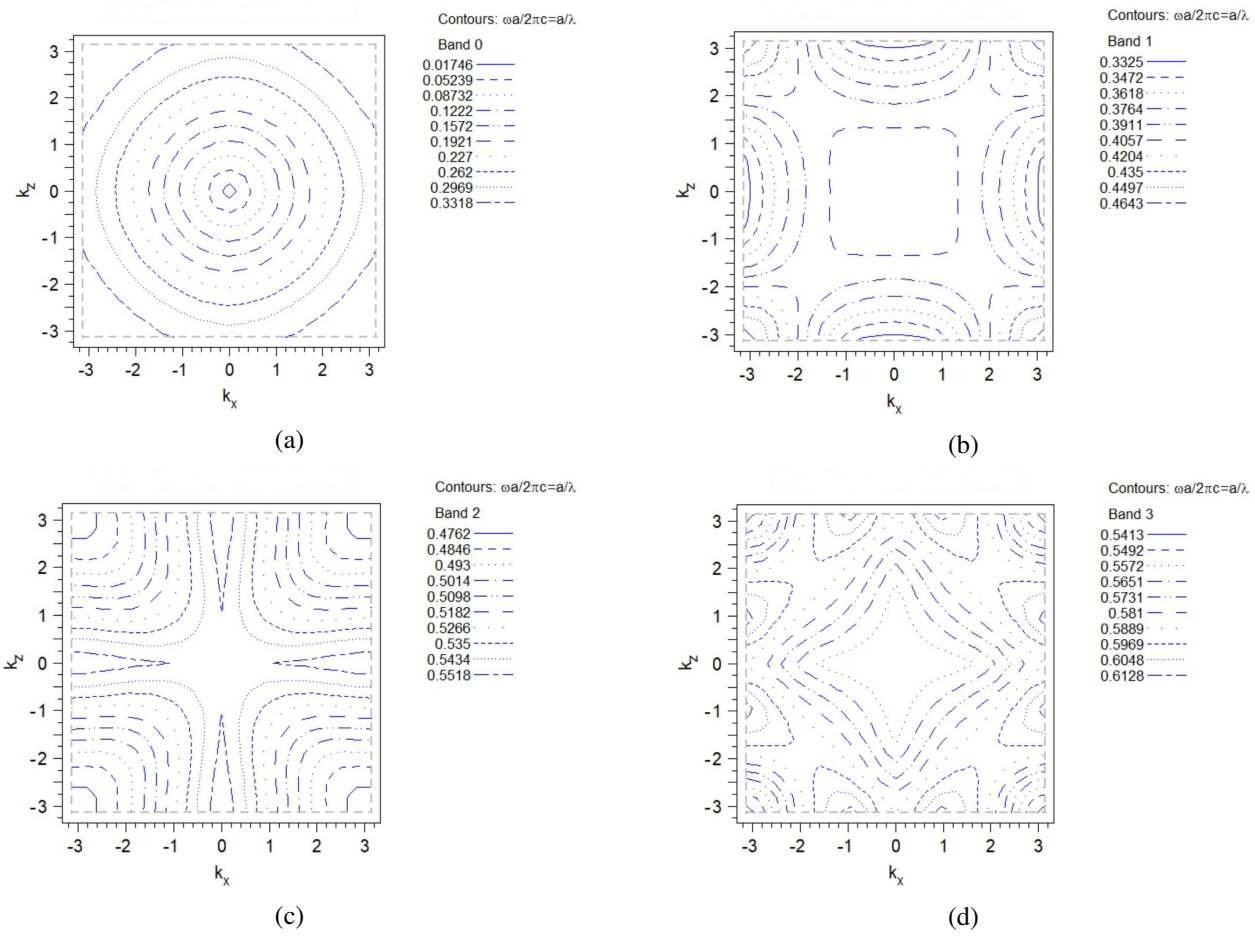

Figure 6.8: The first four EFS contours of TM polarization. The contours can be found by intersecting constant frequency plane with the dispersion surface. (c) Band 2 and (d) Band 3.

for the angle of incidence of 45°, *normalized frequency* < 0.58. In this calculation, the angle of incidence between 10° to 45° Eq.6.10 is not satisfied. Therefore, the diffractive reflection from the PhC interface is not possible. Therefore, the non-evanescent diffractive reflection is not possible for an air-PhC single boundary. The plane EM only reflected away from the air-PhC interface.

TE polarization:

For TE polarization, the components of **E**-field is **E** = *E(x,0,z)*. The direction of **E**-field is in *y*-direction. According to the boundary conditions and Maxwell's equation, the tangential components of the **H**-field, H_x is continuous at the interface of two media. The color map of TE mode for the first band at normalized frequency 0.16 is shown in Fig.6.9 at a different angle of incidence. The amplitude of the incident wave splits into two parts at the boundary of the air-PhC interface- one

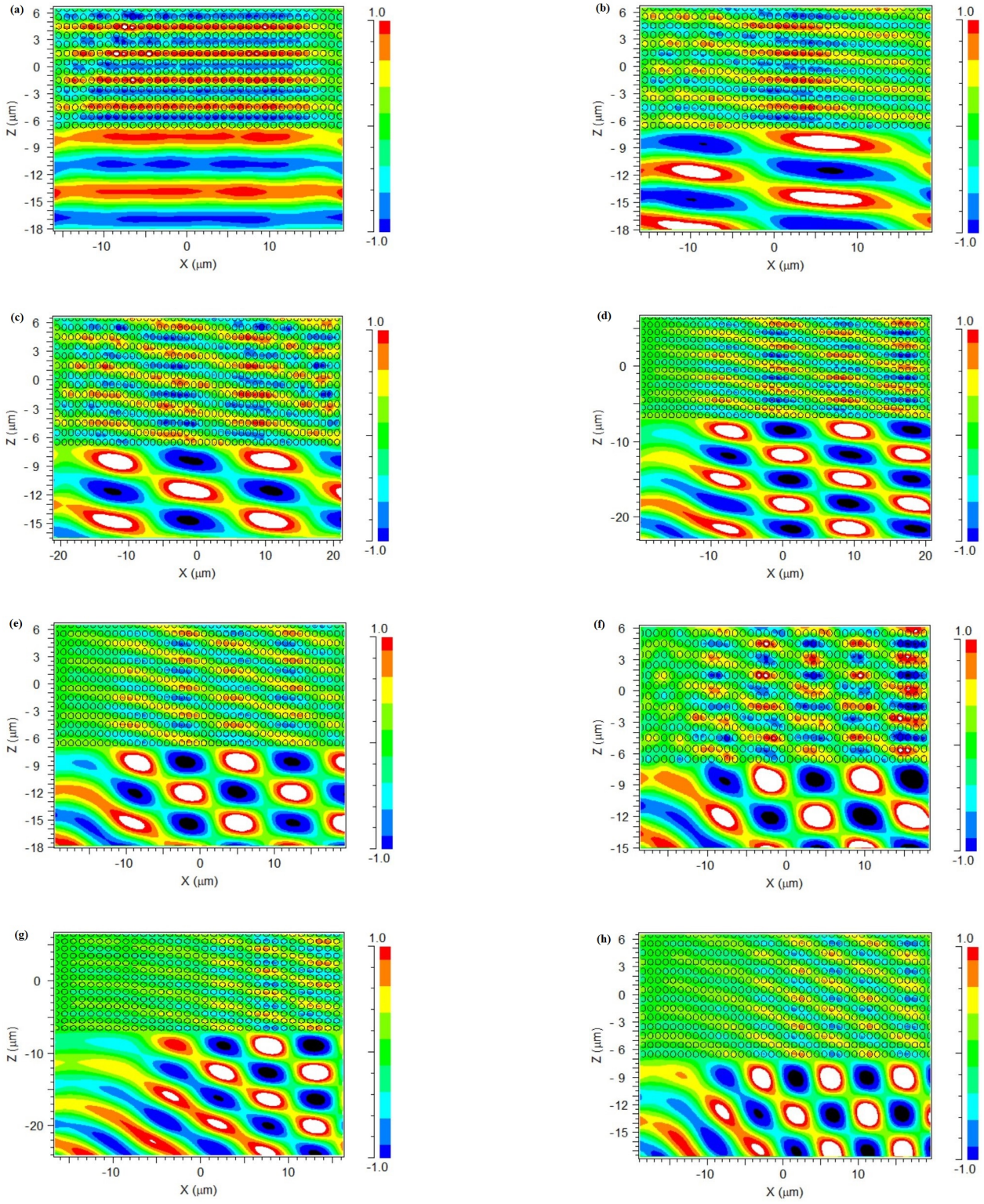

Figure 6.9: Band 0: TE Color map at (a) 0° (b) 10° (c) 15° (d) 20° (e) 25° (f) 30° (g) 35°, and (h) 40°. The normalized frequency of the incident wave is $\Omega = 0.1642$.

part is reflected from the interface, and another is refracted through the PhC. In Fig.6.9, the lower part of the color map shows the sum of the incident amplitude and reflected **E**-field, and the upper region represents the refracted field. The color bar represents the strength of **E**-field. The red color represents the positive **E**-field, the blue color represents the negative **E**-field, and the green color represents the neutral region.

In the lower region of the air-PhC interface, the incident and reflected waves superimpose each other constructively or destructively. During the constructive superposition, the resultant E-field for TE polarization increases. The white region in the red line on the contour map shows the constructive superposition of the incident and reflected waves. In contrast, the dark blue color indicates the destructive superposition in the lower region of the air-PhC system. On the other hand, inside the PhC, the plane EM wave refracted after crossing the air-PhC interface.

To determine the effective index of 2D PhC, we need the angle of refraction of the propagating plane EM wave in that medium. The angle of incidence and index of refraction of the first medium (air) is known. We need to determine the angle of refraction in the PhC. We have determined the angle of refraction in 2D PhC using the method described in ChapterV. The wave vector **k** of the refracted wave is parallel to the air-PhC interface. The angle of the wave vector **k** is calculated in the FBZ of the PhC. Snell's law is applicable in the FBZ. The effective index of refraction of the PhC has been calculated using Eq.6.11. The values of incidence angle, angle of refraction, and the effective index of refraction for Band 0 and TE polarization have been reported in Table.6.1. The 2D PhC has an average effective index of 2.0 in Band 0. We found the positive refraction in 2D PhC, which acts as a homogeneous material.

In Band 1, we used a plane EM wave of normalized frequency 0.3489 ($2.87\mu m$) to model light propagation through the PhC using the FDTD method. We found the positive refraction in PhC for the range of frequencies of Band 1. The color map of the electric field for TE polarization in Band 1 is shown in Fig.6.11. For Band 1 of TE polarization, we determined the effective index of the 2D PhC using the similar method described in Chapter.V. In Band 1, the PhC has average effective index in the range of 2.0, as shown in Fig.6.13b.

Table 6.1: Band 0: TE-mode. Data for effective index of refraction, n_{eff} for different angle of incidence in 2D PhC at normalized frequency $\Omega = 0.1642$ ($\lambda = 6.09\mu m$). The angle of incidence, θ_i and angle of refraction, θ_r are in degree. The effective refractive index of refraction, n_{eff} is dimensionless parameter.

No.	θ_i		θ_r	n_{eff}
	Theoretical	Numerical		
1.	10	10.01	5.04	1.98
2.	15	15.31	7.80	1.95
3.	20	19.97	8.27	2.37
4.	25	25.05	13.15	1.86
5.	30	30.03	13.91	2.08
6.	35	34.97	15.63	2.13
7.	40	39.97	19.76	1.90

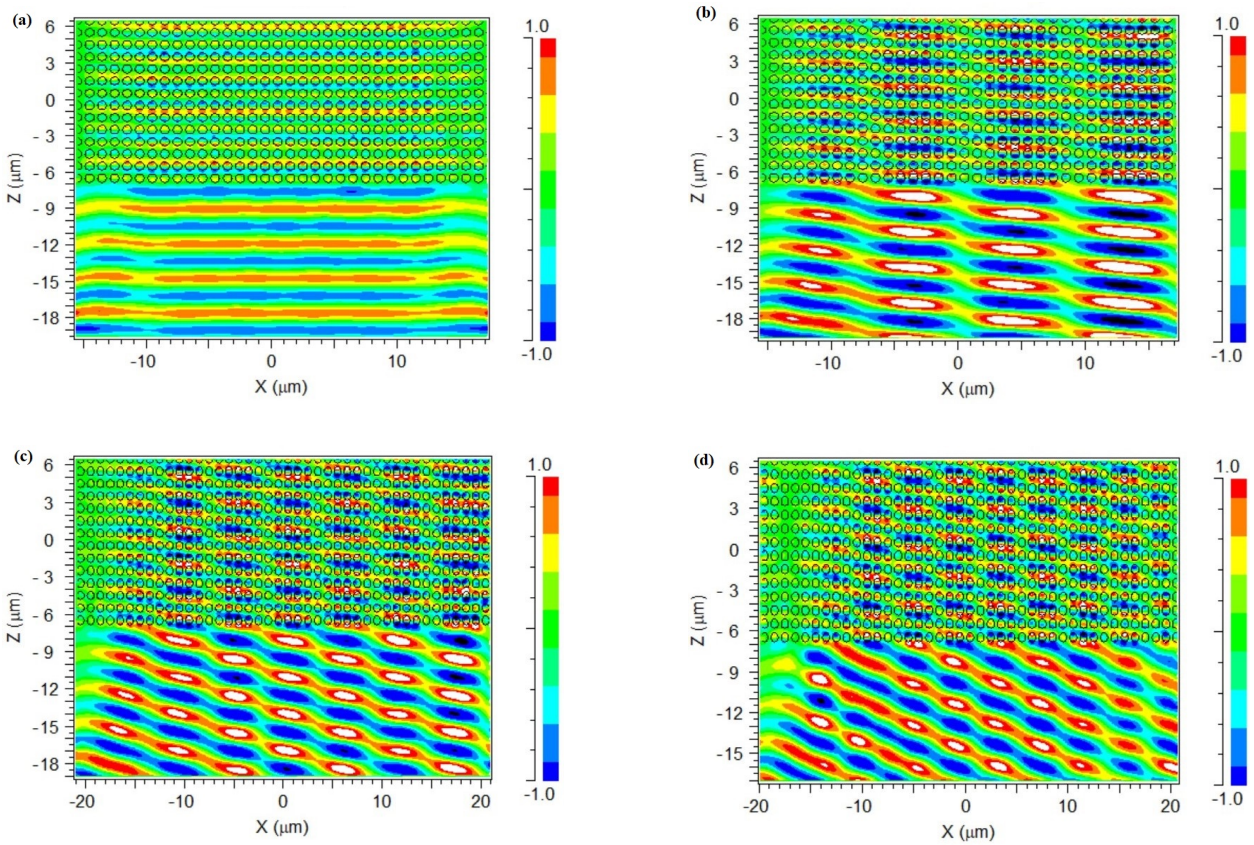

Figure 6.10: Band 1: TE. Contour map of electric field at (a) 0 ◦ (b) 10 ◦ (c) 15 ◦ (d) 20 ◦ (e) 25 ◦ (f) 30 ◦ (g) 35 ◦ , and (h) 40 ◦ . The normalized frequency of the incident wave is Ω = 0.3489.

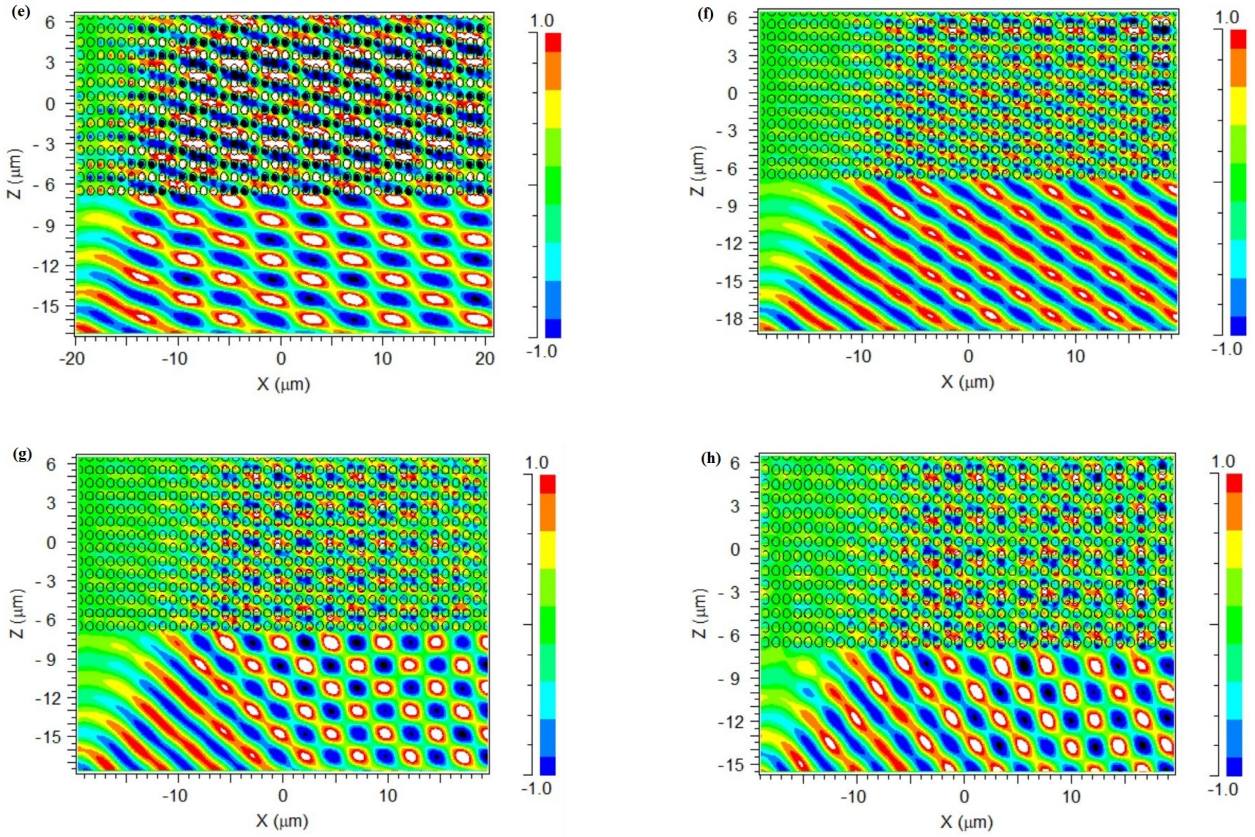

Figure 6.10, continued.

For Band 1 of TE polarization, the data for angle of refraction and effective index of 2D PhC for different angle of incidence is shown in Table.6.2.

Table 6.2: Band 1: TE-mode. Data for effective index of refraction, n_{eff} for various angle of incidence in 2D photonic crystals at normalized frequency, $\Omega = 0.3489$ ($\lambda = 2.87\mu m$). The angle of incidence θ_i and angle of refraction, θ_r are in degree units. The effective index of refraction, n_{eff} is dimensionless.

No.	θ_i		θ_r	n_{eff}
	Theoretical	Numerical		
1.	10	9.83	5.94	1.65
2.	15	15.17	7.72	1.95
3.	20	19.98	9.71	2.03
4.	25	25.23	12.50	1.97
5.	30	29.72	14.27	2.01
6.	35	35.23	16.21	2.07
7.	40	40.24	18.69	2.01

TM Polarization

For TM polarization, the direction of the magnetic field is along y-direction. The component of the magnetic field **H** is $H(x,0,z)$. According to Maxwell's boundary condition, the electric field is continuous along the interface between air-PhC. For Band 0 of TM polarization, we used the normalized frequency 0.3318 ($\lambda = 3.01$ micron) to model the propagation of a plane EM wave through 2D PhC using the FDTD method. The color map of the magnetic field for TM polarization for different angles of incidence is shown in Fig.6.11. In the lower region of the colormap contains the incident and reflected waves, and their superposition gives constructive and destructive interference. The upper region of the colormap shows the refracted wave in the PhC. The magnetic field intensity is maximum for constructive interference and minimum for destructive interference. The white circles in the red background represent the higher intense magnetic field region, and the black circles in the blue background represent the lower intense magnetic field region. The angle of refraction of the

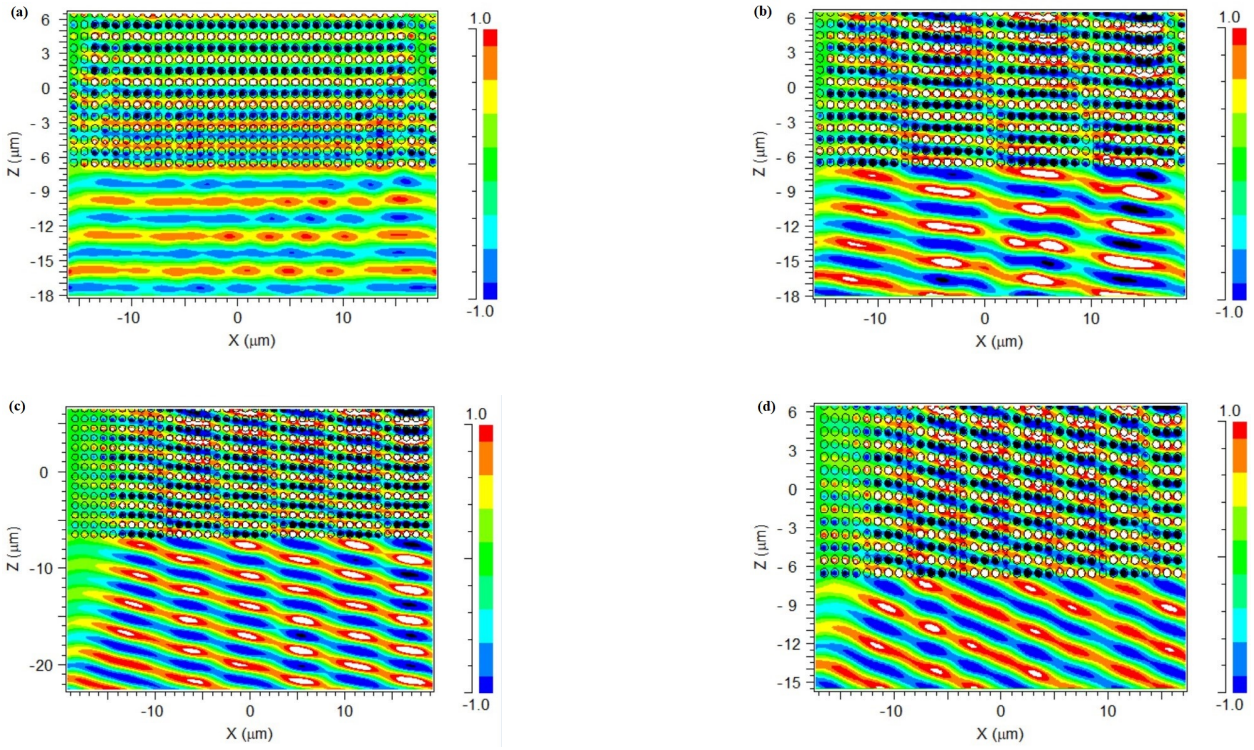

Figure 6.11: Band 0: TM. Contour map of electric field for TM polarization in the PhC (a) 0° (b) 10° (c) 15° (d) 20° (e) 25° (f) 30° (g) 35°, and (h) 40°. The normalized frequency of the incident plane wave is 0.3318.

2D PhC for TM polarization has been determined using a similar method as for TE polarization.

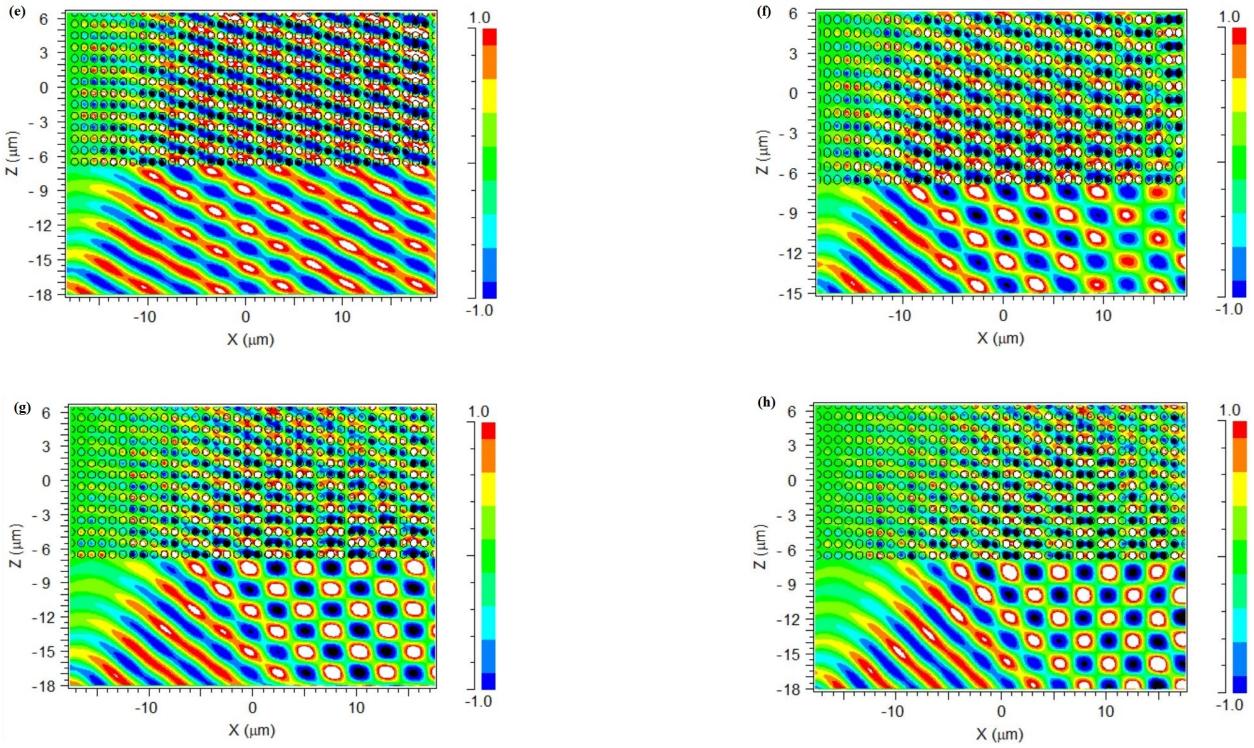

Figure 6.11, continued.

The effective index of the 2D PhC for Band 0 of TM polarization has been determined using Eq.6.11. The data for the angle of refraction and effective index of 2D PhC for different angles of incidence are shown in Table.6.3.

Table 6.3: Band 0: TM-mode. Data for effective index of refraction, n_{eff} for various angle of incidence in 2D photonic crystals at normalized frequency, $\Omega = 0.3319$ ($\lambda = 3.01\mu m$). The angle of incidence θ_i and angle of refraction, θ_r are in degree. The effective index of refraction, n_{eff} is dimensionless parameter.

No.	θ_i		θ_r	n_{eff}
	Theoretical	Numerical		
1.	10	10.01	6.20	1.61
2.	15	14.36	8.73	1.63
3.	20	20.07	13.09	1.51
4.	25	24.90	15.15	1.61
5.	30	30.03	13.91	2.08
6.	35	34.97	15.63	2.12
7.	40	39.99	17.46	2.14

In Band 0, we found the positive refraction in 2D PhC. In the case of TM polarization, the effective index of refraction varies with the angle of incidence, as shown in Fig.6.13a. In the FDTD calculation for Band 0, we found the positive refraction of the incident plane EM wave in the PhC. The PhC has an average index of refraction in the range of 1.8 for TM polarization.

In Band 1 of TM polarization, we set the normalized frequency 0.3618 ($2.76\mu m$) for the plane EM wave and sent it through the PhC for different angles of incidence, as shown in Fig.6.12. For this wavelength in FDTD calculation, we also found positive refraction in the PhC, Fig.6.12. We have calculated the effective index of refraction 2D PhC for TM polarization in Band 1. The data for the angle of refraction for different angles of incidence and the effective index of refraction of the PhC are shown in Table.6.4. The average effective index of refraction is in the range of 1.65 for the TM polarization of Band 1.

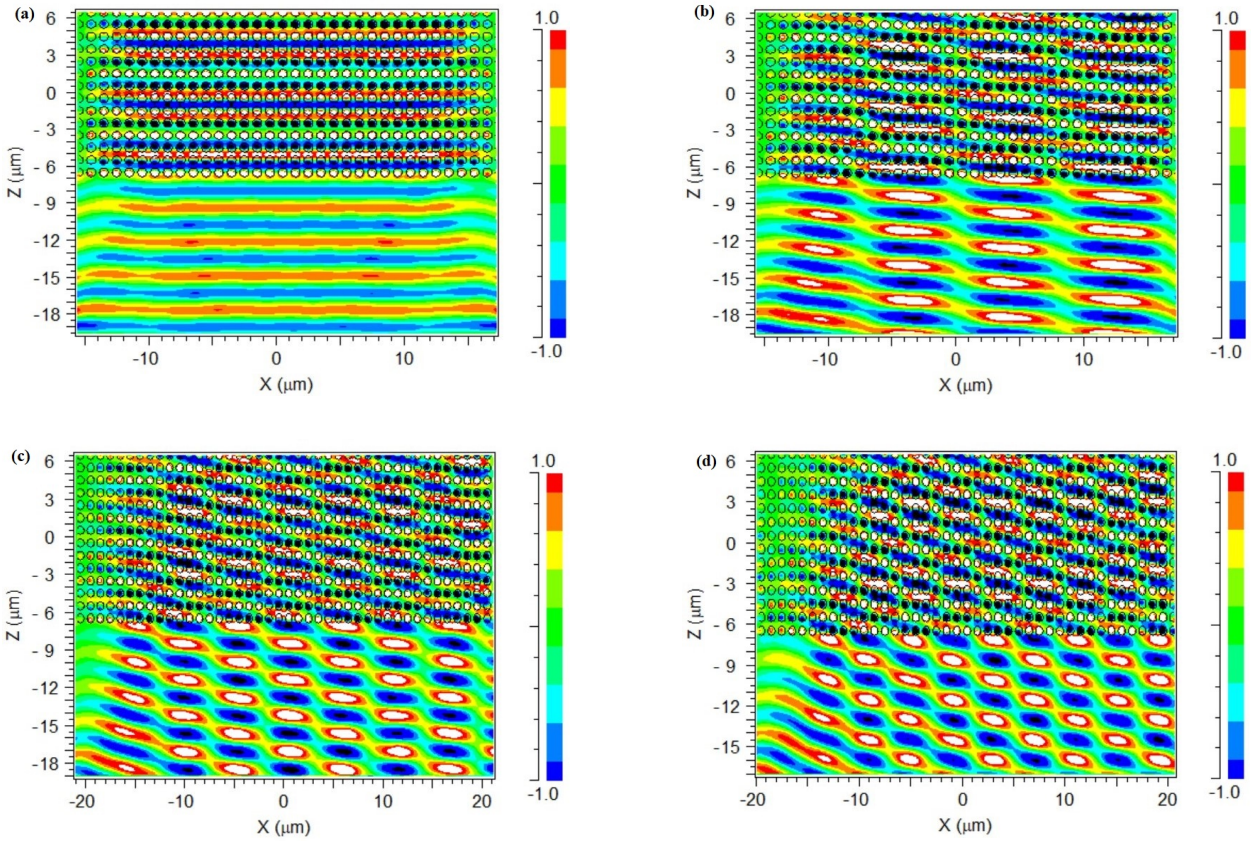

Figure 6.12: Band 1: TM. Contour map of electric field for TM polarization in the PhC at (a) 0° (b) 10° (c) 15° (d) 20° (e) 25° (f) 30° (g) 35°, and (h) 40°. The normalized frequency for the incident wave is $\Omega = 0.3618$.

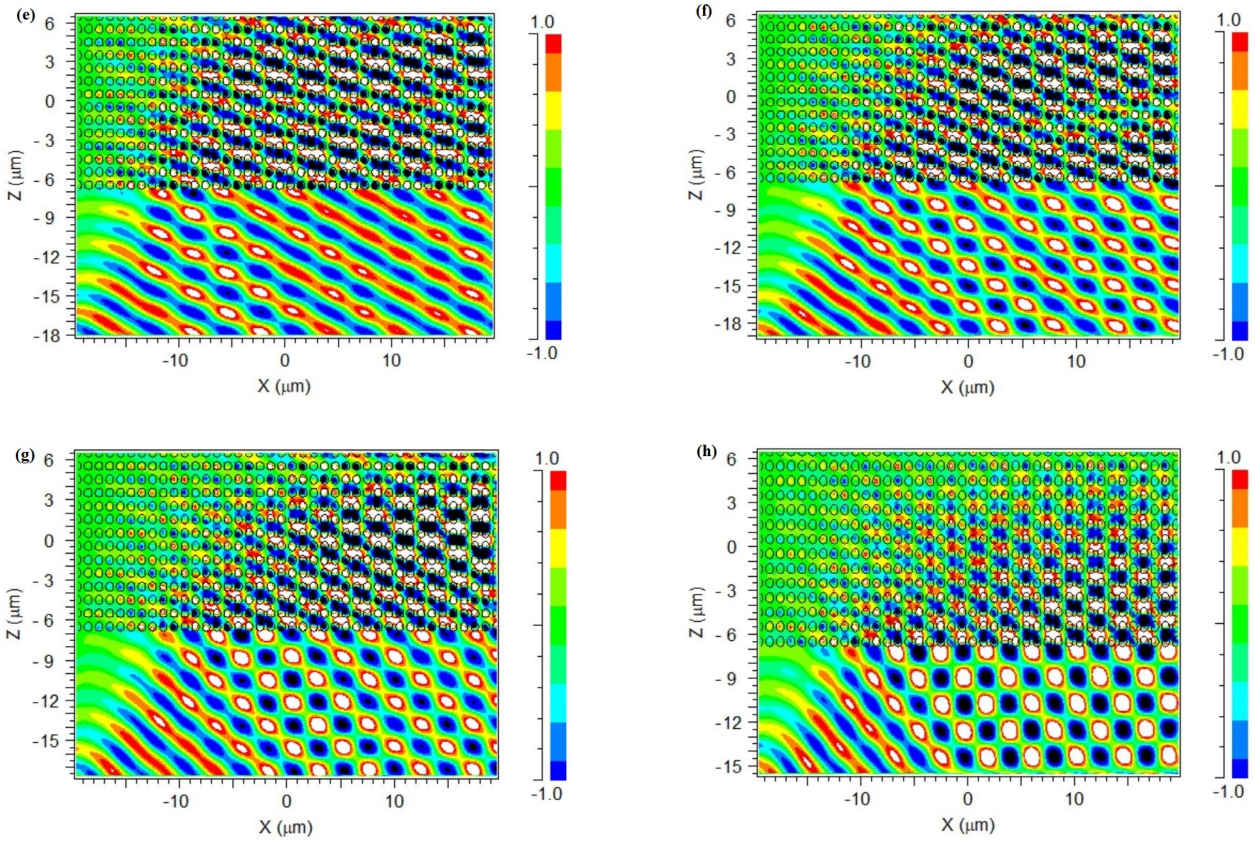

Figure 6.12, continued.

Table 6.4: Band 1: TM-mode. Data for effective index of refraction, n_{eff} for various angle of incidence in 2D photonic crystals at normalized frequency, $\Omega = 0.3618$ ($\lambda = 2.76\mu m$). The angle of incidence θ_i and angle of refraction, θ_r are in degree. The effective index of refraction, n_{eff} is dimensionless parameter.

No.	θ_i		θ_r	n_{eff}
	Theoretical	Numerical		
1.	10	10.02	5.66	1.76
2.	15	15.45	9.42	1.63
3.	20	19.98	11.74	1.68
4.	25	25.23	15.07	1.64
5.	30	29.77	16.97	1.70
6.	35	35.23	20.82	1.62
7.	40	40.16	24.71	1.54

The comparison between the effective index of refraction for TE and TM polarization is shown in Fig.6.13. The effective index of refraction in Band 0 for TE and TM polarization is shown in Fig.6.13a. The In Fig.6.13, we can see that the effective index of 2D PhC varies with the angle of

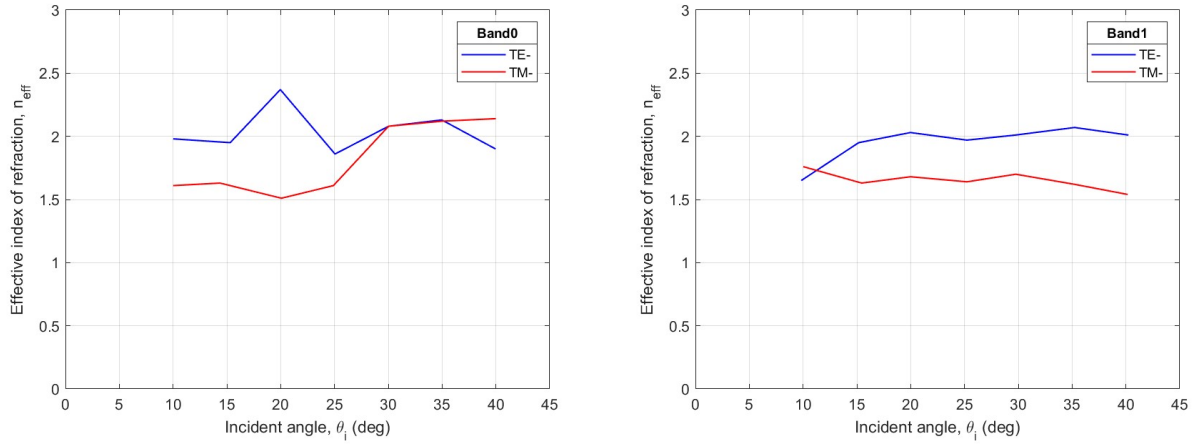

(a) (b)

Figure 6.13: The effective index of refraction, n_{eff} for various angle of incidence in 2D PhC. The blue and red line represents the effective index of refraction for TE and TM polarization, respectively, for (a) Band 0 and (b) Band 1.

incidence of the plane EM waves. In band 0 of TE polarization, the effective index scatters around the value 2.0. for TM polarization, the effective index remains nearly constant up to the angle of incidence of 25 degrees. After that, the effective index starts increasing with increasing the value of the angle of incidence. On the other hand, for band 1 of TE polarization, the PhC has an average effective index in the range of 2.0. For TM polarization of band 1, the average effective index of PhC is in the range of 1.65.

The reason for variation in the effective index is the number of pixels present in the incident and refracted fields. We used the finite-difference method to determine the angle of incidence and refraction in the 2D PhC. In this method, the number of pixels in the fields affects the angles, which affects measurements for the effective index of refraction. When the number of pixels increases, the errors in calculating angles become less; therefore, the error can be minimized for a larger number of pixels.

CHAPTER VII

CONCLUSION

Photonic crystals are interesting structured materials that are currently available for research. In this research, we focused on 2D photonic crystals. We used FDTD, PWE, fft2, and MATLAB to determine the effective index of refraction. A plane EM waves have been used to model the propagation of light in the photonic crystals using the FDTD method. The frequency of the incident plane EM waves has been taken from the first two bands of photonic crystals for both polarization. We studied the refraction phenomenon near Γ symmetry points for TE and TM polarization. A part of the incident field is reflected from the boundary of the air-Photonic crystals, and another part is refracted through the photonic crystals. The incidence and the refraction angle have been calculated in the Fourier domain. The effective index of refraction has been calculated by using Snell's law.

In this work, we applied a new method to determine the effective index of refraction of 2D photonic crystals. We studied the effective index of refraction as a function of the angle of incidence of the incident field for TE and TM polarization. In the case of the first band of TE and TM polarization, we found that the effective index varies with the angle of incidence. On the other hand, the effective index of refraction remains constant with the angle of incidence in the second band for TE and TM polarization. The 2D photonic crystals behave as a homogeneous material in the first band. Furthermore, the effective index of refraction depends on the polarization of the incident field. The effective index of refraction is different for TE and TM polarization. We also found that the effective index depends on the band structure of 2D polarization.

REFERENCES

[1] V. P. Bykov, "Spontaneous emission in a periodic structure," *Soviet Journal of Experimental and Theoretical Physics*, vol. 35, no. 2, pp. 269–273, 1972.

[2] V. P. Bykov, "Spontaneous emission from a medium with a band spectrum," *Soviet Journal of Quantum Electronics*, vol. 4, no. 7, pp. 861–871, 1975.

[3] E. Yablonovitch, "Inhibited spontaneous emission in solid-state physics and electronics," *Physical Review Letters*, vol. 58, no. 20, pp. 2059–2062, 1987.

[4] S. John, "Strong localization of photons in certain disordered dielectric superlattices," *Physical Review Letters*, vol. 58, no. 23, pp. 2486–2489, 1987.

[5] E. Yablonovitch, T. J. Gmitter, and K. M. Leung, "Photonic band structure: The face-centered-cubic case employing nonspherical atoms," *Physical Review Letters*, vol. 67, no. 17, pp. 2295–2298, 1991.

[6] K. M. Leung and Y. F. Liu, "Photon band structures: The plane-wave method," *Physical Review B*, vol. 41, no. 14, pp. 188–190, 1990.

[7] K. M. Ho, C. T. Chan, and C. M. Soukoulis, "Existence of a photonic gap in periodic dielectric structures," *Physical Review Letters*, vol. 65, no. 25, pp. 3152–3155, 1990.

[8] Z. Zhang and S. Satpathy, "Electromagnetic wave propagation in periodic structures: Bloch wave solution of maxwell's equations," *Physical Review Letters*, vol. 65, no. 21, pp. 2650–2653, 1990.

[9] S. G. Johnson and J. Joannopoulos, "Designing synthetic optical media: photonic crystals," *Acta Materialia*, vol. 51, no. 19, pp. 5823–5835, 2003.

[10] M. Qiu, M. Mulot, M. Swillo, S. Anand, B. Jaskorzynska, A. Karlsson, M. Kamp, and A. Forchel, "Photonic crystal optical filter based on contra-directional waveguide coupling," *Applied Physics Letters*, vol. 83, no. 25, pp. 5121–5123, 2003.

[11] K. Masanori, "Wavelength division multiplexing and demultiplexing with photonic crystal waveguide couplers," *J. Lightwave Technol.*, vol. 19, p. 1970, Dec 2001.

[12] O. Frazao, J. L. Santos, F. M. Araujo, and L. A. Ferreira, "Optical sensing with photonic crystal fibers," *Laser & Photonics Reviews*, vol. 2, no. 6, pp. 449–459, 2008.

[13] Q. Liu, Z. Ouyang, C. J. Wu, C. P. Liu, and J. C. Wang, "All-optical half adder based on cross structures in two-dimensional photonic crystals," *Optics express*, vol. 16, no. 23, pp. 18992–19000, 2008.

[14] W. Liu, D. Yang, G. Shen, H. Tian, and Y. Ji, "Design of ultra compact all-optical xor, xnor, nand and or gates using photonic crystal multi-mode interference waveguides," *Optics & Laser Technology*, vol. 50, pp. 55–64, 2013.

[15] M. Plihal, A. Shambrook, A. A. Maradudin, and P. Sheng, "Two-dimensional photonic band structures," *Optics Communications*, vol. 80, no. 3, pp. 199–204, 1991.

[16] M. Plihal and A. A. Maradudin, "Photonic band structure of two-dimensional systems: The triangular lattice," *Physical Review B*, vol. 44, pp. 8565–8571, 1991.

[17] R. Meade, K. Brommer, A. Rappe, and J. Joannopoulos, "Existence of a photonic band gap in two dimensions," *Applied Physics Letters*, vol. 61, no. 4, pp. 495–497, 1992.

[18] P. R. Villeneuve and M. Piche, "Photonic band gaps in two-dimensional square and hexagonal lattices," *Physical Review B*, vol. 46, pp. 4969–4972, 1992.

[19] M. Notomi, "Negative refraction in photonic crystals," *Optical and quantum electronics*, vol. 34, pp. 133–143, 2002.

[20] S. Foteinopoulou, E. N. Economou, and C. M. Soukoulis, "Refraction in media with a negative refractive index," *Physical Review Letters*, vol. 90, no. 10, p. 107402, 2003.

[21] S. Foteinopoulou and C. Soukoulis, "Negative refraction and left-handed behavior in two-dimensional photonic crystals," *Physical Review B*, vol. 67, no. 23, p. 235107, 2003.

[22] R. A. Shelby, D. R. Smith, and S. Schultz, "Experimental verification of a negative index of refraction," *science*, vol. 292, no. 5514, pp. 77–79, 2001.

[23] D. R. Smith, J. B. Pendry, and M. C. K. Wiltshire, "Metamaterials and negative refractive index," *Science*, vol. 305, no. 5685, pp. 788–792, 2004.

[24] J. Bucay, E. Roussel, J. O. Vasseur, P. A. Deymier, A.-C. Hladky-Hennion, Y. Pennec, K. Muralidharan, B. Djafari-Rouhani, and B. Dubus, "Positive, negative, zero refraction, and beam splitting in a solid/air phononic crystal: Theoretical and experimental study," *Physical Review B*, vol. 79, no. 21, p. 214305, 2009.

[25] K. Yee, "Numerical solution of initial boundary value problems involving maxwell's equations in isotropic media," *IEEE Transactions on Antennas and Propagation*, vol. 14, no. 3, pp. 302–307, 1966.

[26] N. W. Ashcroft and D. N. Mermin, *Solid State Physics*. Harcourt College Publishers, 1st ed., 1976.

[27] A. Taflove and S. C. Hagness, *The Finite-Difference Time-Domain Method*. Norwood, MA: Artech House, 3rd ed., 2005.

[28] G. Mur, "Absorbing boundary conditions for the finite-difference approximation of the time-domain electromagnetic-field equations," *IEEE Transactions on Electromagnetic Compatibility*, vol. EMC-23, no. 4, pp. 377–382, 1981.

[29] Z. Sacks, D. Kingsland, R. Lee, and J.-F. Lee, "A perfectly matched anisotropic absorber for use as an absorbing boundary condition," *IEEE Transactions on Antennas and Propagation*, vol. 43, no. 12, pp. 1460–1463, 1995.

[30] S. D. Gedney, "An anisotropic perfectly matched layer-absorbing medium for the truncation of fdtd lattices," *IEEE Transactions on Antennas and Propagation*, vol. 44, no. 12, pp. 1630–1639, 1996.

[31] J.-P. Berenger, "A perfectly matched layer for the absorption of electromagnetic waves," *Journal of Computational Physics*, vol. 114, no. 2, pp. 185–200, 1994.

[32] D. Prather, A. Sharkawy, S. Shi, J. Murakowski, and G. Schneider, *Photonic Crystals, Theory, Applications and Fabrication*. New York: Wiley, 1st ed., 2009.

[33] "BandSOLVE Photonic Band Structure Software - RSoft Photonic Device Tools: Synopsys Photonic Solutions." https://www.synopsys.com/photonic-solutions/rsoft-photonic-device-tools/passive-device-bandsolve.html.

[34] "FullWAVE FDTD Simulation Software - RSoft Photonic Device Tools: Synopsys Photonic Solutions." https://www.synopsys.com/photonic-solutions/rsoft-photonic-device-tools/passive-device-fullwave.html.

[35] J. D. Joannopoulos, S. G. Johnson, J. N. Winn, and R. D. Meade, *Photonic Crystals: Molding the Flow of Light*. New Jersey: Princeton University Press, 2nd ed., 2008.

BIOGRAPHICAL SKETCH

Md. Arafat Hossain comes from Bangladesh, an evergreen country on the Bay of Bengal. He earned his M.S. in Physics from the University of Texas Rio Grande Valley (UTRGV) in May 2023. Mr. Arafat was the Presidential Graduate Research Assistant (PGRA) in the Department of Physics and Astronomy at UTRGV. He worked in Optics Lab. His area of study was Computational Physics.

He finished high school in his home country. He is very keen and eager to learn science and mathematics. His unquenching thirst for knowledge drove him to study Physics. He completed his bachelor of science in Physics in 2016 from Jahangirnagar University, Bangladesh. In 2021, he moved to the USA for higher studies. After graduation, he plans to continue his higher studies in Physics.

Mr. Arafat is an amiable and fun-loving person. He loves to socialize with his friends. His favorite pastime activities are watching moving, riding a bicycle, and watching sports. His favorite sport is cricket. He loves playing cricket in his leisure time.

Md Arafat Hossain

Email: arafathossain097@gmail.com